Calculation Method for the Lateral Deflection of Multi-Storey Timber Modular Buildings

MSc Thesis

Mick Bosse

TU Delft

VAN ROSSUM RAADGEVENDE INGENIEURS

Calculation Method for the Lateral Deflection of Multi-Storey Timber Modular Buildings

Delft University of Technology

by

Mick Bosse

to obtain the degree of Master of Science

at the Delft University of Technology,

to be defended publicly on Tuesday August 27, 2024 at 13:30 PM.

Student number: 4721144

Thesis committee:

Prof. dr. ir. J.W.G. van de Kuilen	TU Delft, Chairman
Dr. ir. G.J.P. Ravenshorst	TU Delft, Supervisor
Dr. ir. P.C.J. Hoogenboom	TU Delft, Supervisor
ir. G.J.T. Brouwers	Van Rossum Raadgevende Ingenieurs, Daily Supervisor

An electronic version of this thesis is available at `http://repository.tudelft.nl/`.

Cover image taken on 12-04-2024 in Odijk.

TU Delft

VAN ROSSUM RAADGEVENDE INGENIEURS

Preface

This master thesis concludes the final part of my study at the Delft University of Technology. It fulfils the requirements for the Master Building Engineering, with the specialisation in Structural Design, at the faculty of Civil Engineering and Geoscience. Successfully defending my thesis will result in the Master of Science degree.

First and foremost, I would like to thank the members of my graduation committee. I want to express my gratitude to Ir. G. Brouwers from Van Rossum Raadgevende Ingenieurs for the numerous meetings where he guided and supported me through the project. The extensive discussions helped me in understanding the different topics and progress with my research. I would like to thank Dr.ir. G.J.P. Ravenshorst for his guidance and advice throughout the process. I would like to show my appreciation to Dr.ir. P.C.J. Hoogenboom for the discussions on the different subjects that helped me grasp the matter and Prof.dr.ir. J.W.G. van de Kuilen for the helpful feedback during the meetings and stepping up as chair when needed.

Furthermore, I am grateful for the opportunity Van Rossum Raadgevende Ingenieurs has given me to perform my thesis at their company. The inspiring environment has provided me with motivation to explore the topic and to finish my thesis. I appreciate all my (future) colleagues for their helpfulness, openness to questions and discussions and for creating a relaxed atmosphere. Finally, I would like to thank the people around me who are not directly involved, but who were a huge support along the journey. A massive thanks to my parents and girlfriend for encouraging and supporting me not only during my thesis, but throughout my entire studies in Delft.

Mick Bosse
Delft, August 2024

Abstract

In the Netherlands, there is a significant housing demand. The Dutch government aims to construct 100,000 houses per year, which presents an enormous challenge. To address this demand and simultaneously tackle the challenge of creating a more sustainable construction industry, timber modular construction emerges as a potential solution. Compared to traditional construction methods, timber modular buildings offer several advantages: lower weight, more sustainable, faster construction, reduced waste, greater efficiency, and higher quality. Currently, most modular components can be prefabricated off-site, except for the stability system. Traditionally, this system involves a concrete core or a steel frame. To eliminate their need, self-supporting modules can be applied, making the building purely modular and more sustainable. Within self-supporting modules, stability is a critical aspect. While incorporating stability elements along the longitudinal side of the module poses no issue, the main challenge lies in the limited available length for stability walls in the transverse direction. Also, the shear wall located in the module conflicts with the preferred open floor area. The design of the module, and in particular the shear wall, has a significant influence on the transverse deflection. Calculating the deflection is crucial to fulfil the requirements for maximum displacements. Therefore, the main research question of this thesis is: *Is it possible to predict the lateral deflection in the transverse direction of multi-storey timber modular buildings with a calculation method based on proposed equations?*. The goal of this thesis is to propose a calculation method that can be used in the design phase, which will give insight in the effect of design choices on the lateral deflection of multi-storey modular buildings.

The approach to answer the main research question consists of several steps. The first step was a literature study that was conducted on modular construction, lateral stability and deformations of modular buildings. Knowledge on the structural design of timber modules and cross-laminated timber was obtained. Also, the deformation mechanisms of multi-storey modular buildings were investigated. The second step was analysing the deformation of individual modules. A general module design and four configurations were established and the numerical modelling method was investigated and validated. Hereafter, the equations to calculate the deformation of individual modules in the transverse direction were proposed for the four module configurations. Based on the numerical model, the equations for the horizontal displacement and rotation were established. Additionally, the formulas were extended to incorporate various design options like connection design, shear wall thickness and shear wall position. The proposed equations were integrated in a calculation method that predicts the lateral deflection of multi-storey modular buildings in transverse direction. Hereby only the deformation of the modules was taken into account and not those from the inter-module connections. The cumulative effect due to rotation of lower modules is added to the individual module displacement to find the total deflection.

The results showed that the proposed equations accurately calculate the deformation of the individual modules. With differences below 10%, the formulas are able to calculate the horizontal displacement and rotation for various designs. The calculation method was validated with two examples. Example 1 was a four-storey, four-span building where at the top a maximum error of 8.7% was found. Example 2 was an eight-storey, eight-span building where the proposed calculation method resulted in a maximum error of 9.5%, which was on the lowest storey. At the top, a difference of 2.6% was found. Both errors were lower than 10% and at the safe side, meaning that the calculation method provides accurate and safe results. A case study was performed to verify the practical applicability of the method. The lateral deflection results showed significant differences (45%), which can be assigned to limitations of the calculation method. These limitations ensure the method is not suited for detailed calculations that are necessary in later design phases. For these detailed calculations, a (parametric) finite element model would be more suited. However, the calculation method offers a solution for early design stages, as it provides quick and easy insight into effects of certain design choices on the building's lateral deflection.

Contents

Preface i

Abstract ii

List of tables v

List of figures x

1 Introduction 1
- 1.1 Background . . . 1
- 1.2 Research specification . . . 1
  - 1.2.1 Problem definition . . . 1
  - 1.2.2 Scope . . . 2
  - 1.2.3 Research contribution and objectives . . . 2
  - 1.2.4 Research questions . . . 3
- 1.3 Work approach . . . 3

2 Modular Construction 5
- 2.1 Introduction . . . 5
  - 2.1.1 Advantages . . . 6
  - 2.1.2 Disadvantages . . . 7
  - 2.1.3 History and reference projects . . . 7
- 2.2 Structural design of timber modular buildings . . . 8
  - 2.2.1 Module types . . . 8
  - 2.2.2 Connections . . . 9
  - 2.2.3 Fire safety . . . 10
  - 2.2.4 Robustness . . . 11
- 2.3 Cross-laminated timber . . . 12
  - 2.3.1 Structural design with cross-laminated timber . . . 13
  - 2.3.2 Modelling of CLT . . . 15
- 2.4 Connection types . . . 17
  - 2.4.1 Intra-module connections . . . 17
  - 2.4.2 Inter-module connections . . . 20

3 Lateral deformation of modular buildings 22
- 3.1 Lateral load resisting systems . . . 22
  - 3.1.1 Core . . . 22
  - 3.1.2 Bracing system . . . 23
  - 3.1.3 Shear walls . . . 23
- 3.2 Self-supporting modular buildings . . . 23
  - 3.2.1 Shear wall deformation . . . 23
  - 3.2.2 Diaphragms . . . 25
- 3.3 Modular buildings versus conventional buildings . . . 25
- 3.4 Lateral deflection of modular buildings . . . 26
  - 3.4.1 Force distribution . . . 27
  - 3.4.2 Deflection due to shear . . . 27
  - 3.4.3 Deflection due to bending . . . 28
  - 3.4.4 Deflection due to rotation . . . 28
  - 3.4.5 Deflection due to translation . . . 29

3.4.6 Deflection due to rotation of the foundation . . . 30
3.4.7 Total deflection . . . 30
3.5 Loading . . . 30
3.5.1 Wind load . . . 31
3.5.2 Gravity load . . . 31
3.5.3 Notional loads . . . 32
3.5.4 Second-order effect . . . 33
3.6 Code requirements . . . 34

4 Design and modelling of individual modules 35
4.1 Module configurations . . . 35
4.2 Module design . . . 36
4.3 Deformation calculation . . . 37
4.4 Numerical modelling . . . 39
4.4.1 Validation . . . 40
4.4.2 Mesh size . . . 40
4.4.3 Modelling of the module . . . 40

5 Equation proposal for individual modules 42
5.1 Assumptions . . . 42
5.2 Main equation proposal . . . 42
5.2.1 Standard shear and bending stiffness . . . 44
5.2.2 Module 0 . . . 44
5.2.3 Module 1 . . . 47
5.2.4 Module 2 . . . 50
5.2.5 Module 3 . . . 52
5.2.6 Summary and validation of the equations . . . 54
5.3 Moment induced deformation . . . 55
5.3.1 Moment induced rotation . . . 55
5.3.2 Moment induced displacement . . . 58
5.4 Extension of the equation . . . 59
5.4.1 Connection stiffness . . . 59
5.4.2 Shear wall thickness . . . 62
5.4.3 Shear wall position . . . 64
5.4.4 Test of the extensions . . . 65
5.5 Workflow . . . 66

6 Calculation method for multi-storey modular buildings 69
6.1 Individual module deformation . . . 69
6.2 Multi-storey deformation . . . 70
6.3 Modelling of vertical and horizontal stacked modules . . . 71
6.4 Calculation method . . . 72
6.4.1 Horizontal stacking . . . 72
6.4.2 Vertical stacking . . . 73
6.4.3 Force spread factor . . . 74
6.4.4 Correction factor . . . 76
6.5 Workflow . . . 77
6.6 Examples . . . 78
6.6.1 Example 1 . . . 78
6.6.2 Example 2 . . . 80

7 Case study verification 82
7.1 Poppies . . . 82
7.1.1 Structural design . . . 82
7.2 Predicting the lateral deflection . . . 84
7.2.1 Design . . . 84

7.2.2 Calculation. 84
7.3 Results 85

8 Discussion **87**

9 Conclusions and recommendations **90**
9.1 Conclusions. 90
9.2 Recommendations 91

Bibliography **94**

Appendix A: Numerical validation **95**

Appendix B: Mesh size influence **105**

Appendix C: Bending and shear stiffness determination **107**

Appendix B: Results **112**

List of Figures

1.1 Thesis outline 4

2.1 Modular concepts: (a) linear, (b) planar and (c) volumetric [5] 6
2.2 Typical time planning for modular and traditional construction [7] 6
2.3 Examples of timber modular buildings 8
2.4 Modular connection types[13] 9
2.5 Application of sound bearing strips 10
2.6 Direct and indirect robustness design methods [19] 12
2.7 Cross-laminated timber [21] 12
2.8 CLT cross section with out of plane stresses [23] 14
2.9 (a) Stiffness directions, (b)planes and directions corresponding to stiffness matrix [25] . . 17
2.10 Slip of different timber-concrete connection types [26] 18
2.11 Dimensions of screw from Rothoblaas. [27] 18
2.12 Characteristics of the load-displacement graph of the connection [28] 19
2.13 Tested connection setups [29] 19
2.14 Angle brackets and hold downs [30] 20
2.15 Steel WHT plate for timber-to-timber connection [27] 21
2.16 Acoustic anchor Straviwood Modulink [33] 21

3.1 Illustration of the different deformation contributions of a shear wall [35] 23
3.2 Diaphragm action [20] 25
3.3 Bending deformation with cumulative effect of a modular building [37][38] (adjusted) . . 26
3.4 Shear force and bending moment distribution in a multi-storey modular building [37] . . 27
3.5 Deflection due to shear [37] 28
3.6 Rotation deformation of a modular building [37] 29
3.7 Translation deformation of a modular building [37] 29
3.8 Rotation of the foundation due to horizontal loads 30
3.9 Wind pressure distribution over the building height following the Eurocode EN 1991-1-4 31
3.10 Construction tolerances of modular buildings [1] 32
3.11 Displacement components [3] 33
3.12 Inter-storey drift [40] 34

4.1 Design of the four module configurations: M0-M3 36
4.2 3D view of the basic module 36
4.3 Cross-sections of the basic module 37
4.4 Shear wall clamped at the bottom: a) model of the shear wall, b) total deflection, c) shear deflection, d) bending deflection 38
4.5 Shear wall supported with pinned supports at the bottom corners: a) numerical model, b) total deformation, c) shear deformation, d) bending deformation 38
4.6 Orientation joint with degrees of freedom in SCIA 40
4.7 SCIA model with the local coordinate systems 41
4.8 SCIA model with the loading, connections and supports 41

5.1 Numerical model of module 0 44
5.2 Deformation of module 0 (standard dimensions) with the horizontal displacement (left) and rotation (right) 45

5.3 Module 0: a) relation width and displacement, b) relation height and displacement, c) relation force and displacement, d) relation width and rotation, e) relation height and rotation, f) relation force and rotation 46
5.4 Relation stiffness and width for module 0 47
5.5 Numerical model of module 1 47
5.6 Deformation of module 1 with the horizontal (left) and vertical displacement (right) . . . 48
5.7 Module 1: a) relation width and displacement, b) relation height and displacement, c) relation force and displacement, d) relation width and rotation, e) relation height and rotation, f) relation force and rotation 49
5.8 Relation stiffness and width for module 1 49
5.9 Numerical model of module 2 50
5.10 Deformation of module 2 with the horizontal (left) and vertical displacement (right) . . . 50
5.11 Module 2: a) relation width and displacement, b) relation height and displacement, c) relation force and displacement, d) relation width and rotation, e) relation height and rotation, f) relation force and rotation 51
5.12 Relation stiffness and width for module 2 51
5.13 Numerical model of module 3 52
5.14 Deformation of module 3 with the horizontal (left) and vertical displacement (right) . . . 52
5.15 Module 3: a) relation width and displacement, b) relation height and displacement, c) relation force and displacement, d) relation width and rotation, e) relation height and rotation, f) relation force and rotation 53
5.16 Relation stiffness and width for module 3 53
5.17 Deflection due to the bending moment: left) tension and compression force due to the horizontal load, right) deflection due to the tension and compression forces 55
5.18 Numerical model for the moment induced rotation 56
5.19 Equations for the modules plotted next to the numerical results 57
5.20 Equations for the module configurations (dashed curve) plotted next to the numerical results (continuous curve) 58
5.21 Cross-section of a module at the shear wall with the positions of the 5 intra-module connections 60
5.22 Details 1-5 60
5.23 non-linear function of connection 1, option A 61
5.24 Relations for the connection design options of module 0 62
5.25 Deflection of the diaphragm in symmetric and asymmetric designs 64
5.26 Relation between the concentrated wind load F and Δ_l 65
5.27 Design of the four module configurations 66
5.28 Module dimensions H, b and H_{sw} (left) and the corresponding shear wall design (right) . 67

6.1 The four deformation contributions θ_M, u_M, θ_V and u_V 70
6.2 Force distribution and deformation behaviour of a six-storey building [37][38] (adjusted) 70
6.3 Simplified model of vertical (left) and horizontal (right) stacked modules 71
6.4 Modelling detail of horizontal and vertical connected modules 72
6.5 Numerical models of the four module configurations for a 6 x 1 building 73
6.6 Lateral displacements of the four module configurations for a 6 x 1 building 73
6.7 Lateral deflection of an m x 1 modular buildings 74
6.8 Visualization of the normal force spreading in a multi-storey modular building due to an applied lateral load at the top. 75
6.9 Lateral displacements of an m x 1 modular buildings. Situation with the force spread factor 76
6.10 Lateral displacements of an m x 1 modular buildings. Situation with the force spread- and correction factor 77
6.11 Numerical analysis of Example 1 79
6.12 Lateral displacement of Example 1 80
6.13 Numerical analysis of Example 2 80
6.14 Lateral displacement of Example 2 81

7.1 Cross section of Poppies with block A indicated [41] . . . 82
7.2 Van Rossum model of Poppies [41] . . . 83
7.3 Numerical analysis of Van Rossum [41] . . . 84
7.4 Lateral deflection of Poppies . . . 86

9.1 Orientation joint with degrees of freedom in SCIA . . . 96
9.2 Shear wall with geometry [35] . . . 97
9.3 Numerical model . . . 97
9.4 Load displacement curves . . . 99
9.5 Analytical models of the CLT shear walls with: (a) basic shear wall, (b) coupled shear walls and (c) shear wall connected to a perpendicular wall and floor . . . 100
9.6 Numerical models of the CLT shear walls with: (a) basic shear wall, (b) coupled shear walls and (c) shear wall connected to perpendicular wall and floor . . . 101
9.7 3D view and top view of the one-storey CLT structure [45] . . . 102
9.8 SCIA model of the 3D building . . . 103
9.9 Load displacement curve of the 3D reference (paper) and validation (SCIA) model for both building configurations . . . 104
9.10 Deformation for different mesh sizes, with the focus on compression at the supports . . . 106
9.11 Dimensions of the wall and the corresponding cantilever model . . . 107
9.12 Model of module 0 used to determine the stiffness . . . 109
9.13 Module 1 shown as I-section . . . 110
9.14 Effective width related to transverse wall width - Full cooperation [47] . . . 110
9.15 Relations for the varying shear wall thickness, module 0 . . . 113
9.16 Relations for the varying shear wall thickness, module 1 . . . 114
9.17 Relations for the varying shear wall thickness, module 2 . . . 114
9.18 Relations for the varying shear wall thickness, module 3 . . . 115
9.19 Relations for the varying connection stiffness, module 0 . . . 115
9.20 Relations for the varying connection stiffness, module 1 . . . 116
9.21 Relations for the varying connection stiffness, module 2 . . . 116
9.22 Relations for the varying connection stiffness, module 3 . . . 117

List of Tables

2.1 Strength and stiffness properties of CLT class C24 (prEN1995-1) . . . 13
2.2 Results of tested setups [29] . . . 19
2.3 CLT connections with strength and stiffness [31] . . . 20
2.4 Properties of the WHT Rothoblaas plate [27] . . . 21

5.1 Standard shear and bending stiffnesses of the module configurations . . . 44
5.2 Validation of the displacement equations for three module designs . . . 54
5.3 Validation of the rotation equations for three module designs . . . 54
5.4 Accuracy determination of the equations for varying parameters . . . 58
5.5 Validation of the moment induced displacement equations for three module designs . . . 59
5.6 Translation spring stiffness of the intra-module connections [29] . . . 61
5.7 Modelling line-to-line stiffness of the three options. Spacing in mm and stiffness in MN/m/m 61
5.8 Factor k_c for the three connection design options . . . 62
5.9 Standard stiffnesses for the three shear wall thicknesses . . . 63
5.10 Values for $k_{t,u}$ . . . 63
5.11 Values for $k_{t,\theta}$ . . . 63
5.12 Validation of the displacement equations for three module designs . . . 66
5.13 Validation of the rotation equations for three module designs . . . 66
5.14 Equations for the module configurations . . . 67
5.15 Determination of the constants . . . 67
5.16 Standard stiffnesses for the three shear wall thicknesses . . . 68
5.17 Values for $k_{t,u}$ . . . 68
5.18 Values for $k_{t,\theta}$ . . . 68
5.19 Factor k_c for the three connection design options . . . 68

6.1 Displacement due to spreading of the force . . . 75
6.2 Force spread factor per storey . . . 76
6.3 Correction factor . . . 77
6.4 Results of the numerical analysis and hand calculation . . . 77
6.5 Force spread factor per storey . . . 78
6.6 Correction factor . . . 78
6.7 Design characteristics example 1 . . . 79
6.8 Lateral displacement of Example 1 . . . 79
6.9 Design characteristics example 2 . . . 80
6.10 Lateral displacement Example 2 . . . 81

7.1 Design characteristics Poppies . . . 84
7.2 Lateral deflection prediction of Poppies . . . 85

9.1 Properties of CLT shear wall . . . 97
9.2 Influence of simplification in modelling . . . 99
9.3 Properties of the CLT shear walls . . . 100
9.4 Displacement results . . . 101
9.5 Geometrical and mechanical parameters of the building . . . 102
9.6 Stiffness of the connections used in the numerical validation model . . . 103
9.7 Lateral stiffness of the models . . . 104
9.8 Total deflection and local deflection for varying mesh sizes. . . . 105

9.9 Comparison of calculated stiffness values 111

1

Introduction

1.1. Background

Multi-storey timber buildings have experienced massive interest in the last decade because of the awareness of the environmental benefits and the demand to build more sustainable. In addition, there are new developments in timber construction methods which have become popular and are promising for the future. A relatively new construction method is modular construction, where buildings are erected with primarily prefabricated 2D or 3D elements. Modular construction has been gaining popularity due to many advantages like controlled manufacturing, little waste and quick installation capabilities, reducing the construction time drastically. In combination with timber, it could become an import future construction method as it is both fast and sustainable.

1.2. Research specification

This section describes the framework of the thesis by appointing the problem definition, scope, objectives and research questions. It forms the outline of the study.

1.2.1. Problem definition

In most developed countries, the built environment represents more than 40% of the total energy consumption. Therefore, the European Commission requires significant reduction of CO2 emissions in new buildings in order to mitigate climate change [1]. This means that not only the energy consumption during the utilization phase should be reduced, but also during the construction phase. This, in combination with the plan of the Dutch government to built 100,000 houses per year to resolve the extreme housing demand in the Netherlands, asks for sustainable and fast building methods [2]. One way of doing this is by using the sustainable material timber. In the last decades this building material has made its reappearance in the construction industry and timber high-rise buildings are already constructed. Over the past few years, a relatively new construction method has also appeared, the modular construction method. This construction method proves to be promising in combination with timber to create timber modular buildings. As with any new system, the lack of guidelines and unknown structural behaviour are however two reasons why designers and contractors might hesitate to choose this construction method. To increase its popularity, these challenges have to be overcome.

Nowadays, timber modular buildings are being constructed, but in most cases they are supported with an external stability element made from traditional materials. To make timber modular construction fully sustainable and modular, self-supporting buildings are required. However, more structural knowledge about these self-supporting timber modular structures is needed. A major challenge is to provide the lateral stability in transverse direction, which is done by the shear wall inside the modules. Different shear walls designs are possible that all have varying stiffness and thus contribute differently to the stability. The engineer and architect together choose a suitable module design, such that the lateral

stability is provided and the floor plan layout is convenient. However, in the early design stage, it is difficult to quickly calculate the structure lateral deflection and check whether the chosen design fulfils the code requirements.

1.2.2. SCOPE

The scope of the research is given in this section. As modular construction is a broad topic, not all aspects can be considered within the given time frame. The scope is limited by the following boundary conditions:

- Materials: The materials used of the design of the modules is limited to cross-laminated timber (CLT). In the connections, steel is used.
- Foundation: The design of the foundation is outside the scope of this research. The connection between the modules and foundation is modelled as a hinged line support. The stiffness of the foundation is therefore not included.
- Building dimensions: The maximum number of vertical stacked modules that is investigated is 10, because the focus is on low- and mid-rise buildings.
- Fire safety: The fire safety aspects of timber are assessed during the literature study. However, no calculations will be performed in this thesis.
- Progressive collapse: In the literature research, the progressive collapse of modular buildings is qualitatively described. In theory, the inter-module connections provide both horizontal and vertical ties. In this thesis, no calculations are performed on progressive collapse.
- Building physics: No attention is paid to the building physics of the modular buildings. Therefore, acoustics, thermal insulation and ventilation are not considered. Additionally, building services such as ducts, wiring, plumbing and lift shafts are outside the scope of this research.

1.2.3. RESEARCH CONTRIBUTION AND OBJECTIVES

Focusing on timber shear wall behaviour has been an interest to researchers for years. The focus however has been mainly on light-frame- or cross-laminated timber shear walls and the analyses of the wall parameters such as aspect ratio, panel thickness and connections. Additionally, the individual contribution of the four-term deflection equation (bending, shear, overturning and sliding) has been investigated for timber shear walls. Where research has lacked, is in investigating the deformation of timber modular buildings and the influence of the different shear wall designs on the deformation of self-supporting multi-storey timber modular buildings.

The objective of this thesis is to create a calculation method, based on proposed equations, that predicts the lateral deflection in transverse direction of timber modular buildings. This will be done for multiple module configurations to allow for variation in the building design. Additionally, the equations are extended to incorporate different design options such as intra-module connections, shear wall thickness and shear wall position. The main goal is to develop a calculation method that provides insight in the effects of the design choices on the lateral deflection of modular buildings. The main goal is obtained with the help of the following sub goals:

1. Choose a general applicable module design and commonly used module configurations.
2. Build a reliable structural model in Finite Element Software program SCIA, that analyses the module deformation behaviour correctly.
3. Propose equations, based on the numerical model, for the horizontal displacement and rotation of the different module configurations.
4. Extend the equations for several parameters like connection stiffness, shear wall thickness and shear wall position.

5. Integrate the equations into a calculation method that determines the lateral deflection of multi-storey timber modular buildings.

1.2.4. RESEARCH QUESTIONS

The main research question that will be answered in this thesis is:

Is it possible to predict the lateral deflection in transverse direction of multi-storey cross-laminated timber modular buildings with a calculation method based on proposed equations?

SUB RESEARCH QUESTIONS

In order to answer the main research question, several sub-questions have been formulated:

1. What does the existing literature state about modular construction and lateral deformation of modular buildings?
2. What is a general applicable module design and what common shear wall configurations are applied?
3. How can the designed modules be realistically modelled in the Finite Element Analysis program SCIA?
4. Can accurate equations be proposed that calculate the horizontal displacement and rotation of individual modules?
5. What is the influence of intra-module connections, shear wall thickness and shear wall location on the deformation and how could these be incorporated in the proposed equations?
6. Can the equations be integrated in the calculation method that predicts the lateral deflection of multi-storey modular buildings?

1.3. WORK APPROACH

The literature will focus on the structural aspects concerning timber modular buildings. R. Gijzen investigated in his thesis [3] the structural behaviour of cross-laminated timber buildings. It contains a comprehensive research about all aspects influencing the structural behaviour of modular buildings. This will form a basis for the literature research which will be performed in this thesis.

After the literature study is performed and sufficient knowledge is gained on modular construction, Cross-laminated timer, connections and Finite Element Methods, the research part can start. First, a general module design is chosen, for which four module configurations are determined. Then, the module is modelled in the FEA software SCIA (version 22), where the modelling methods are validated and tested to obtain a trustworthy model. With this model, the relations between the chosen parameters with the displacement and rotation are determined. Subsequently, the equations for the horizontal displacement and rotation of individual modules are established based on the found relations. Next, the equations are extended with several factors that allow for various design options like: connection stiffness, shear wall thickness and shear wall position. Hereafter, the proposed equations will be integrated in a calculation method that can predict the lateral deflection of modular buildings. Finally, the practical applicability is verified with a case study. The described work approach is visualized in Figure 1.1.

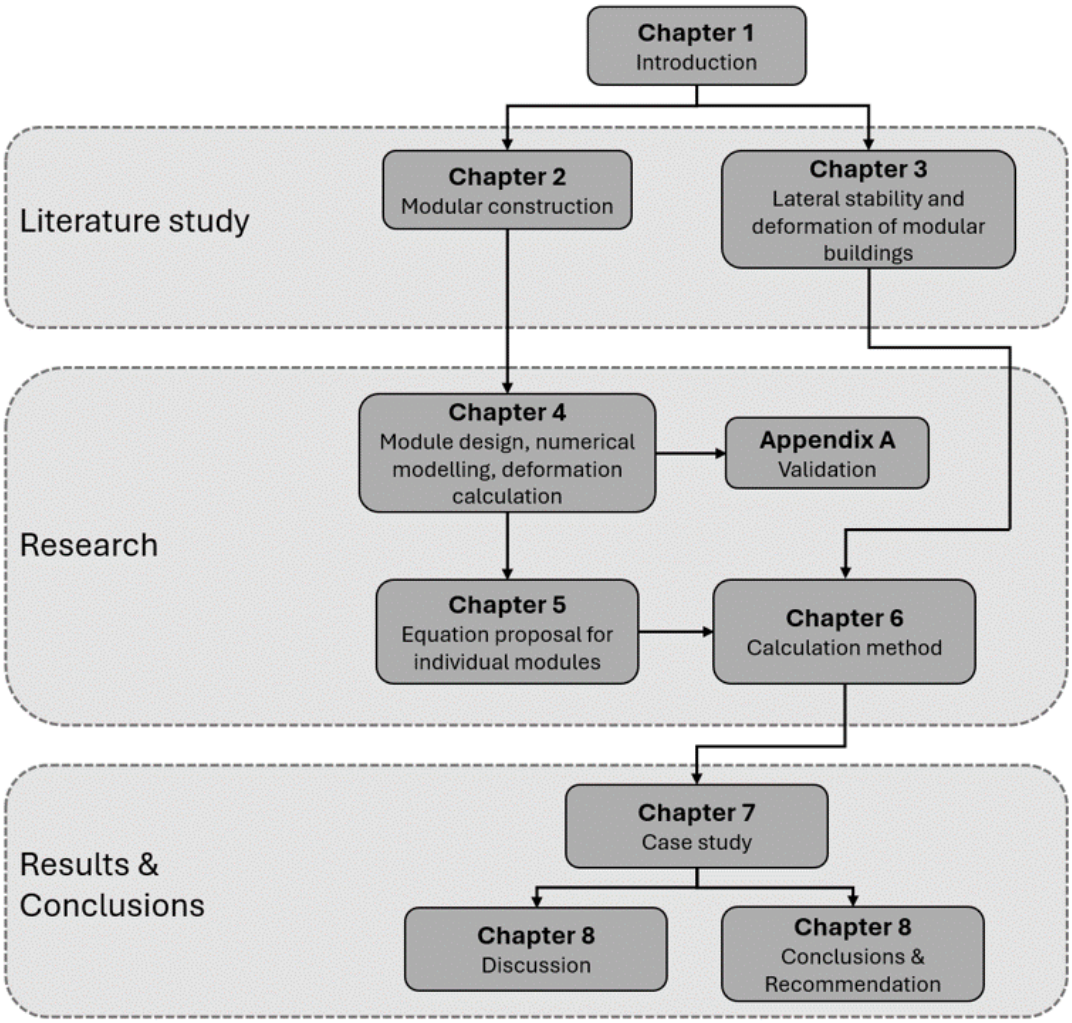

Figure 1.1: Thesis outline

2

Modular Construction

This chapter serves an introduction to modular construction. It will give background information and an overview of structural aspects. First, an introduction on modular construction will be given in Chapter 2.1. It describes advantages and disadvantages, as well as reference projects. Hereafter, Chapter 2.2 discusses the structural design of timber modular building focusing on module types, connections, fire safety and robustness. Chapter 2.3 entail information on cross-laminated timber. Finally, Chapter 2.4 will dive deeper into the intra- and inter-module connection types.

2.1. INTRODUCTION

The building industry switches to using more and more prefabricated elements for construction. These can be prefabricated facade elements or prefabricated structural elements. When prefabrication is extended, the modular construction type arises. Muse et al. [4] defines modular construction as "a construction method that produces a building consisting of modular units or modules that are mass-produced off-site in a manufacturing facility". A module is an element that is part of the final product and has substantial functionality to this product. The degree to which the prefabricated modular concepts can be applied varies in terms of geometry. Components may be linear, planar or volumetric as shown in Figure 2.1. Linear components are the most simple ones, columns and beams are made with predrilled joints and assembled on site. The planar components consist of walls and slabs forming larger elements, which also come with precut slots and technical installations could be included when fabricated. Finally, the volumetric components corresponds to room modules. These are large units assembled off-site, where entire room modules can be manufactured. They can be completely prefabricated, including interior like kitchens and bathrooms. This latter option has the potential to build very quickly by delivering fully finished modules, which can be stacked on top of each other to create a building. When authors speak about modular construction, they only talk about the volumetric units, which is also the case is this thesis [5].

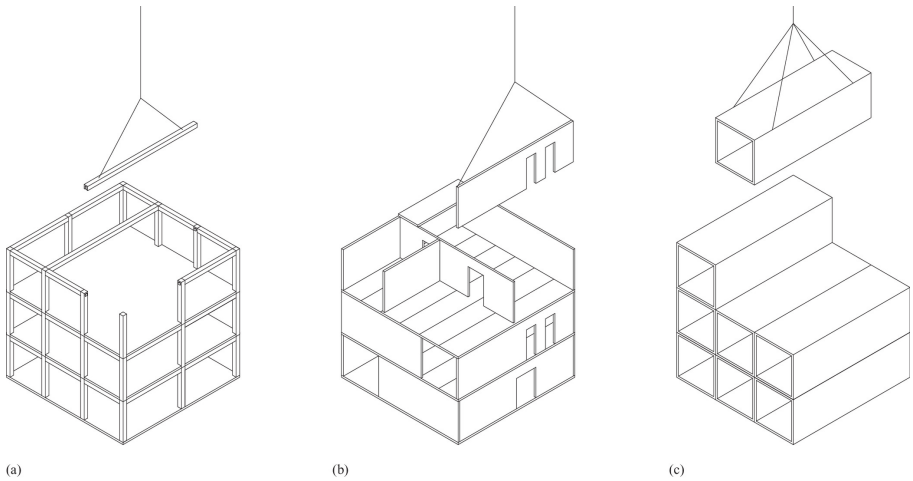

Figure 2.1: Modular concepts: (a) linear, (b) planar and (c) volumetric [5]

2.1.1. ADVANTAGES

The choice for modular construction by the design team usually results in highly repetitive buildings. Compartmentalized layouts such as hotels, hospitals, student residences, prisons and social housing are all well-suited for this building method. The advantages of this building type are extensive and established by different parties. They are elaborated in the paragraphs below.

SPEED OF CONSTRUCTION

Modular construction can increase building time drastically due to the efficient off-site fabrication. The prefabrication can be done simultaneously with the on-site construction, reducing construction time. In addition, the repetitive character of the modules ensures efficient fabrication, resulting in increased productivity. Due to the indoor and centralized manufacturing location, all key parties can work effectively together in good environmental conditions, which make them independent of weather conditions[6]. According to Lawson et al. [1], time savings for of construction for a modular building of 6 storeys can be up to 50% in comparison to traditional construction. Because on-site construction time is massively reduced, and off-site manufacturing can be started early, the finishing time is reduced. A typical time planning is shown in Figure 2.2.

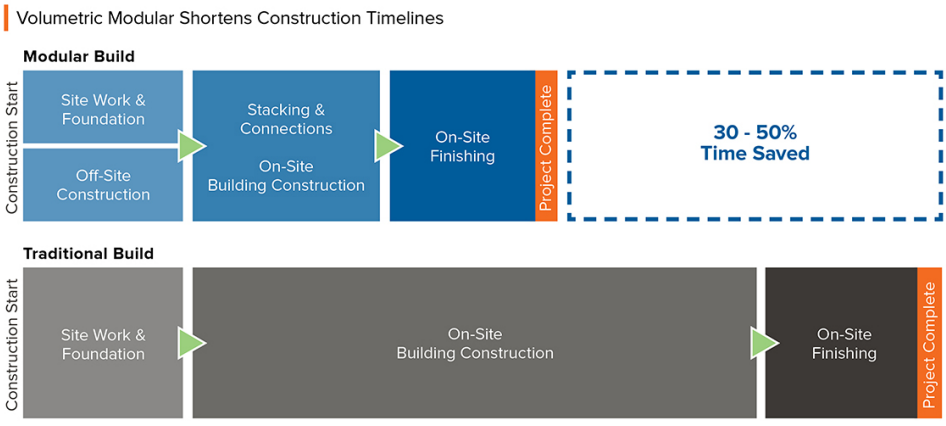

Figure 2.2: Typical time planning for modular and traditional construction [7]

IMPROVED QUALITY AND SAFETY
Manufacturing and assembly of the modules takes places in a factory, where climate conditions can be regulated, leading to better environmental conditions for the modules as well as the workers. Due to the repetitiveness process, fewer errors and imperfections occur, minimizing damage and waste. Finally, the indoor controlled environment reduces risk of rust, sun damage and mould to the materials [1]. Modular construction methods leads to more safety because less people, equipment and traffic is present at the construction site. At the same time, the indoor environment makes sure the workers do not have to deal with extreme weather.

SUSTAINABILITY
An important benefit of modular construction is its sustainability, which is caused by several aspects. Due to material efficiency, limited waste, reuse potential, limited nuisance and (for timber) CO2 absorption, this method is seen as very sustainable. At the same time, these advantages also provide economic benefits[6].

2.1.2. DISADVANTAGES
Besides benefits, there are also disadvantages to modular construction. The main drawback lies in the limited flexibility regarding building design due to the repetitive nature of the modules. Furthermore, dimensions are restrained due to transportation requirements for road transport. Without police transport, the maximum width is 3.5 meter. Larger modules could be transported with police escorts, but costs will increase[8].

2.1.3. HISTORY AND REFERENCE PROJECTS
Historically, modular buildings started in markets with high housing demands and low availability of labour. After the war, this method gained interest in especially the United Kingdom and the United States due to the rapid need of social housing and fast construction methods. Nowadays, the housing demand has accelerated again and therefore modular construction gained renewed attention. With the additional problem of climate change, the combined advantages of modular construction and the sustainable material timber has led to the increased popularity of timber modular buildings.

Over the years, multiple timber modular buildings have been built. From these projects, lessons can be learned and future potential can be evaluated. Figure 2.3 shows four example projects where buildings have been constructed with CLT modules. Hotel Jakarta is a nine-storey, 30 meter high triangular building situated in Amsterdam. This timber framed building is 16500 m2, gathering 176 modular rooms of 30 m2 each (3.25 x 9.50 m). The module consists of a concrete floor with CLT walls and ceiling. Assembling the modules took 3 months in total, resulting in 12 modules per day. Woodie is a student accommodation consisting of 371 modules covering 13500 m2 over six floors. The modules vary from 3.30 x 6.80 m to 3.30 x 7.20 m. The modules were placed in a record rate of 18 a day[5]. Robin Wood and Poppies are two buildings which are still under construction in Amsterdam, they both have parts of the building which are self-stabilizing while other parts rely on stabilizing cores.

(a) Hotel Jakarta [5]

(b) Woodie [5]

(c) Robin Wood [9]

(d) Poppies [9]

Figure 2.3: Examples of timber modular buildings

2.2. STRUCTURAL DESIGN OF TIMBER MODULAR BUILDINGS

The primary vertical load bearing component of a modular building is the module itself. In general, three types of modules can be distinguished for the local system: continuously supported, corner supported and non-load bearing modules. They differ in the way of transferring the load and their application range for building designs. Looking at the global system, there are several approaches to ensure a stable structure. It could be done by using a core, bracing system or shear walls. This latter assures a self-supporting structure, which means that the modules should provide the lateral stability by themselves. For low-rise buildings this is possible, but for medium and high-rise it is more difficult. The core and bracing systems are suitable for medium to high-rise buildings. Furthermore, the intra- and inter-module connections play an important role in transferring the loads.

2.2.1. MODULE TYPES

In general, three load-bearing module types can be distinguished: Continuously supported, corner-supported and non-load bearing modules. This study focuses on continuously supported modules. The three types are briefly discussed.

In corner-supported modules, forces are transferred by edge beams to the columns. For longer modules, it is common to add an extra column in the middle to keep the height of the beam minimal. The connections could be made moment resisting so that the module is stiff by itself. Another option is to make simple connections and use bracing along the edges to create stiffness. Due to the open sides, this topology allows for flexibility in creating larger floor spaces [1]. The safety of these types of timber modules is still being investigated. For example, the robustness was investigated by J. Knudde and K. Zutt [10][11]. Non-load bearing modules are non-structural units which are directly supported on the floor of the building. They are often called 'pods' and commonly used for highly served areas such as kitchens, small rooms like toilets or bathrooms [1]. Continuously supported modules, also known as load-bearing or volumetric modules, are modules where the walls are load bearing. They have cross-laminated timber panels trough where loads are transferred. The vertical loads are transferred through

the side walls by direct wall-to-wall bearing. The walls serve as a barrier between individual modules and thus have no openings. Because the walls are closed, limited freedom for composition of floor area is possible. It is possible to create openings in the wall panels, but this depends on the loading situation.

2.2.2. CONNECTIONS

Construction of a modular building requires multiple connections and these can be grouped as inter-module connections and intra-module connections. Inter-module connections connect individual modules, while intra-module connections connect elements within a module. Since intra-module connections are done in the factory during prefabrication, the fastening of the inter-module connections affect the overall on site work the most [12].

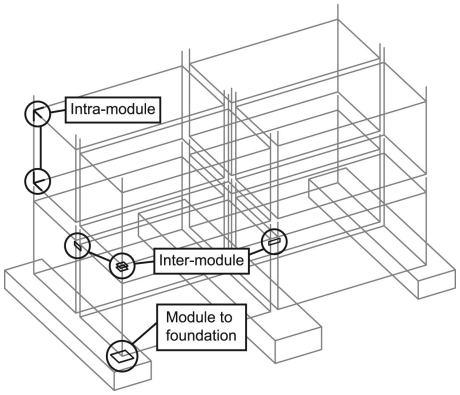

Figure 2.4: Modular connection types[13]

INTRA-MODULE CONNECTION SYSTEMS

As mentioned, intra-module connections connect all elements within an individual module, such as wall-to-wall, floor-to-wall and ceiling-to-wall elements. The connections should provide enough strength and should be stiff enough to enable the module to act as a whole. Chapter 2.4 describes the different types of connections and discusses their structural performance.

INTER-MODULE CONNECTION SYSTEMS

Inter-module connections are connections that are located between individual modules (Figure 2.4). They connect modules to each other and therefore play an important role in ensuring structural integrity, stability and robustness of modular buildings [14]. Inter-module connections can connect a module to another module in vertical and horizontal direction, or to the foundation. Depending on the load direction, the joints may transfer tension, compression and shear forces horizontally and vertically. According to Li et al. [15] the following connection types can be used when designing the inter-module connections: steel plates with screws, steel rods, a notched CLT panel or an advanced interlocking connection.

The limited accessibility of inter-module connections is a widely recognised challenge in volumetric modular construction. External access is required for the installation of conventional timber connections, while accessibility for these type of connections has long been a key challenge [15]. Especially when volumetric modules become enclosed, the inter-module connections become entirely inaccessible. The consequence of this is, that in some CLT volumetric structures, the inter-module connections are absent and lateral resistance is provided by friction between modules. For self-stabilizing buildings, this can decrease the lateral stability significantly. Therefore, the inaccessibility of inter-module connections is considered as one of the main obstacles in achieving tall CLT volumetric buildings with sufficient lateral stiffness, due to the importance of these connections in defining the integrity and stability of the structures.

SOUNDPROOFING BEARING STRIPS

Sound transmission takes place between modules and according to a case study by Getzner, 90% of the transmission happens through the walls of the modules [16]. To significantly reduce transmission of sound and vibrations, Sylomer bearing strips can be used to transfer loads from one module to another without causing sound- and vibration bridges. Figure 2.5a shows such a bearing strip. It is placed between the ceiling of the lower module and the wall of the upper module, as can be seen in Figure 2.5b. The type of strip is chosen in collaboration with an acoustic designer.

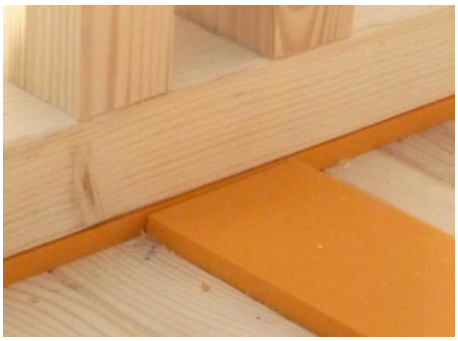

(a) Sound bearing strip [16]

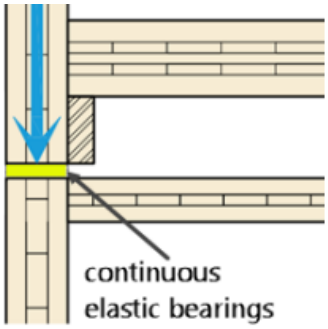

(b) Position of the sound bearing strip [17]

Figure 2.5: Application of sound bearing strips

The design of a bearing strip is not only acoustic based but also structural. Because the flexibility of the strip causes displacements in horizontal and vertical directions, the stiffness must be determined carefully. Next to stiffness, the strength should be sufficient to ensure that the bearing strip does not fail in ultimate limit state. These structural values must be provided by the manufacturer. [15].

2.2.3. FIRE SAFETY

The main two objectives in fire safety design are to prevent casualties and avoid damage to adjacent buildings. To meet these goals, the Building Decree contains minimum requirements for all structures in the Netherlands. In short, the requirements are explained below [18].

- Fire resistance values: The fire resistance of a building must have a specific period of time that it should withstand the fire without the risk of structural failure. This can be 30, 60, 90 or 120 minutes.
- Fire performance characteristics: For timber elements, performance requirements are given. Load bearing capacity, integrity and thermal insulation should be provided by the elements.
- Fire compartments: To prevent fire and smoke spread, the building is separated into compartments. A minimal fire resistance of 60 minutes applies to the separating elements.
- Fire protection systems: Next to passive measures, active measures could be applied. Examples are smoke detection systems, fire hoses and sprinkler systems.

In the case of fire, the timber elements in the module are exposed to sufficient heat and pyrolysis takes place. This is a process of thermal degradation where gas is produced. When this process of charring occurs, it reduces the cross-sectional area and a charred layer is formed on the side surface at the fire-exposed side. To calculate the remaining properties of the reduced cross-section, formulas stated in Eurocode 5 can be used. A thickness $k_0 d_0$ is affected by the increased temperatures and will not be able to transfer forces any more. At the same time, there is a charring rate, which determines how much of the material chars per hour. Expressions for the effective charring depth and rate are shown below. Important to mention is that if a laminate has a residual thickness of less than 3 mm, it should not be incorporated in the strength calculations any more. In general, often $k_0 d_0$ is taken as 7 mm and β_n is taken as 0,65 mm per minute.

$$d_{eff} = d_{char,n} + k_0 d_0 \tag{2.1}$$

$$d_{char,n=\beta_n * t} \tag{2.2}$$

Because CLT is build out of multiple board layers which are glued together, there is a possibility of delamination of the glued interfaces. High temperatures in case of fire can lead to charring layers falling off due to failure of the glued interfaces. When the charred layers fall off, the charring rate is increased significantly because the wood is no longer protected. Additionally, the position of the element, for example walls, floor or ceilings, has an influence on the charring rate because of the susceptibility to delamination. However, there is not a universally valid structural design method to incorporate this effect. Therefore, the effect is often not included.

For verification of the fire situation, safety factors can be neglected and 20% fractile higher strengths can be used.

$$\sigma_{fi,d} \leq f_{fi,d} \tag{2.3}$$

$$\sigma_{fi,d} \leq k_{mod,fi} * \frac{f_{20}}{\gamma_{M,fi}} \tag{2.4}$$

$$\sigma_{fi,d} \leq k_{fi} * k_{mod,fi} * \frac{f_k}{\gamma_{M,fi}} = 1,15 * f_k \tag{2.5}$$

where:

$k_{mod,fi} = 1,00$	Modification factor in the event of fire
$f_{20} = 20\%$	fractile of strength at normal temperature
$k_{fi} = 1,15$	Conversion coefficient for CLT from 5% to 20% fractiles
$\gamma_{M,fi} = 1,00$	Partial safety factor for timber in the event of fire

While the timber elements can be designed such that they provide fire safety, another option is to add fire protective cladding to the elements. Although it takes away the timber look in the building, it is an effective method to provide a fire safe design.

2.2.4. ROBUSTNESS

A building should be designed such that progressive collapse is prevented. Robustness is the ability of a structure to withstand events such as explosions, fire, impact or errors, without being damaged to an extent disproportionate to the original cause (EN 1991-1-7 2006). In other words, failure of a small part of the building does not lead to failure of a bigger part. Providing this can be done by redistributing loads in the case of damage. In the literature, two indirect and three direct progressive collapse prevention methods are given (Figure 2.6).

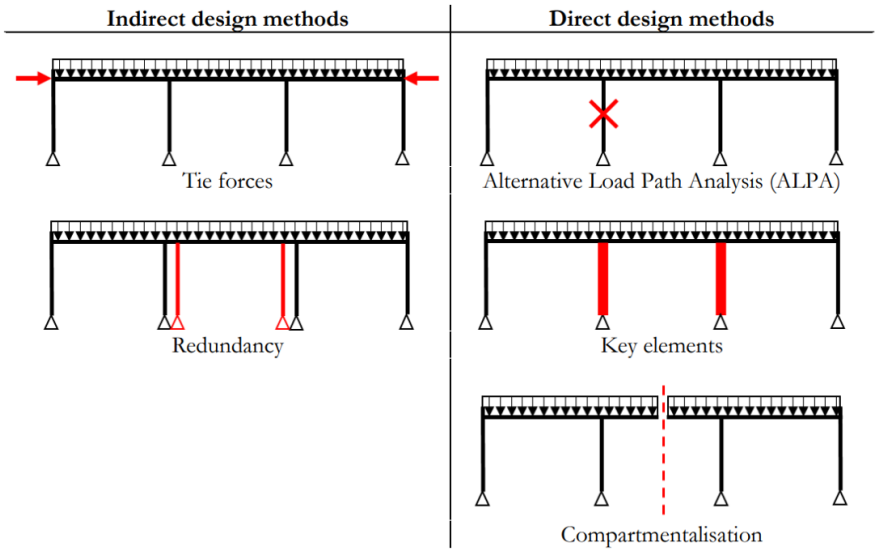

Figure 2.6: Direct and indirect robustness design methods [19]

In modular buildings, the redistribution of loads can be achieved by alternative load path design or by tie forces between the modules [11]. Both methods have the principle that adequate tying of the modules is crucial. In the case of removal of a module, the forces can be redistributed via the connections and an alternative load path is created, assuming sufficient capacity of the connections. Investigating the robustness is outside the scope of this study. It is assumed that progressive collapse is prevented by alternative load paths.

2.3. CROSS-LAMINATED TIMBER

Cross-laminated timber (CLT) is a solid timber element used for load bearing applications and has been developed around 15 years ago in Central Europe. It consists of cross-wise glued lamellas which lie at 90 degrees of each other as is illustrated in Figure 2.7. The cross-wise layering brings the advantage of two directional load bearing, increased shear capacity and the elimination of shrinkage and swelling. Other advantages are the high level of prefabrication, low weight compared to traditional materials and easy fastening. CLT panels are build-up of uneven layers, usually 3, 5 or 7. The timber which is being used for CLT elements in general is spruce wood with strength class C24. The dimensions of CLT panels can be up to 16 m in length, 3.5 m in width and 0,5 m in thickness, but very often transportation is the limiting factor [20].

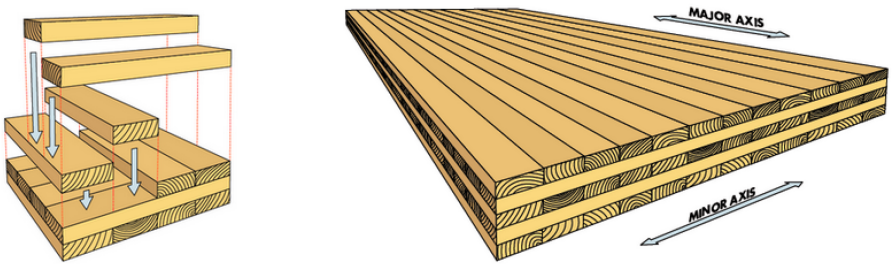

Figure 2.7: Cross-laminated timber [21]

2.3.1. STRUCTURAL DESIGN WITH CROSS-LAMINATED TIMBER

This section discusses the design of cross-laminated timber. The European standard for timber structures, EN 1995-1-1 and NEN-EN 16531, does not cover everything. Therefore, several papers and manufacturing guides are used to analyse CLT.

MATERIAL PROPERTIES

The material characteristics of cross-laminated timber are listed in the table below. Stiffness and strength properties of CLT with strength class C24 are presented according to EN1995-1 and manufacturer DERIX [22].

Table 2.1: Strength and stiffness properties of CLT class C24 (prEN1995-1)

Property	Loading direction	Symbol	Value	Unit
Density	-	ρ_k	450	kg/m^3
Bending strength	Out of plane	$f_{m,k}$	24	N/mm^2
	In plane	$f_{m,edge,k}$	21	N/mm^2
Tension strength	In plane	$f_{t,0,k}$	14,5	N/mm^2
	Perpendicular to plane	$f_{t,90,k}$	0,4	N/mm^2
Compressive strength	In plane	$f_{c,0,k}$	21	N/mm^2
	Perpendicular to plane	$f_{c,90,k}$	2,5	N/mm^2
Shear strength	Out of plane	$f_{v,k}$	2,5	N/mm^2
	Rolling shear	$f_{r,k}$	1,1	N/mm^2
	Perpendicular to plane	$f_{v,xy,k}$	5,0	N/mm^2
Modulus of elasticity	In and out of plane	E_{mean}	11000	N/mm^2
	In and out of plane	$E_{0,05}$	9166	N/mm^2
	Perpendicular to plane	$E_{90,mean}$	370	N/mm^2
Shear modulus	Out of plane	G_{mean}	690	N/mm^2
	Rolling shear	$G_{r,mean}$	50	N/mm^2

CROSS SECTIONAL VALUES

The basis of the limit state verification is the cross-sectional value calculations. CLT is usually treated as a panel strip when there is a dominating direction of loading. For the ultimate limit state verification, the net cross-sectional values may be analysed without considering shear flexibility. For the serviceability limit state, shear flexibility must be considered via multiple possible calculation methods for the effective cross-sectional values. Generally, in ultimate limit state procedures, the modulus of elasticity of the transverse boards to the fibre corresponding to the load direction is assumed as $E_{90} = 0$. Here, it is assumed that the cross-sections are symmetrical and the same material is used for all layers. This means that there is no difference in moduli of elasticity between the layers.

NET CROSS-SECTIONAL VALUES

Normal and shear stresses in CLT panels can be determined with the net cross-sectional values. Due to the orthogonal composition, these values have to be determined for the main span direction which is equal to the grain direction of the outer two layers and denoted with subscript 0. Analogously, the values can be calculated for the contrary direction. The described method only takes into account the contribution of the layers parallel to the main direction of loading. The parallel layers can be neglected because limited or no transfer of normal stresses can take place due to cracks and gaps in longitudinal direction within these layers. Moreover, the modulus of elasticity of the longitudinal direction is 30 times higher than the timber loaded perpendicular to the grain [3].

Calculating the net cross-sectional values with the described method can be done with the image and formulas below. Figure 2.8 shows the used designation and corresponding out of plane stresses.

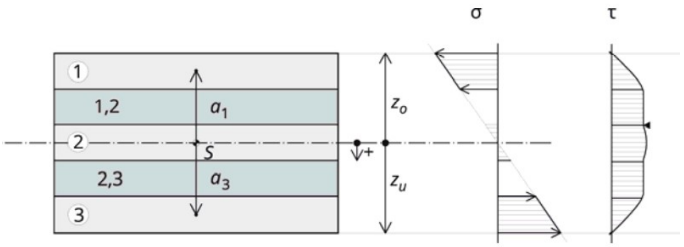

Figure 2.8: CLT cross section with out of plane stresses [23]

Area:

$$A_{0,net} = \sum_{i=1}^{n} b * h_i \tag{2.6}$$

Moment of inertia:

$$I_{0,net} = \sum_{i=1}^{n} (I_i + I_{i,Steiner}) = \sum_{i=1}^{n} (\frac{b * h_i^3}{12} + b * h_i * a_i^2) \tag{2.7}$$

Section modulus:

$$W_{0,net} = \frac{I_{0,net}}{z} \tag{2.8}$$

Static moment (rolling shear):

$$S_{0,net} = \sum_{i=1}^{m_L} b * h_i * a_i \tag{2.9}$$

where:

b = Width of the CLT panel (usually 1 meter)
h_i = Thickness of the boards in the layer parallel to the loading direction
a_i = Distance from centre of gravity to the middle of the considered layer
z = Distance from centre of gravity to the edge of the cross-section
n = Number of layers in longitudinal direction
m_L = Index of the longitudinal layer closest to the position of the centre of gravity as seen from the top edge

EFFECTIVE CROSS-SECTIONAL VALUES

In contrary to stress related calculations, the contribution of the transverse boards to deformations can not be neglected. To perform calculations on the out of plane deformations (including buckling), the effective moment of inertia should be used. These deformations of a CLT panel consists of pure bending and a shear portion due to rolling deformation in the transverse layers. This latter depends on the build-up of the cross-section and the element's slenderness. To include this shear deformation, there are three methods; the shear analogy method, the Timoshenko beam theory and the γ-method, [3].

The Timoshenko theory and shear analogy method are based on a shear reduction factor. It results in a separate calculation of bending and shear deformation. The γ-method is used in Eurocode 5 and is a commonly used method to calculate the effective cross-sectional value. A study which compared the three methods showed that all three methods are suitable for CLT and the differences are negligible when the length to thickness ratio is higher than 15, which is usual for engineering practices.[3]

The γ-method has the benefit that it allows the calculation to be through pure bending, in which shear flexibility is already included. That is why this method will be used in this research. The idea behind the

method is that the CLT section is considered as a mechanically jointed beam according to the Möhler theory. The transverse layers are modelled as equivalent joints between the layers in longitudinal direction. To determine the effective moment of inertia, the Steiner equation is used, where the longitudinal layers are reduced with a factor γ which accounts for the rolling shear flexibility in the transverse layers. The downside of this method is that γ depends on the length of an element. The formulas which are used are mentioned below for 3 and 5 layered CLT elements [23].

$$\gamma_i = \frac{1}{1 + \frac{\pi^2 * E_i * (b * h_i)}{L_i^2} * \frac{h_i}{G_r * b}} \tag{2.10}$$

$$I_{0,eff} = \sum_{i=1}^{n} (I_i + \gamma_i * I_{i,Steiner}) = \sum_{i=1}^{n} (\frac{b * h_i^3}{12} + \gamma_i + b * h_i * a_i^2) \tag{2.11}$$

where:

b = Width of the element (usually calculated for a 1m strip)
h_i = Height of longitudinal layer
l_i = Reference length of considered element
h = Thickness of intermediate layer (for a 3-layered element, h/2)
G_r = Rolling shear modulus of the intermediate layers
a_i = Distance from neutral axis of element to the middle of longitudinal layer
n = Number of layers in longitudinal direction

2.3.2. MODELLING OF CLT

Cross-laminated timber is an orthotropic material, meaning that it has different properties in the different directions, depending on the thickness, orientation, strength and number of layers. Modelling the layers individually is time-consuming and costly, therefore it is proposed to use an equivalent orthotropic shell element that is used to create a stiffness matrix, which subsequently can be inputted in the finite element models. The calculations are based on equivalent shear- and bending stiffness. Because the CLT panels will be used for stability as well, it is useful to incorporate shear deformations in the numerical analysis and therefore the Mindlin plate theory should be used [24]. The stiffness matrix is computed to describe the behaviour of CLT of various thicknesses and is shown in below.

$$M = \begin{bmatrix} D_{11} & D_{12} & 0 & 0 & 0 & 0 & 0 & 0 \\ D_{21} & D_{22} & 0 & 0 & 0 & 0 & 0 & 0 \\ 0 & 0 & D_{33} & 0 & 0 & 0 & 0 & 0 \\ 0 & 0 & 0 & D_{44} & 0 & 0 & 0 & 0 \\ 0 & 0 & 0 & 0 & D_{55} & 0 & 0 & 0 \\ 0 & 0 & 0 & 0 & 0 & D_{66} & 0 & 0 \\ 0 & 0 & 0 & 0 & 0 & 0 & D_{77} & 0 \\ 0 & 0 & 0 & 0 & 0 & 0 & 0 & D_{88} \end{bmatrix}$$

Determining the stiffness values given in the matrix can be done with the following formulas based on the code from Austria (ÖNORM B 1995-1-1) [23]. The Poisson's ratio v_{xy} and v_{yx} are assumed to be zero according to Aondio et al. [23] as if the boards are 'unglued'. Because CLT consists of a symmetrical build-up, the stiffness matrix can be reduced to a diagonal matrix, given the assumption that the Poisson's ratio is 0 in all directions. The diagonal terms can be calculated by the following formulas.

- Bending stiffness in the (main) x-direction $D_{11} = \frac{E_{0,mean} * I_{0,net}}{(1 - v_{xy} v_{yx})}$; in practice: $D_{11} = E_{0,mean} * I_{0,net}$
- Bending stiffness in the (secondary) y-direction $D_{22} = \frac{E_{0,mean} * I_{90,net}}{(1 - v_{xy} v_{yx})}$; in practice: $D_{22} = E_{0,mean} * I_{90,net}$

- Bending moment influenced by transverse strain: $D_{12} = D_{21} = \sqrt{\upsilon_{xy} * \upsilon_{yx} * D_{11} * D_{22}}$; in practice (no Poisson effects): $D_{12} = D_{21} = 0$
- Torsional twist: $D_{33} = k_{twist} * G_{0,mean} * \frac{b*d^3}{12}$
- Shear stiffness: $D_{44} = \frac{1}{\kappa_{0,z}} * G_{0,mean} * A_{0,net}$
- Shear stiffness: $D_{55} = \frac{1}{\kappa_{90,z}} * G_{0,mean} * A_{90,net}$
- Axial stiffness in plane: $D_{66} = \sum h_{i,0,net} * E_{0,mean}$
- Axial stiffness in plane: $D_{77} = \sum h_{j,90,net} * E_{90,mean}$
- Axial stiffness in plane $D_{88} = G_{0,mean} * d * K_{shear}$

where:

$E_{0,mean}$ = Mean elasticity modulus in the main bearing direction
$G_{0,mean}$ = Mean shear modulus in the main bearing direction
I = Moment of inertia of layer
υ_{xy},υ_{yx} = Poisson ratios
k_{twist} = reduction factor to torsional stiffness ($\approx 0,65$)
d = thickness of the CLT panel
b = Width of CLT element
$A_{0,net}$ = Net area in the main bearing direction
$A_{90,net}$ = Net area in the secondary bearing direction
K_{shear} = reduction factor for shear rigidity (=0,70)

$I_{0,net}$ = Net moment of inertia in the main bearing direction:

$$I_{0,net} = \sum \frac{E_i}{E_c} * \frac{b * d_i^3}{12} + \sum \frac{E_i}{E_c} * b * d_i * a_i^2 \tag{2.12}$$

$I_{90,net}$ = Net moment of inertia in the secondary bearing direction:

$$I_{90,net} = \sum \frac{E_i}{E_c} * \frac{b * d_i^3}{12} + \sum \frac{E_i}{E_c} * b * d_i * a_i^2 \tag{2.13}$$

where:

E_i = E-modulus of respective layer
E_i = reference E-modulus
b = width
d_i = thickness of respective layer
a_i = distance between centre of gravity of the whole panel and the layer

$\kappa_{0,z}$ = correction factor for shear

$$\kappa_{0,z} = \frac{\sum G * A}{(E * I_{0,net})^2} * \int \frac{[E_{(z)} * S_{(z)}]^2}{G_{(z)} * b} dz \tag{2.14}$$

Guideline values for CLT panels with standard slats of different thicknesses:
Type 3s: $0.15 \leq \kappa_o \leq 0.18$
Type 5s: $0.18 \leq \kappa_o \leq 0.20$
Type 7s: $0.25 \leq \kappa_o \leq 0.29$
Type 9s: $0.26 \leq \kappa_o \leq 0.29$

Guideline values for CLT panels with standard slats of equal thicknesses:
Type 3s: $\kappa_o = 0.21$
Type 5s: $\kappa_o = 0.24$
Type 7s: $\kappa_o = 0.26$
Type 9s: $\kappa_o = 0.27$

$\kappa_{90,z}$ = correction factor for shear

$$\kappa_{90,z} = \frac{\sum G * A}{(E * I_{90,net})^2} * \int \frac{[E_{(z)} * S_{(z)}]^2}{G_{(z)} * b} dz \tag{2.15}$$

Same guideline values as described above also apply here but for $\kappa_{90} = \frac{1}{\kappa_{90,z}}$

Special attention should be given to assigning the correct local coordinate system. The inputted stiffness matrix should correctly represent the material it is supposed to model. Figure 2.9 shows the intended directions and local coordinate system which coincides with the stiffness matrix.

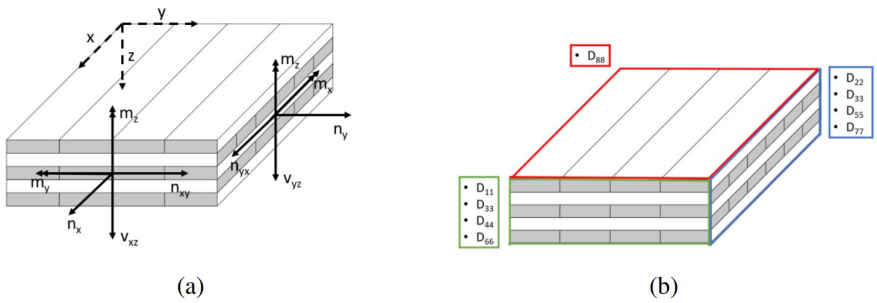

Figure 2.9: (a) Stiffness directions, (b)planes and directions corresponding to stiffness matrix [25]

The above explained calculation method of the stiffness matrix can be used for input of the required parameters. However, SCIA 22 has a built-in function that will calculate the stiffness matrix. Therefore, the only input parameters are the layer thickness, board width and the material properties.

2.4. CONNECTION TYPES

As discussed, connections in modular buildings play an important role. Different types of connections can be used for the intra- and inter-module connections. This section gives an overview of the possibilities.

2.4.1. INTRA-MODULE CONNECTIONS

Connections are critical in timber engineering, because they will in most cases govern the failure mode. Especially the displacement behaviour of the joints is important as they contribute a lot in the total displacement. There are multiple ways to connect timber elements, all having different displacement behaviour. Figure 2.10 gives an overview of this behaviour for the different connection types. It can be seen that glued joints are the most stiff, followed by notched joints. The downside of these joints is that they are difficult to assemble and therefore are not commonly used for timber modular buildings. Only mechanical joints, which have much less stiffness, are considered and discussed in this section.

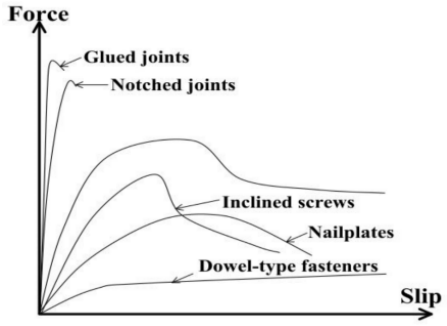

Figure 2.10: Slip of different timber-concrete connection types [26]

FASTENERS

Fastener connectors consist of bolts, screws, dowels and nails and are used to connect multiple timber elements. In this thesis, only screws will be used because of their favourable properties. Figure 2.11 shows a screw from Rothoblaas with dimensional parameters.

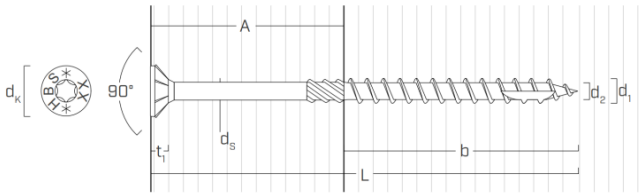

Figure 2.11: Dimensions of screw from Rothoblaas. [27]

STRENGTH

A screw can be loaded axially or laterally. For the lateral strength of connections with fasteners, Eurocode 5 can be consulted. There, equations for calculating characteristic load carrying capacity of fasteners according to the Johansen yield theory are provided. Three main parameters which influence the load carrying capacity of dowel type joints are the bending capacity, the embedding strength of the timber and the withdrawal strength of the dowel. This latter can be calculated according to the NEN-EN 1995-1-1:2005+A2:2014+NB:2013.

STIFFNESS

Next to load carrying capacity, the load deformation behaviour is important. The design equations for the slip and stiffness for fastener type connections are given in section 7.1 of Eurocode 5. However, these equations are very basic and based on a linear calculation. Therefore, next to equations from the Eurocode, experimental results should be considered.

For different type of fasteners, different equations should be used. For dowels, bolts and nails with predrilling the stiffness can be determined with: $K_{ser} = \frac{\rho^{1.5} * d}{23}$ and for nails without predrilling: $K_{ser} = \frac{\rho^{1.5} * d^{0.8}}{30}$. For connections with multiple fasteners the stiffness can be calculated with: $K_{ser} = \frac{n * \rho^{1.5} * d^{0.8}}{30}$ where d is the diameter of the fastener in mm, ρ_m is the average density of the secondary beam in kg/mm^3 and n is the number of fasteners. If the densities are different, the mean density can be calculated with $\rho_m = \sqrt{\rho_{m1} * \rho_{m2}}$. When timber to steel or concrete connections are considered, the density of the timber should be multiplied with 2.

Important to note is that the equations are an estimation of the real load-displacement behaviour. In Figure 2.12 two graphs with the real load deformation behaviour of timber connections is shown. An initial deformation (slip) is followed by linear load-deformation and non-linear load-deformation [28].

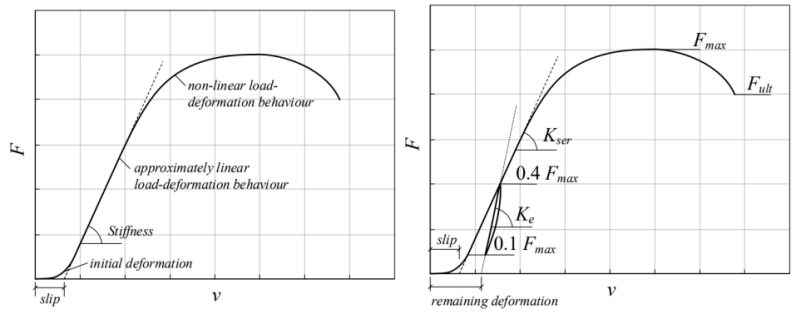

Figure 2.12: Characteristics of the load-displacement graph of the connection [28]

PERFORMANCE OF SCREWED JOINT ASSEMBLY

To be able to model the screwed connections, the capacities in terms of strength and stiffness have to be known. Experiments on the axial and lateral behaviour of self-tapping screws have been done by Flatscher et al. [29] which focused also on different screw angles, as can be seen in Figure 2.13. The test results showed a higher stiffness and strength for the axially loaded screw in comparison with the lateral loaded screw for an angle of 90 degrees. To overcome the relatively low properties for the lateral loaded screws an inclination of 45 degrees can be used for the screw to increase the strength and stiffness, seen in table 2.2

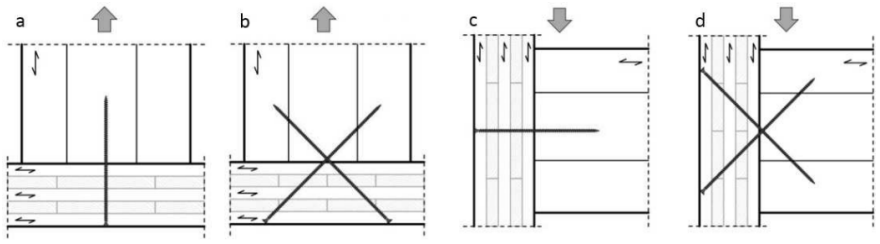

Figure 2.13: Tested connection setups [29]

Table 2.2: Results of tested setups [29]

Setup		**Screw angle**	F_{max} **[kN]**	K_{ser} **[kN/mm]**
Axial	a	90	20,8	17,6
	b	45 (per pair)	33,6	16,6
Lateral	c	90	10,3	0,5
	d	45 (per pair)	30,0	19,9

ANGLE BRACKETS AND HOLD-DOWNS

Another possibility to connect two timber elements is with angle brackets and hold-downs, as shown in Figure 2.14. Both of these connectors are designed to connect the walls to the floors below, but hold downs have as primary function to withstand the rocking behaviour and thus tensile forces, while angle brackets should resist sliding and thus shear forces. However, angle brackets can resist tensile forces and help to withstand rocking, but their contribution is often neglected [30]. The mechanical connectors are placed with screws or nails. The mechanical behaviour depends on the dimensions of the metal plates but also on the grain direction of the timber. Because this is difficult to capture in equations, the strength and stiffness are determined with experimental tests.

Experiments on angle brackets and hold-downs are done by Shahnewaz et al. [31]. The study investigated the strength and stiffness of a steel bracket with dimensions 90 x 48 x 116 mm fastened with

different type and number of fasteners. Next to the angle brackets, two hold-downs are investigated, a HTT16 and HTT22 with 9 and 12 fasteners respectively. In case of the angle-brackets, both shear and tension tests were performed, whereas the hold-downs were only tested in tension. Table 2.3 shows the strength and stiffness results of the tests. Larger metal brackets can be used to when higher strength and stiffness are required.

Table 2.3: CLT connections with strength and stiffness [31]

Connection type	ID	Fasteners	Type of test	Strength P_y [kN]	Stiffness K_e [kN/mm]	Type of test	Strength P_y [kN]	Stiffness K_e [kN/mm]
Angle bracket 90 x 48 x 116 mm	B1	18 16d SN 3.9 x 89 mm	Tension	45,5	6,6	Shear	38,1	5,0
	B2	18 SFS screw 4 x 70 mm		48,0	5,9		50,0	5,9
	B3	10 SFS screw 5 x 70 mm		37,3	4,8		43,0	4,2
	B4	12 RN 3.8 x 76 mm		35,2	7,7		37,3	5,6
	B5	11 RN 4 x 60 mm		20,2	2,5		23,9	2,2
Hold-down HTT16	HD1	9 RN 3 x 60 mm		32,4	2,5	-	-	-
Hold-down HTT22	HD2	12 RN 4 x 60 mm		41,8	4,9		-	-

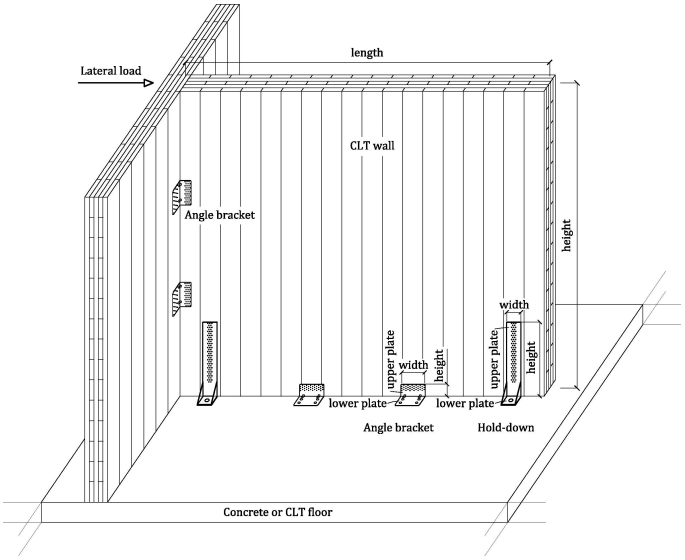

Figure 2.14: Angle brackets and hold downs [30]

2.4.2. INTER-MODULE CONNECTIONS

Inter-module connections connect modules to each other, either vertically or horizontally. For both cases, the often used connection types are discussed.

VERTICAL COUPLING

Tensile connections, where high forces should be transferred, can be designed with metal plates. These plates can connect two inter-storey timber elements and prevent uplift generated by the rotation of the wall (see Figure 2.15). It is mostly used in platform-type construction but can also be used in balloon-type construction. Multiple sizes and thickness can be selected depending on the resulting force that has to be transferred. The plates are attached to the timber by screws and for acoustic damping bearing strips can be placed [32].

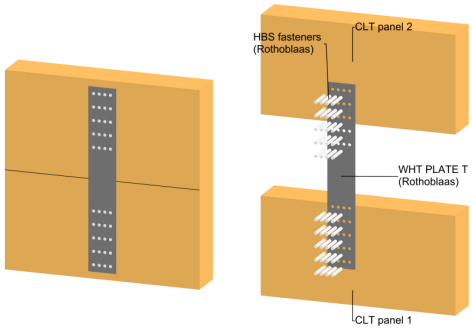

Figure 2.15: Steel WHT plate for timber-to-timber connection [27]

Table 2.4 shows strength and stiffness properties of the connection. The stiffness is based on an assumption related to hold-down connectors of Rothoblaas and the equation for coupled nails.

Table 2.4: Properties of the WHT Rothoblaas plate [27]

Type	**Fasteners**	**d x L [mm]**	**nv1 [pcs]**	**nv2 [pcs]**	$R_{1,k,timber}$ **[kN]**	$R_{1,k,steel}$ **[kN]**	K_{ser} **[kN/mm]**
WHTPT720	HBS	8 x 100	28	28	115,8	135.9	21.2
WHTPT720	HBS	8 x 100	40	40	176,1	206.6	30.3

HORIZONTAL COUPLING

Horizontal coupling is necessary to create the diaphragm action for transferring horizontal loads to vertical stability elements. Connecting two modules can be done in multiple ways. One of the options is by a metal plate as discussed previously, but acoustic damping should be considered. Therefore, a horizontal anchor (Straviwood Modulink) is designed by Delta-L which acoustically uncouples the modules (see Figure 2.16). The Straviwood ModuLink is constructed from two steel profiles (electro-galvanized) that are acoustically decoupled from each other by means of a natural rubber or polyurethane foam. The anchors are prefabricated and pre-stressed and only need to be screwed on location [33].

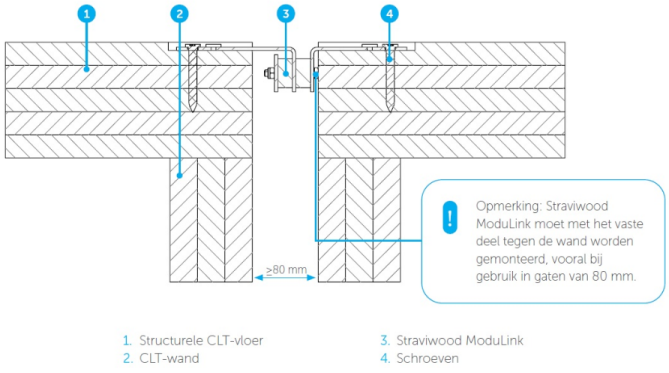

Figure 2.16: Acoustic anchor Straviwood Modulink [33]

3

Lateral deformation of modular buildings

Horizontal load acting on a building causes the building to deform. To prevent the structure from excessive deflections, the lateral stability of the structure should be provided. In modular construction, the lateral stability can be provided by an external stability system (in the form of a core or bracing system) or by the modules themselves (with shear walls). Next to the structural system, there are several factors that influence the lateral stability of modular buildings. The inter- and intra-connections should allow the structure to act as a unified system. The foundation needs to prevent the building from rotating. Geometry and layout of the building has effect on the position and orientation of the stability elements. All these factors together determine how the lateral stability of a modular building is provided and how much the building will deform. This chapter will discuss the lateral stability and deformation of modular buildings. First, the different lateral load resisting systems are described in Chapter 3.1, followed Chapter 3.2 that goes into more detail about self-supporting modular buildings. Chapter 3.3 discusses the differences between the deformation of modular buildings and conventional buildings. Subsequently, Chapter 3.4 discusses the lateral deformation terms of multi-storey modular buildings. Chapter 3.5 describes the load acting on the structure. At the end, Chapter 3.6 elaborates on the requirements of the building codes.

3.1. LATERAL LOAD RESISTING SYSTEMS

When modules are stacked on top of each other, multi-storey modular buildings are created. When the height of the multi-storey buildings increase, the wind load increases as well, resulting in higher horizontal impact on the building causing the danger of overturning. The overall stability should be checked to see if there is a risk of overturning. This risk is especially a problem in lightweight structures such as timber buildings. Next to preventing overturning, the deflection of the building should be kept under certain limits. This can be done by stabilizing the building with for example a core, a bracing system or shear walls. These three options are the most common and are briefly discussed below. Because, this research focuses on self-supporting modular buildings with volumetric modules, the shear walls are discussed more thoroughly in the next section.

3.1.1. CORE

The most used stability system is a core. This is a stiff and strong part of the building, where the lifts and staircases are located. Because that part has a regular shape and is relatively closed, the walls can carry high forces to the foundation. It is especially used in high-rise modular buildings where the modules themselves can not provide the stability. Often, corner-supported modules are used in combination with a core. The horizontal forces are transferred from the facade to the core and subsequently to the

foundation. The vertical forces are transferred directly through the modules. Although this system allows for high-rise buildings to be stable, the downside is that the concrete core has to be constructed on site, reducing time efficiency drastically. The benefits of modular construction do not come forward this way.

3.1.2. BRACING SYSTEM

Another possible stability system is a bracing system. Here, the modules are placed in a framework that is kept stable with braces. The modules themselves do not contribute in the horizontal force transfer. In contrary to the core system, the bracing system can be realized by attaching modular elements on site, but this will take extra time and the system does only apply to low-rise buildings.

3.1.3. SHEAR WALLS

When the stability has to come from the modules themselves, shear walls are used. They are placed inside the module and can have different configurations. The side walls provide stability in longitudinal direction and the internally placed shear wall in transverse direction.

3.2. SELF-SUPPORTING MODULAR BUILDINGS

Most multi-storey modular buildings found around the world are assemblies of corner-supported modules connected to a cast in situ concrete core. Although this is an effective method, it does not characterize the structures as purely modular nor provide them with the benefits of modular construction. Besides, the external stability elements would be made of traditional materials, reducing the sustainability of the project [34]. If external stabilizing elements are therefore not desired, the modules should provide the stability themselves. This is possible, but requires the modules to be designed in such a way that horizontal forces can be transferred to the foundation. This is done by the floors and shear walls of the modules in such a way that the lateral load is transferred through the floors by diaphragm action to the shear wall, which bring the force downwards via the other shear walls. When carrying the load, the shear walls deform under the horizontal load. This will cause lateral displacement and rotation of the modules.

3.2.1. SHEAR WALL DEFORMATION

Cross-laminated timber is well suited as a shear wall, due to its high strength and stiffness. It has large capacities to provide the lateral stability of a module. In such a module, the shear wall is responsible for the horizontal displacement caused by horizontal loads. In general, there are four shear wall deformation contributions [35] as can be seen in figure 3.1. The total displacement at the top is the sum of the bending (Δ_B), shear (Δ_S), translation (Δ_T) and rotation (Δ_R) deformation. Equations 3.1-3.4 show how these terms can be calculated. The bending and shear deformation is a result of the CLT plate itself, while the translation and rotation are caused by the connections.

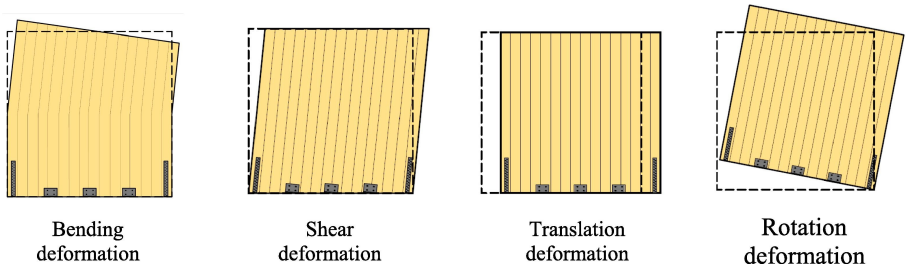

Figure 3.1: Illustration of the different deformation contributions of a shear wall [35]

Determining the strength and stiffness values of CLT shear walls can be done with analytical calculations. In the literature, several calculation methods are identified to calculate these values [35]. Common for the strength calculation methods is that they assume a rigid CLT panel and thus neglecting

bending and shear and that the calculations are based on static equilibrium equations. For the strength of the shear wall, it means that the load carrying capacity F can be simplified as $F = min(F_r; F_t)$. Since this chapter focuses on the lateral stability, the stiffness assessment of CLT shear walls is important. The stiffness can be determined from the load-displacement relation. With the maximum force acting on the wall and knowing the stiffness of the connections, the corresponding displacement can be calculated resulting in the stiffness. Simple hand calculations of the displacement can be done in five ways [35]. One of the methods is presented by Wallner-Novak et al. [23] and takes into account a reduced flexural stiffness and a 25% reduction of the shear modulus. The equations for calculating the deformations are presented below. It must be noted that the translation and rotation equations only hold for hold-down and angle-bracket connections, but the principle can also be used for other type of connections such as screws.

$$\Delta_B = \frac{F * h^3}{3 * EI_{ef}} \tag{3.1}$$

$$\Delta_S = \frac{F * h}{GA} \tag{3.2}$$

$$\Delta_T = \frac{F}{k^H} \tag{3.3}$$

$$\Delta_R = (\frac{F * h}{w} - \frac{q * w}{2}) * \frac{h}{w * k^V} \tag{3.4}$$

where:

F = the horizontal load

h = the height of the shear wall

k^H_{conn} = the horizontal stiffness of the connection

k^V_{conn} = the vertical stiffness of the connection

w = the width of the shear wall

EI_{ef} = the effective flexural stiffness:$(EI)_{ef} = E_0 * (t_{ef} * w^3)/12$ where t_{ef} is the thickness of the vertical layers

GA = the shear stiffness: $GA = (0.75 * G) * (t * w)$

Although these mechanisms interact at a certain degree, this can be ignored and the shear wall can be idealised as four springs in series: one for each mechanism. The total displacement Δ_{total} can be calculated by adding the individual deflection as shown in the equation below.

$$\Delta_{total} = \Delta_{Bending} + \Delta_{Shear} + \Delta_{Translation} + \Delta_{Rotation} \tag{3.5}$$

The total stiffness of the shear wall k_{total} can be calculated as follows:

$$k_{total} = \frac{1}{\frac{1}{k_{bending}} + \frac{1}{k_{shear}} + \frac{1}{k_{translation}} + \frac{1}{k_{rotation}}} \tag{3.6}$$

3.2.2. DIAPHRAGMS

Horizontal wind loads should be transferred to the vertical stability elements to bring the forces to the foundation. This transfer is done by diaphragm action of the horizontal elements that act as a diaphragm. In modular buildings, this diaphragm consists of the ceilings together with the horizontal inter-module connections. Figure 3.2a provides a schematic overview of a diaphragm connected to two shear walls. The acting horizontal load is transferred by the diaphragm to the two shear walls. Figure 3.2b shows how this causes the structure to displace.

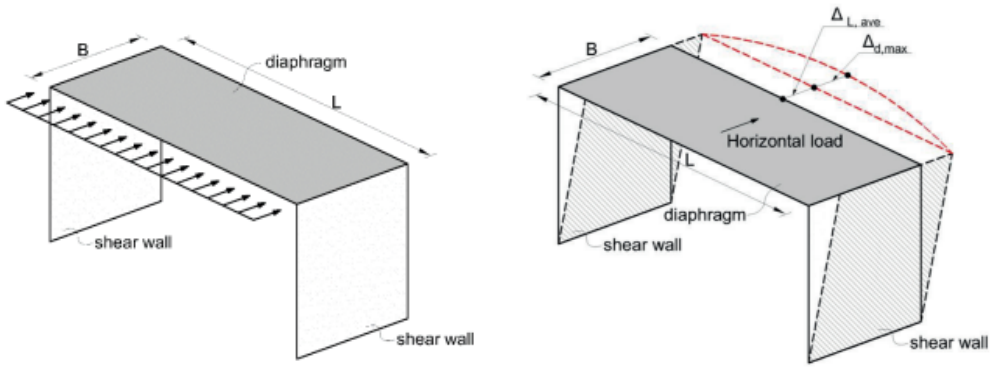

(a) Floor diaphragm

(b) Diaphragm displacement

Figure 3.2: Diaphragm action [20]

Depending on the stiffness of the roofs and connections, the diaphragm can act as rigid or flexible. This depends on the maximum in-plane deformation of the floor diaphragm ($\Delta_{d,max}$) and the average inter-storey drift ($\Delta_{L,ave}$), which are displayed in figure3.2b. Often, CLT diaphragms are considered as rigid concerning the shear walls, but if the deflection is 1.1 times the average inter-storey drift they should be considered flexible [20]. The panel and connection stiffness k_{panel} and k_c influence the total diaphragm stiffness and can be calculated as follows:

$$k_{panel} = \frac{F}{\Delta_{d,max}} \tag{3.7}$$

$$k_c = \frac{F}{2 * \Delta_{con}} \tag{3.8}$$

$$k_{diaphragm} = \frac{1}{\frac{1}{k_{panel}} + \frac{1}{k_c}} \tag{3.9}$$

3.3. MODULAR BUILDINGS VERSUS CONVENTIONAL BUILDINGS

Modular buildings with shear walls have the deformation behaviour of a combination between a pure bending and pure shear beam. The side walls in combination with the floor and ceiling creates a frame which would deform due to shear. The shear wall inside a module experiences both shear and bending deformation as explained before, but also compression at the supports, which will be discussed in chapter 4.3. Because the shear walls are not continuous, they can not act as one stiff shear wall. Normally, high shear walls have mainly bending deformation, but in this case that does not apply.

Besides, the difference between traditional and modular buildings is in the internal force distribution. The main reason can be attributed to the existence of inter-module connections, leading to a different frame design. For conventional frames with a "single-beam and single-column" configuration in the connection zone, releasing the rotational restraint to the upper column would result in bending

moments being transferred only between the beam and the lower column. In this situation, the bending moment in the lower part of the upper column will be lower. In contrary, modular frames have a "double-beam and double-column" configuration in the connection zone. Here the module columns extend to the connection zone for the end-to-end connection and they are also connected with the floor and ceiling of the modules. Therefore, when releasing the rotational constraint to the upper module, bending moments at the bottom of the upper module will still exist due to the restraint provided by the floor beams [36].

Even though the system is more complex than traditional buildings, summation of the individual deformation mechanisms results in the prediction of the lateral displacement.

3.4. LATERAL DEFLECTION OF MODULAR BUILDINGS

The module deformation mechanisms, as described, can be extended to calculate the deflection of multi-storey modular buildings. The total deflection is the sum of all the individual components. However, the cumulative effect has to be incorporated in some of the deflection mechanisms. This effect and the method to calculate the total deflection of multi-storey modular buildings is explained on the basis of a six-storey modular building. The bending and shear deformations are dependent on the module design, while the rotational and translational deformation depend on the inter-module connections. Figure 3.3 shows for the six-storey building how the inter-storey drift and the cumulative effect result in the total deflection. The cumulative effect is the displacement that is induced by the horizontal rotation of lower storeys. This rotation causes the module to stand at an angle θ. The angle theta times the height gives the cumulative effect. Because every storey has its own rotation, the displacement due to the tilt of these storeys should be accumulated to obtain the total storey cumulative displacement.

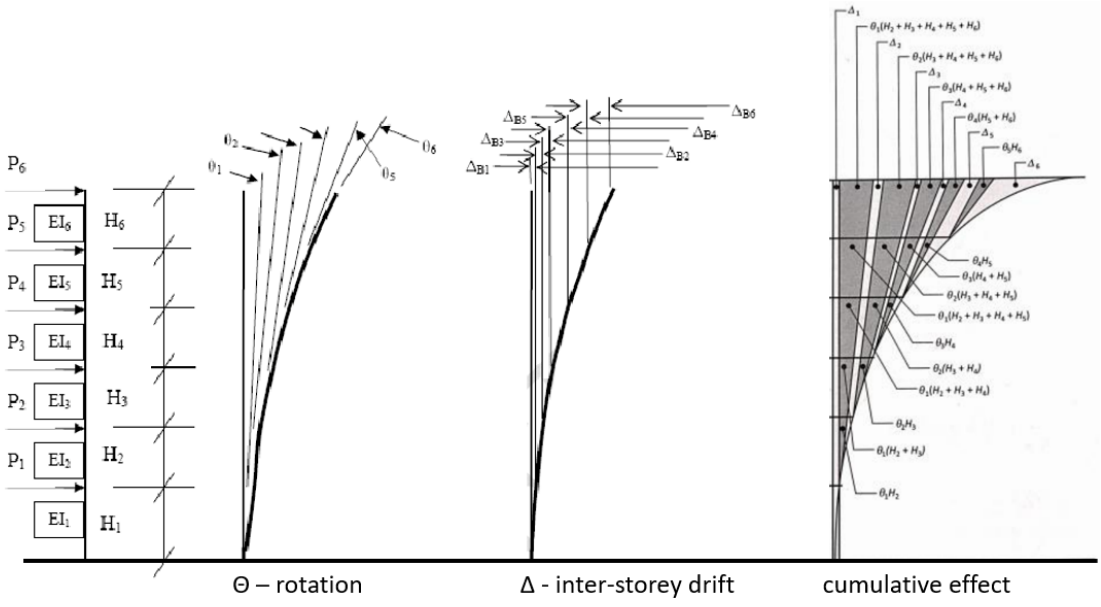

Figure 3.3: Bending deformation with cumulative effect of a modular building [37][38] (adjusted)

The total inter-storey drift Δ_i^{total} is:

$$\Delta_i^{total} = \sum_{j=1}^{i} \Delta_i^{storey} \tag{3.10}$$

where:

Δ_i^{total} = the total deflection at the i-th level
Δ_i^{storey} = the inter-storey drift at the i-th level

The inter-storey drift Δ_j^{storey} is expressed as:

$$\Delta_i^{storey} = \Delta_{S,i}^{storey} + \Delta_{B,i}^{storey} + \Delta_{R,i}^{storey} + \Delta_{T,i}^{storey} \tag{3.11}$$

where:
$\Delta_{S,i}^{storey}$ = the inter-storey drift at the i-th level due to shear
$\Delta_{B,i}^{storey}$ = the inter-storey drift at the i-th level due to bending
$\Delta_{R,i}^{storey}$ = the inter-storey drift at the i-th level due to rotation
$\Delta_{T,i}^{storey}$ = the inter-storey drift at the i-th level due to translation

3.4.1. FORCE DISTRIBUTION

Before looking at the deflection components, the shear force and bending moment in the structure is determined, see Figure 3.4. The external horizontal load is modelled as point loads acting at the top of the storey, representing the wind load that acts on the building.

The shear force V_i at the i-th storey is the sum of the applied horizontal force of the above storeys [37]. m is the number of storeys.

$$V_i = \sum_i^m P_i \tag{3.12}$$

The bending moment M_i is the sum of the shear force V_i times the height of storey H_{i+1} [37].

$$M_i = \sum_i^m (V_i * H_{i+1}) \tag{3.13}$$

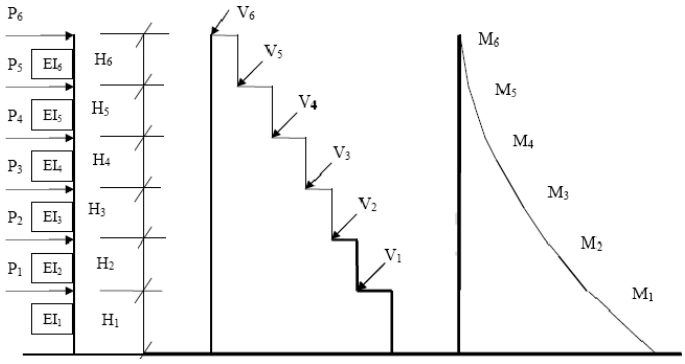

Figure 3.4: Shear force and bending moment distribution in a multi-storey modular building [37]

3.4.2. DEFLECTION DUE TO SHEAR

For the shear deflection there is no cumulative effect in multi-storey modular buildings, therefore the total deflection is the sum of the individual deflections as is shown in Figure 3.5.

$$\Delta_{S,i}^{storey} = \Delta_{S,i} \tag{3.14}$$

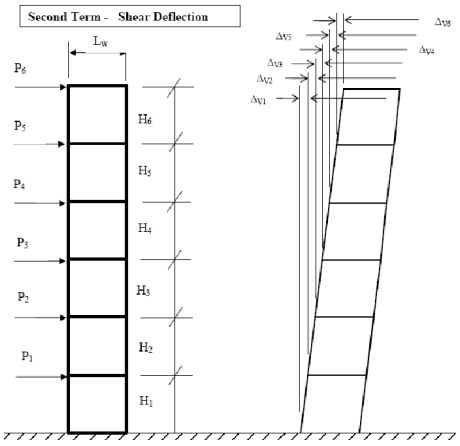

Figure 3.5: Deflection due to shear [37]

3.4.3. DEFLECTION DUE TO BENDING

Deformation due to bending moments at the i-th level causes a horizontal displacement and rotation. The rotation leads to the cumulative effect. This effect should be accounted for in the total deformation. Therefore, the deflection of the i-th storey is the bending of the module plus the cumulative effect due to rotation of the bottom levels. This is visualized in Figure 3.3.

$$\Delta_{B,i}^{storey} = \Delta_{B,i} + H_i(\sum_{j=1}^{i-1} \theta_j) = \Delta_{B,i} + H_i(\theta_1 + \theta_2 + ... + \theta_{i-1}) \tag{3.15}$$

where:

$\Delta_{B,i}$ = the deflection of the module

H_i = the storey height

θ_j = the total deflection due to the cumulative effect

3.4.4. DEFLECTION DUE TO ROTATION

Similar to bending, the rotation at lower levels due to elongation of the vertical inter-module connection causes cumulative deflection at top levels as follows:

$$\Delta_{R,i}^{storey} = H_i(\sum_{j=1}^{i} \alpha_j) = H_i\alpha_i + H_i(\sum_{j=1}^{i-1} \alpha_j) \tag{3.16}$$

with:

$$\alpha_j = \frac{\Delta_{ar,j}}{L_w} \tag{3.17}$$

where:

$\Delta_{ar,j}$ = the total vertical elongation of the connection

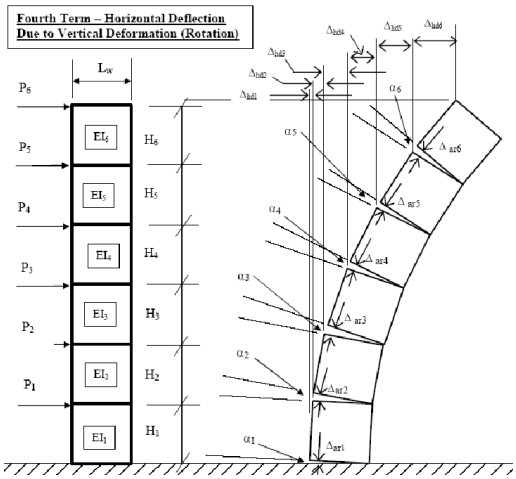

Figure 3.6: Rotation deformation of a modular building [37]

3.4.5. DEFLECTION DUE TO TRANSLATION

The translation of the modules does not have a cumulative effect in multi-storey buildings, therefore the total deflection is the sum of the individual deflections (see Figure 3.7).

$$\Delta_{T.i}^{storey} = \Delta_{T,i} \tag{3.18}$$

With:

$$\Delta_{T,i} = \frac{V_i}{k} \tag{3.19}$$

where:

V_i = the shear force at the storey i

k = the stiffness of the inter module connections

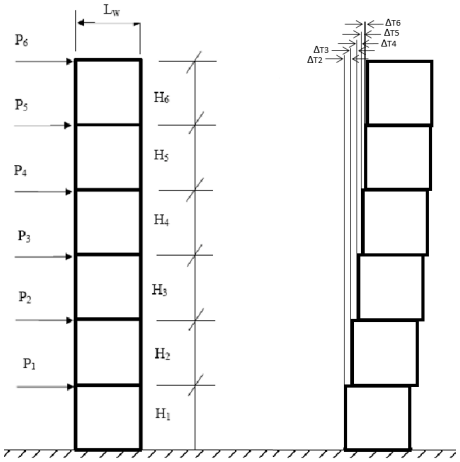

Figure 3.7: Translation deformation of a modular building [37]

3.4.6. DEFLECTION DUE TO ROTATION OF THE FOUNDATION

In addition to the described deformation mechanisms, there is another effect that has to be taken into account when determining the total building deflection. The rotation of the foundation due to horizontal loading leads to a deflection along the height of the building. Although the detailed calculation is outside the scope of this research, the deflection should be included when checking for the Serviceability Limit State (SLS). The total deflection at the i-th storey is the rotation times the height to storey i:

$$\Delta_{F,i}^{storey} = \phi_F * i * H \tag{3.20}$$

where:

ϕ_F = the rotation of the foundation

H = the storey height, assuming H is equal for all storeys

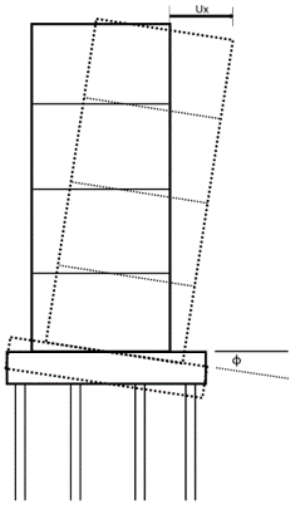

Figure 3.8: Rotation of the foundation due to horizontal loads

3.4.7. TOTAL DEFLECTION

The total deflection is the sum of the individual storey deflection and the cumulative effect. The total displacement Δ_i^{storey} can be calculated as follows:

$$\Delta_i^{storey} = \Delta_i + H_i(\sum_{j=1}^{i-1} \theta_j) = \Delta_i + H_i(\theta_1 + \theta_2 + ... + \theta_{i-1}) \tag{3.21}$$

where:

Δ_i = the storey deflection

H_i = the storey height

θ_i = the storey rotation

3.5. LOADING

The load that acts on a modular building is described in this section. Some are only quantitative described, because they are not considered in this research, and other qualitative.

3.5.1. WIND LOAD

The wind load acting on a building can be determined following NEN-EN 1994-1-4. The load depends on the height of the building, which in modular buildings is related to the number of stacked modules. The wind force acting on a building can be determined with equation 5.4 in section 5.3 of the NEN-EN 1991-1-4:

$$F_w = c_s c_d * c_f * q_p(z) * A_{ref} \tag{3.22}$$

where:

$c_s c_d$ = the structural factor
c_f = the force coefficient
$q_P(z)$ = the peak velocity wind pressure at height z
A_{ref} = the reference area

For the distribution of the wind force, three cases can be distinguished depending on the dimensions of the building as illustrated in Figure 3.9:

1. Building height smaller or equal to the building width: Uniform wind pressure along the building.
2. Building height between one and two times the building width: Wind pressure is divided into two blocks.
3. Building taller than two times the width: Wind pressure is divided into three blocks.

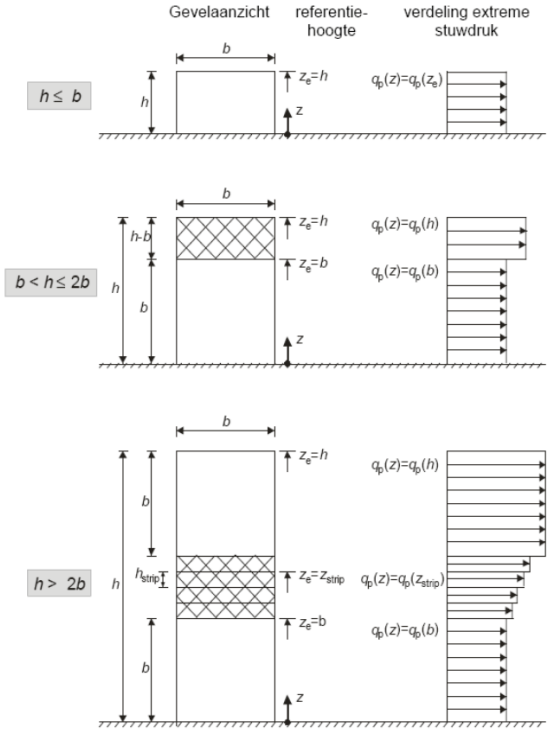

Figure 3.9: Wind pressure distribution over the building height following the Eurocode EN 1991-1-4

3.5.2. GRAVITY LOAD

Gravity loads are forces that act downwards on a structure. They are categorized into dead and live loads. Dead load is the weight of the structural components themselves and are permanent live loads

are variable loads and depend on the intended use of the buildings. The magnitude is guided by building codes, which also provide information for the snow load.

3.5.3. NOTIONAL LOADS

The initial eccentricities due to installation tolerances of modular buildings are shown in Figure 3.10. These tolerances are significantly important for the overall performance of the structure and differ from conventional buildings. When designing with this method, the effects of construction tolerances should be accounted. Both the tolerances which occur due to manufacturing of a single module and the misalignment during placing of the modules in their final position are contributing to the total imperfections. The maximum tolerances which are allowed are based on the Eurocode for steel and aluminium structures (EN 1090-2). For a large number of modules, the average allowable manufacture imperfection is taken as h/1000 resulting in a total error for n number of floor of n*h/1000 [39].

During installation of the modules, errors can occur when placing them in the right position. Misalignment may arise when stacking the modules. The cumulative allowable error should be limited to 5 mm per module. According to Lawson and Richardson [39] it is recommended to limit the total out of verticality to 80 mm for 10 or more modules.

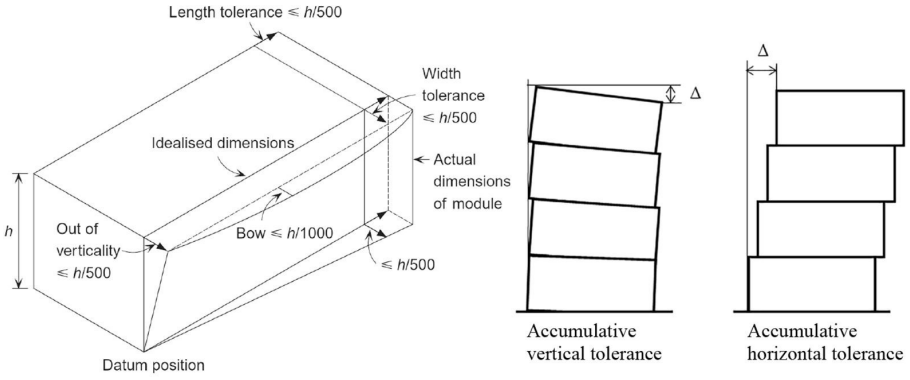

(a) Single module (b) Entire building

Figure 3.10: Construction tolerances of modular buildings [1]

The above-mentioned tolerances cause eccentricities may lead to additional horizontal forces. When the vertical force is due to misalignment applied with eccentricity, moments occur which result in these additional horizontal forces. When the side walls are unable to resist these bending moments, the ceiling, floor and shear wall have to take these extra forces by shear force. To calculate these additional moments that act on the base of the module, Lawson et al. [1] came up with a good approximation for the effective eccentricity of a vertical group of modules:

$$\Delta_{eff} = 3 * n^{1.5} \tag{3.23}$$

The following equation can be used to convert this eccentricity to a horizontal force that acts on each floor level:

$$F = 0.2 * n^{0.5} \tag{3.24}$$

This notional force is expressed as a percentage of the factored vertical load of a module and varies between 0.5% and 0.8% for 6 and 16 storeys respectively. These additional horizontal loads should be applied in combination with wind loading.

3.5.4. SECOND-ORDER EFFECT

The second-order effect results from deformations caused by horizontal loads like wind and notional forces. It occurs when a structure experiences a displacement in horizontal direction which has the effect that the centre of gravity will shift respectively to the structure. Therefore, the shift and vertical force will cause a bending moment, resulting in additional horizontal displacement. Usually these phenomena may be neglected due to small effects, but sometimes can cause failure.

Calculations can be done to check whether a structure is vulnerable to second-order effects. This is called the critical loading method, where the stabilizing elements are modelled as a column with a certain bending and shear stiffness uniform over the building height and a rotational spring at the base (Figure 3.11). Generally, the second-order effect is composed of three displacement components, which are also shown in Figure 3.11.

$$y_{bending} = \frac{q * l^4}{8 * EI} \tag{3.25}$$

$$y_{shear} = \frac{q * l^2}{2 * GA} \tag{3.26}$$

$$y_{foundation} = \frac{q * l^3}{2 * C} \tag{3.27}$$

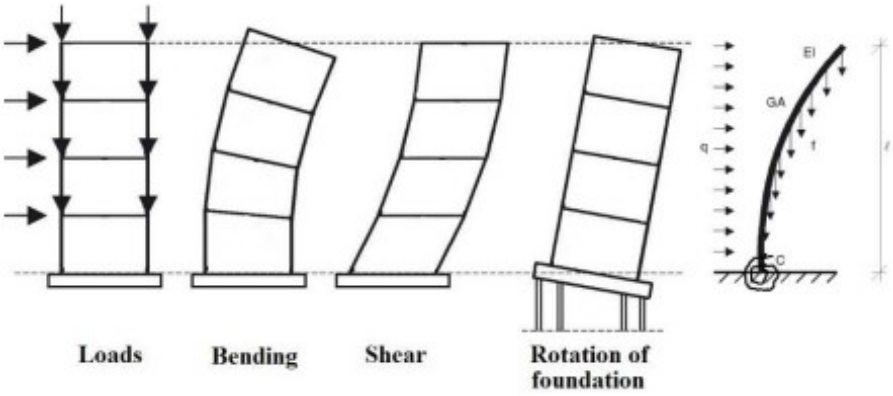

Figure 3.11: Displacement components [3]

When evaluating a structure for the susceptibility to second-order effects, the critical buckling load of the modelled column is calculated. This is done by determining the stiffnesses which corresponds to the displacement components as discussed above. The next equation can be used:

$$\frac{1}{P_{cr}} = \frac{1}{P_{cr,b}} + \frac{1}{P_{cr,s}} + \frac{1}{P_{cr,f}} = \frac{1}{\frac{7.837}{L^2}} + \frac{1}{2GA} + \frac{1}{\frac{2C}{L}} \tag{3.28}$$

Dividing the critical buckling load with the total vertical load belonging to the stabilizing element will result in a ratio n and using this factor n for the magnification factor for the second order effects:

$$n = \frac{F_{cr}}{F} \tag{3.29}$$

$$\frac{n}{n-1} \tag{3.30}$$

Eurocode 2 for concrete describes in art. 5.8.2 that the second order effects can be neglected if it is less than 10% of the corresponding first order effects. When the second-order effects are significant, the effects have to be incorporated in the Ultimate Limit State (ULS) and Serviceability Limit State (SLS) calculations via additional horizontal forces. In this study, only the deformation of the module itself is considered.

3.6. CODE REQUIREMENTS

The total horizontal deflection at the top of the building is caused by several mechanisms that were explained in this chapter. All the contribution must be added up to obtain the total displacement that can be checked for building code compliance. The national codes and Eurocodes recommend a maximum horizontal displacement. This is because non-structural elements such as cladding or windows can be damaged if the movements are too large. Also, displacements should be kept low for users comfort. At the same time, the second order effect can become too large if displacements become large. Therefore, engineers must make sure the building is sufficient stiff to full-fill the requirements. According to the Eurocode, the maximum horizontal displacement of a building is H/500 and for a storey h/300, H and h being the height of the building and storey respectively. The inter-storey displacement is shown in Figure 3.12.

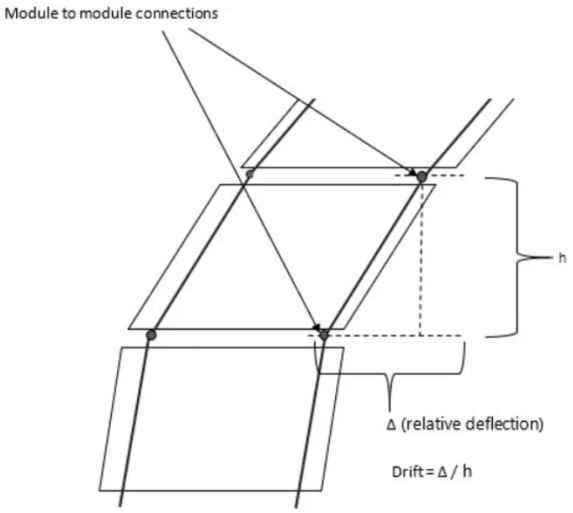

Figure 3.12: Inter-storey drift [40]

4

Design and modelling of individual modules

With the understanding of the deformation mechanisms of modular buildings and the knowledge on modular construction, the focus will be on the research part. The first step is to focus on the individual modules. Designing the module is an important step in the process, as it influences the building layout and overall performance of the structure. Especially for lateral deformation, structural design choices have a significant influence on the total lateral deflection. In the longitudinal direction, the side walls provide sufficient stiffness to limit these deflections. However, due to the limited available length for the transverse shear wall, lateral stability in transverse direction is a critical aspect. This shear wall is located inside the module, meaning that it affects the floor plan of the module and therefore the architectural freedom of the building layout.

This chapter focuses on the individual module configurations and design, as well as the deformation calculation and numerical modelling. General applicable module configurations are determined in Chapter 4.1, after which Chapter 4.2 describes the module design. Hereafter, Chapter 4.3 discusses the deformation calculation of a module and the problems that occur with the superposition principle. Finally, the numerical modelling approach is explained in Chapter 4.4.

4.1. Module configurations

In this study, equations for the transverse deflection of four different module configurations will be proposed. The transverse direction is the direction of the shorter side. The module configurations are based on commonly used designs and dimensions and differ in the design of the transverse shear wall. The four configurations are shown in Figure 4.1, with the shear wall displayed in dark brown. Module 0 is chosen as the basic module. Although it is not very applicable in practice due to the lack of openings, it is still considered because it allows for hand calculations for verification purposes. The presented dimensions of the shear walls in Figure 4.1 show the values for the standard module width of 3.5 m. The standard dimensions will be elaborated in the next section. As mentioned, the modules vary in the setup of the shear wall. The module configurations are briefly described:

- Module 0 (M0): Module with a fully closed shear wall
- Module 1 (M1): Module with a shear wall with a door opening in the middle
- Module 2 (M2): Module with a shear wall with an opening at one side
- Module 3 (M3): Module with half a shear wall

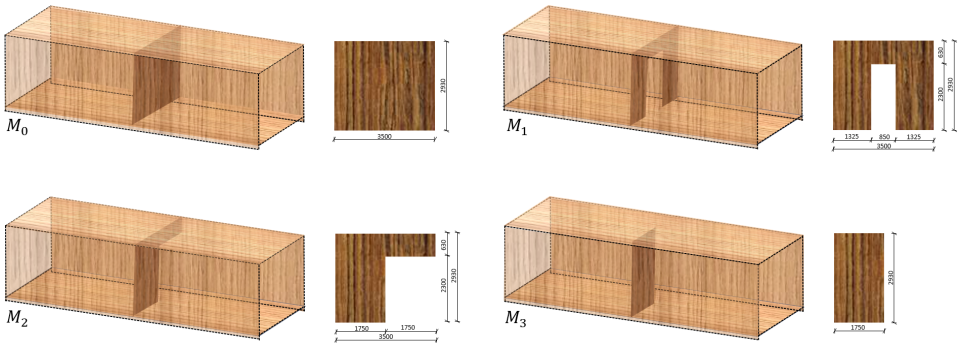

Figure 4.1: Design of the four module configurations: M0-M3

4.2. MODULE DESIGN

This section describes the design of the modules, focusing on their global dimensions and CLT elements. The description is done for the basic module (module 0), but applies to all configurations. Figure 4.2 shows a 3D view of module 0, with the parameters for length, width and height. In the figure, the longitudinal and transverse direction are indicated. In this research, standard dimension are considered and are 12, 3.5 and 3.1m for the length, width and height respectively. These dimensions are referred to as the 'standard' dimensions and will be used across the study. The corresponding dimensions of the shear wall configurations are given in Figure 4.1.

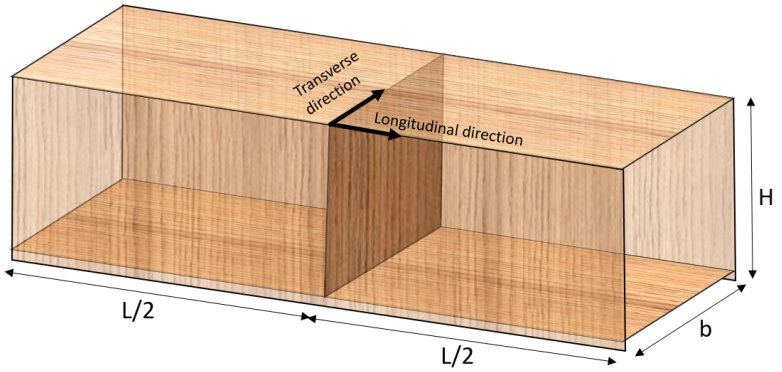

Figure 4.2: 3D view of the basic module

The CLT panels are cut from a single piece, so no longitudinal joints are necessary. Below, the thickness and composition of the panels are listed:

- Floor: 120 mm thick 3-ply (40/40/40)
- Wall: 140 mm thick 5-ply (40/20/20/20/40)
- Ceiling: 80 mm thick 3-ply (30/20/30)
- Shear wall: 260 mm thick 7-ply (40/30/40/40/40/30/40)

Cross-sections of the module are given in Figure 4.3. A horizontal cross-section of the module is given in Figure 4.3a, showing the build-up of the shear- and side walls. Figure 4.3b shows a vertical cross-section of the module, including the build-up of the side walls, floor and ceiling. Important to note is that high compression stresses perpendicular to the grain are prevented by using the balloon construction type. This means that the floor and ceiling are attached at the inside of the side walls. Also, the floor is raised with 170 mm. The module design is based on a general design that is used in multiple buildings.

The dimensions of the elements could vary slightly depending on the situation, but overall, the chosen design is applicable to many buildings.

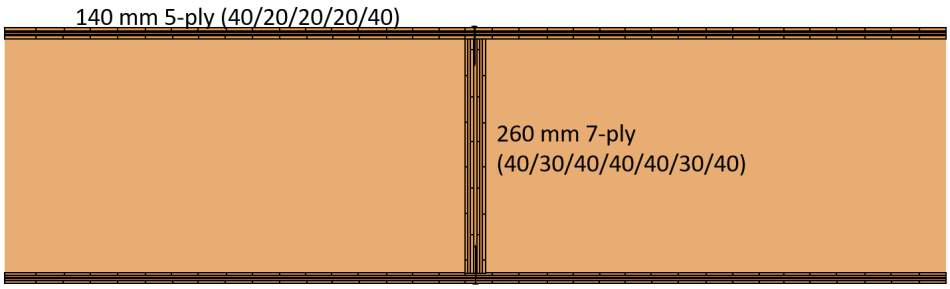

(a) Horizontal cross-section

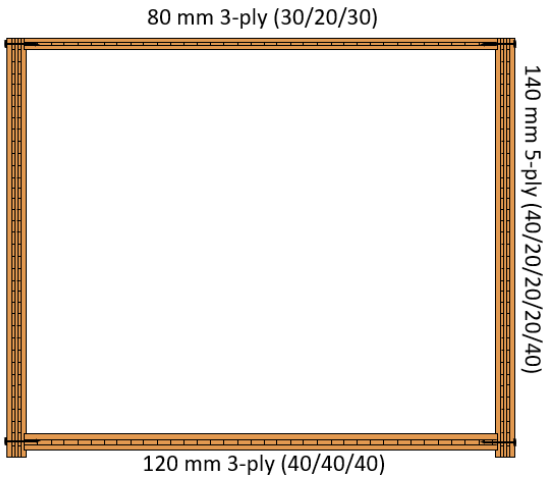

(b) Vertical cross-section

Figure 4.3: Cross-sections of the basic module

4.3. DEFORMATION CALCULATION

The aim of the study is to predict the lateral deflection of modular buildings. For conventional buildings, the calculation method is known. The structure is modelled as a cantilever or frame, for which the deflection can be calculated. In those cases the deformation can be separated in bending and shear deformation by using an infinitely high bending or shear modulus and with superposition the two are added to obtain the total deflection. Modular buildings are different due to the raised floor and, consequently, the transverse shear wall. Therefore, the modules have not the typical form to model it as a clamped cantilever or conventional frame. It should be investigated how the lateral deflection could be calculated. Using superposition to calculate the deflection would be the simplest. To see whether this is possible, the possibility for superposition is investigated with a Finite Element Software SCIA.

The numerical modelling is done in SCIA, where the shear modulus (G) and bending modulus (E) must be assigned. The first test that is performed is to check if it is possible to separate the bending and shear deformations in SCIA by alternately assigning them infinite values (10^{10}). This is done for a simple CLT shear wall of 9 m high and 3 m wide. A point load of 500 kN is applied at the top. The CLT wall is modelled as a 260 mm thick 7-ply (40/30/40/40/40/30/40) orthotropic plate. The model is shown in Figure 4.4a. The maximum deflection is taken at the top right, ignoring the local effect at the top left that occurs due to the concentrated load.

The results show that in the normal situation, with realistic moduli ($G = 690 N/mm^2, E = 11000 N/mm^2$, see table 2.1, the deflection at the top is 44.9 mm, as can be seen in Figure 4.4b. For shear defor-

mation ($G = 10^{10} N/mm^2$), the deflection is 12.4 mm (Figure 4.4c) and for bending deformation ($E = 10^{10} N/mm^2$) 30.4 mm (Figure 4.4d). Superposition results in a total deflection of 42,8 mm which is, compared to the total deflection, a deviation of 5%. Since the difference is so small, it can be concluded that superposition works with the use of infinitely high moduli.

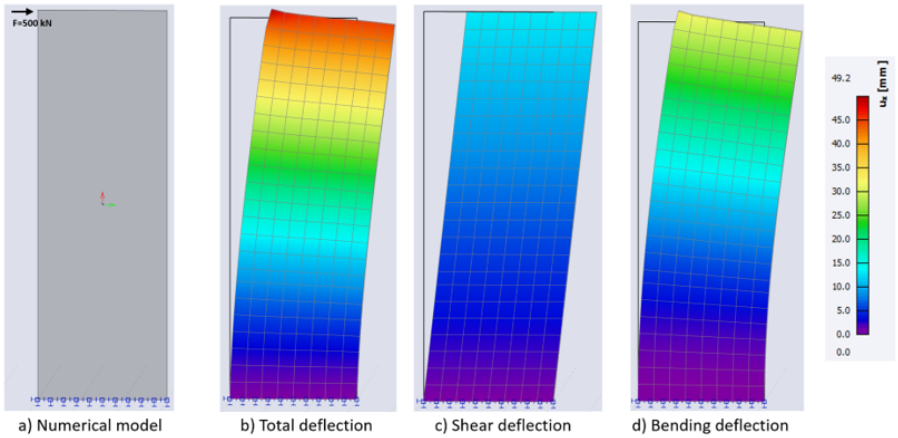

Figure 4.4: Shear wall clamped at the bottom: a) model of the shear wall, b) total deflection, c) shear deflection, d) bending deflection

As explained before, the modules that are investigated in this research are not clamped at the bottom, but are supported by the side walls. Consequently, the structural model is a shear wall with two hinged supports at both sides. It should be verified whether superposition is also possible in that case. The same shear wall is now modelled with two hinged supports at the bottom corners, see Figure 4.5a. The results are shown in Figure 4.5b-d. The total deflection at the top is 81.7 mm, while the shear and bending deflection is 12.4 mm and 44.7 mm respectively. Superposition of the latter two gives 57.1 mm, which is a 30% deviation compared to the total deflection. From this it can be concluded that superposition is not possible.

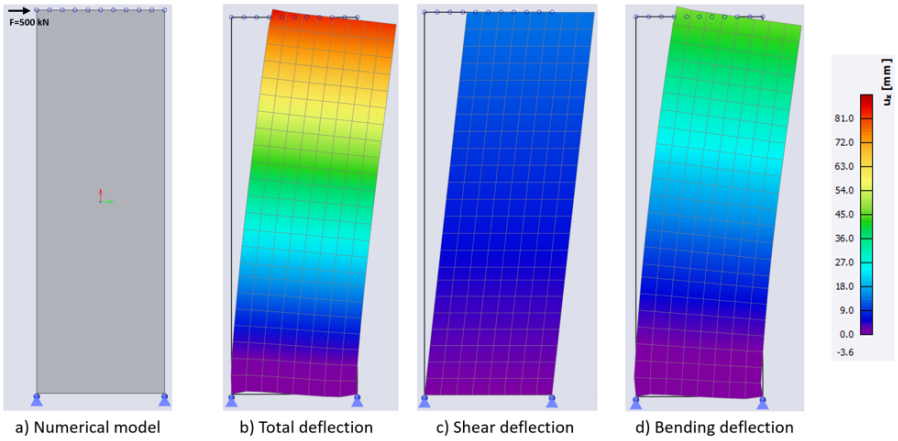

Figure 4.5: Shear wall supported with pinned supports at the bottom corners: a) numerical model, b) total deformation, c) shear deformation, d) bending deformation

The explanation for the failed superposition of the bending and shear deflection lies in a third deformation mechanism. The horizontal force causes a local stress concentration at the supports and as a result, the material compresses and causes local deformations. This leads to a curvature along the

height of the wall in the horizontal cross-section, which is the largest at the bottom. Due to this rotation, the wall will have an extra cumulative effect, resulting in a higher deflection at the top. Because the superposition of bending and shear deflection does not include this compression at the supports, it only gives 70% of the total deflection. Looking at the bottom of the wall in Figure 4.5, it can be seen that due to the curvature, the bottom of the wall moves vertically. The maximum vertical displacement indicates how large the curvature is. For shear deformation, there is no curvature. In the bending only situation, some curvature is visible (maximum vertical displacement is 2 mm) and for the normal situation a larger curvature occurs (maximum vertical displacement is 4.8 mm). Remarkable is that for the total deformation situation, the curvature is larger than in the bending situation. This indicates that the curvature is prevented in the shear only situation. With the E-modulus being infinitely high, the vertical shear is avoided and thus no curvature occurs.

To confirm that the compression at the supports is the cause of the extra deflection, a rigid beam is placed between the supports so that horizontal curvature is prevented. The results are in this case the same as for the clamped shear wall of Figure 4.4. This confirms that the supports themselves do not cause the inability to use superposition, but the curvature that occurs due to compression at the supports. Additionally, the shear wall was modelled with one pinned and one roller support to see whether that influences the results and the possibility to use superposition. The results show that the same behaviour occurs as for the shear wall with two pinned supports, but due to elongation of the wall the displacement is slightly higher.

The compression at the supports is a mechanism that can not be expressed in equations and calculated accordingly. Consequently, it is for a hinged supported structure, like the modules, not possible to calculate the deflections with simple formulas like the forget-me-nots. Therefore, equations should be proposed, to incorporate the compression at the supports. The equations are proposed based on the numerical model.

4.4. NUMERICAL MODELLING

Before the equations can be proposed, the modules should be correctly modelled. The Finite Element Software that is used to for modelling is SCIA. SCIA is a comprehensive finite element software for structural analysis and design. Modelling a structure is always a representation of reality, captured as good as possible in the model to approach real behaviour of the structure. When modelling the modules, choices have to be made to model the behaviour of the CLT panels, connections, supports and loads in the software. These modelling choices result in the following modelling methods.

CROSS-LAMINATED TIMBER

As described in chapter 2.3.2, CLT is an orthotropic material. It is important to model this correctly by incorporating the right stiffness matrix. SCIA has an option to select cross-laminated when creating the build-up of a 2D element, that calculates the stiffness matrix automatically. As input parameters it needs a material, which is generated separately, and information on the build-up of the CLT. The material can be selected from the database and adjusted if necessary, while the following parameters should be entered: plate thickness, number of layers, thickness of each layer and board width. Based on the German and Austrian National code (ÖNÖRM B 1995-1-1) the stiffness matrix is determined. To ensure that the stiffness matrix coincides with the intended direction in the models, the local coordinate system of the CLT elements needs to follow the correct convention: the x-axis is the 'main' longitudinal direction, the y-axis in the transverse direction and the z-axis is the out-of-plane direction.

CONNECTIONS

Modelling of the connections can be done as rigid, free, flexible or nonlinear depending on the connection type. Most connections are modelled correctly as flexible, simplifying the connection as a spring with a certain stiffness. Connecting elements is done in SCIA by applying a hinge between the members, where the degrees of freedom K_x, K_y, K_z and φ_x can be assigned. When non-linear connections are used, the stress-strain relationship should be given as a function. The connections are modelled continuous by line elements representing the stiffness per meter length. Figure 9.1 shows the orientation

of the degrees of freedom of the 2D line-to-line connection. K_x represents the in-plane shear stiffness, K_y the out-of-plane shear stiffness, K_z the axial stiffness of the connection and φ is the rotation.

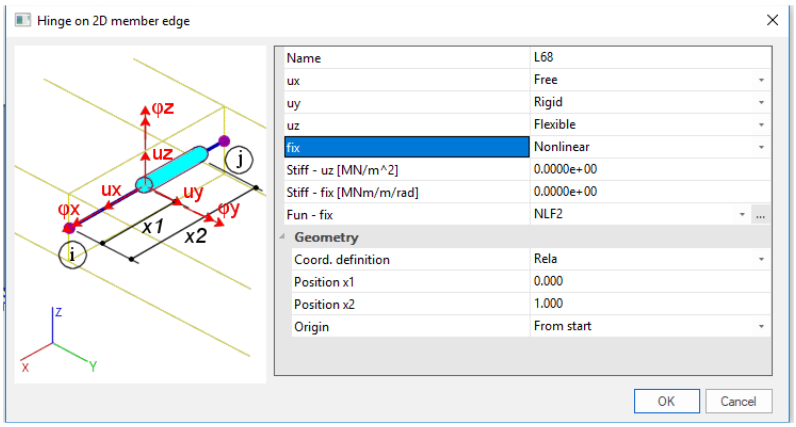

Figure 4.6: Orientation joint with degrees of freedom in SCIA

LOADING

The lateral load is the wind load that acts on the structure. As we are only investigating the transverse stability, the wind load in longitudinal direction is not considered. The side walls transfer the load to the floor and ceiling, where it acts as a line load. It is simplified such that the wind load on the floor is distributed to the ceiling of the lower module. Therefore, the wind load is only modelled at the ceiling. Vertical load is not included in the research, meaning that dead and live loads are not modelled.

SUPPORTS

Supports can be modelled to support the building. The degrees of freedom that can be assigned are: $K_x, K_y, K_z, \varphi_x, \varphi_y$ and φ_z. The degrees of freedom can be constrained based on the type of support.

4.4.1. VALIDATION

Validation of the model has to be done to ensure the methods and assumptions used in modelling are accurate and give results that are reliable and in accordance with real structural behaviour. Because there is no experimental test of an entire CLT module, the validation has to be done with different CLT elements and structures. For example, with shear wall experiments or other CLT structures. Appendix A describes this validation process. It starts with a simple shear wall connected with hold-downs and angle brackets subjected to lateral load. After that, more complex shear walls with perpendicular walls and roofs, coupled walls and screw connections are checked. Finally, a one storey CLT structure is validated. As all validations showed accurate results, the modelling method is validated.

4.4.2. MESH SIZE

In finite element analysis, the elements are divided into small elements for which the software perform calculations. The size of the finite elements is called the mesh size and has influence on the results. Normally the finer the mesh, the better the results but the longer the computational time. However, in this specific module design, a finer mesh results in concentrated stresses which could overestimate certain results. An optimal should therefore be found. Appendix B provides a study on this optimization and it was found that the most optimal mesh size is 400 mm. This will be used throughout the study when the numerical analyses are performed.

4.4.3. MODELLING OF THE MODULE

Now that the validation of the modelling methods is finished, the modules can be modelled. This section will describe the modelling process of module 0. The modelling process consists of multiple steps. First, the material(s) should be created. After that, the build-up of the panels should be established and

the material assigned to it. Next, the members must be placed, after which the connections between the members can be modelled. Finally, the loads and supports are added. The modelling process for module 0 is comprehensively explained below.

For the CLT panels, the timber material that is used is C24, since this material is widely used and available. The material properties of C24 are listed in table 2.1. Higher material strengths could provide extra performance of the structure, but large quantities of high strength timber can be difficult to find.

The CLT panels are 2D elements that are modelled as shell elements. A shell element is a combination of a plate element and plane stress elements. Plane stress elements have only in-plane loading and plate elements have only out of plane loading. Shell elements thus have both in and out of plane loading. Figure 4.7 show how the CLT panels form the module. The local coordinate systems are visualized.

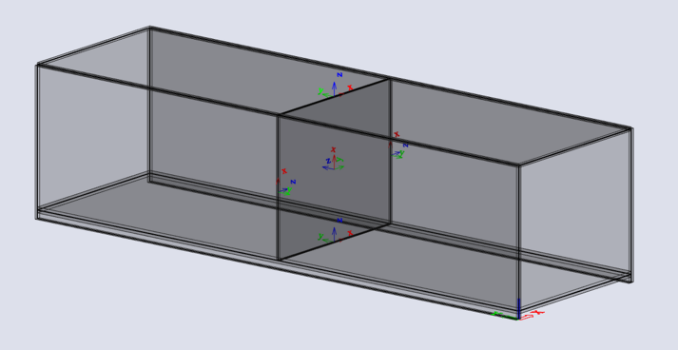

Figure 4.7: SCIA model with the local coordinate systems

The module elements are connected with hinges as is shown in Figure 4.8. In the figure, the hinge connection is visualized with circles between the elements. In the initial situation, the translational stiffnesses K_x, K_y and K_z are 0. Later, a realistic value based on certain connection types are introduced. As explained, the wind load is applied at the top of the module. As a starting point, a distributed load of 5 kN/m is applied, acting on the total length of the module. However, when the modules are stacked, the horizontal load will be transferred through the transverse shear walls to the lower module, causing a more concentrated load at that lower module. Therefore, the load will be applied to 1 m width around the shear wall. This width is found realistic, because it gives a good approximation of the situation with multiple stacked modules and at the same time large local effects are avoided. The length (12 m) times the distributed load (5 kN/m) is divided by the applied width (1 m) and results is the total applied load of 60 kN/m (see Figure 4.8. This concludes the complete numerical model of the designed modules.

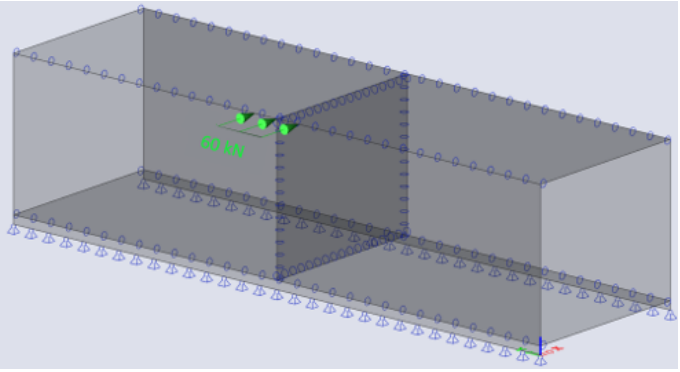

Figure 4.8: SCIA model with the loading, connections and supports

5

Equation proposal for individual modules

As it is concluded that existing calculation methods can not be applied to calculate the deflection of the designed timber modules, equations based on the numerical results are proposed. Beforehand, assumptions that apply to the equations are mentioned in Chapter 5.1. Hereafter, the main equations are established in Chapter 5.2 and 5.3. Several design options are given and incorporated in the equations in Chapter 5.4. The equations are extended for three situations: connection stiffness, shear wall thickness and shear wall position. To conclude the equation proposals, a workflow on how to use them is presented in Chapter 5.5.

5.1. ASSUMPTIONS

The assumptions that apply to the proposed equations follow from the design, modelling or other agreements and are as follows:

- The build-up and thickness of the CLT elements are fixed.
- The floor is raised by 170 mm for all module dimensions.
- The side walls remain closed, no openings are allowed.
- In all situations, the uplift force due to the horizontal wind loading must be smaller than the vertical load, meaning that there is no tension between the modules that causes the module to rotate. Therefore, only lateral loads are considered and no vertical loads are taken into account.
- The fire safety is fulfilled by protective gypsum layers or other non-structural measures.
- Only wind load is considered for the horizontal loads, no earthquake loads are taken into account

5.2. MAIN EQUATION PROPOSAL

In the previous chapter, the modelling of the modules has been comprehensively discussed. Together with Appendix A, where the modelling methods are extensively validated, it can be stated that the numerical model describes the real structure accurately. That being said, it is possible to establish equations based on the numerical model. In this section, the main equations will be proposed for the four module configurations. These are the equation for the horizontal displacement and rotation induced by the horizontal wind loading.

As discussed in Chapter 4.3, the deformation can not be obtained by superposition of bending and shear, due to the extra deformation caused by the compression at the supports. This extra deformation

mechanism makes the use of the existing forget-me-nots not possible. Proposing the equations will be done however on the basis of the forget-me-nots, but will be adjusted such that they calculate the module deformation. The starting equations for the lateral displacement u and horizontal rotation θ are stated below. For the parameters force F, height H and width b the relations with u and θ are obtained with the numerical model. The bold noted factors A, B, C, b and H are used to match the found relations. In the proposed equations, the bending stiffness $(EI)_s$ and shear stiffness $(GA)_s$ for the standard dimensions is introduced. Because calculating the stiffnesses for a module is complex, it is done only for the standard dimensions. This way, the stiffnesses have to be calculated only once. Subsequently. the factor bH takes into account the deviation of the shear and bending stiffness due to varying width and height. This factor will be turned into a constant afterwards so that the units of the equations are correct. For equation 5.1 this will be α for the first term and β for the second term. In equation 5.2 this will be γ.

$$u = \frac{\mathbf{A}FH^2b}{(EI)_s(\mathbf{bH})} + \frac{\mathbf{B}FH}{(GA)_s(\mathbf{bH})} \tag{5.1}$$

$$\theta = \frac{\mathbf{C}FHb}{(EI)s(\mathbf{bH})} \tag{5.2}$$

where:

F = the total horizontal load $[kN]$
H = the module height $[m]$
b = the module width $[m]$
E = the elastic modulus $[kN/m^2]$
G = the shear modulus $[kN/m^2]$
I = the second moment of area $[m^4]$
A = the area on which the force acts $[m^2]$
$(EI)_s$ = the standard bending stiffness $[kNm^2]$
$(GA)_s$ = the standard shear stiffness $[kN]$

Equations 5.1 and 5.2 form the basis of the main equations. To propose the equations, the relation between the parameters and the deformation terms are needed. In SCIA these relations can be explored by modelling the modules with varying values for the parameters. By plotting the corresponding displacement and rotation, the relation between the parameter and the unknown is determined. Plotting is done in Excel and by activating the trend line, excel computes the mathematical formula that describes the relation. With the help of the trend line, the equations will be proposed. The range of the parameters is chosen around the standard dimensions and represent realistic values.

The steps that are taken to establish the main equations apply to all four module configurations are as follows. First, the numerical model in SCIA is created with the standard dimension and horizontal dummy load of 60 kN. This load is spread over a meter around the shear wall, as explained in Chapter 4.4. From the model, the lateral displacement and horizontal rotation of the module will follow. The displacement is taken at the top corner of the shear wall and is measured in millimeters. The horizontal rotation is the vertical displacement at the top corners of the shear wall, divided by the length of the shear wall and is measured in milliradian. The next step is to obtain a relation between the three parameters width, height and force with the displacement and rotation. Therefore, one parameter at a time is adjusted, resulting in corresponding values for u_x and θ. With the data, the relations between the parameters and the displacement and rotation is plotted. Knowing the relations, the equations can be proposed. It begins with determining the standard bending and shear stiffness and entering them

in the equation. Hereafter, the bold noted factors are adjusted such that the proposed equations match the found relations. This results in three equations that have the best fit for each parameter. Finally, one equation is proposed that has the best agreement with all parameters.

5.2.1. STANDARD SHEAR AND BENDING STIFFNESS

Before the equations are established, the standard shear and bending stiffness is determined. With the method explained in appendix C, the shear and bending stiffness can be determined for the standard module dimensions (H x b x L = 3.1 x 3.5 x 12 m). These stiffnesses are referred to as the standard stiffness ($(GA)_S$ and $(EI)_s$) of the module and are listed in table 5.1. Important to note is that the stiffness depends on the dimensions of the module and therefore should be adjusted for different heights and widths. In most 2D structures the height is not of influence on the shear and bending stiffness, but as the modules are modelled in 3D the effective width of the side walls is increasing as the height increases, i.e. the higher the module, the larger the part of the side wall cooperates. This phenomenon is difficult to describe and is therefore not specifically investigated in this research, but is indirectly taken into account when the equations are proposed. The influence of the width depends on the module configuration and is therefore investigated separately. With the determined values for $(GA)_S$ and $(EI)_s$, the equations for the module configurations can be proposed.

Table 5.1: Standard shear and bending stiffnesses of the module configurations

Module	$(EI)_s$ $[kNm^2]$	$(GA)_s$ $[kN]$
0	$9.20 * 10^6$	$4.79 * 10^5$
1	$3.49 * 10^6$	$3.37 * 10^5$
2	$2.96 * 10^6$	$2.34 * 10^5$
3	$1.42 * 10^6$	$1.98 * 10^5$

5.2.2. MODULE 0

The numerical model of module 0 with standard dimensions is shown in Figure 5.1. The model is created with the modelling methods explained in Chapter 4.4. With this model the research into the relations is done from which the equations are proposed. A linear elastic analysis is performed in SCIA to obtain the results. The mesh size is taken as 400 mm as explained in Chapter 4.4.

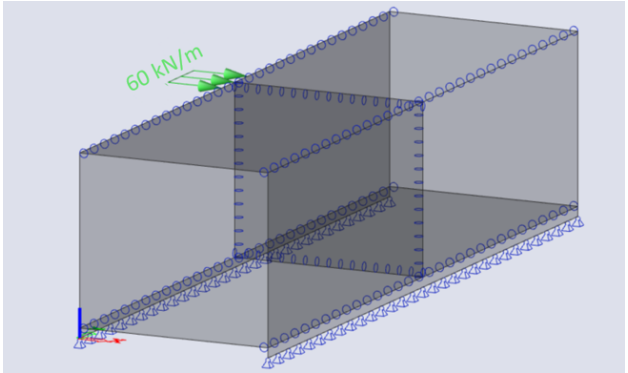

Figure 5.1: Numerical model of module 0

The results of the deformed mesh are presented in Figure 5.2. On the left, the horizontal displacement U_x is displayed. At the top right of the shear wall the displacement is taken, which is 0.80 mm. The right image shows the vertical displacement U_z. At the top corners of the shear wall the values are shown. From the vertical displacement, the horizontal rotation can be determined by adding them and dividing by the width. In this case 0.04 mrad. Performing the same analysis for different parameters gives the relations between the parameters and the unknown displacements.

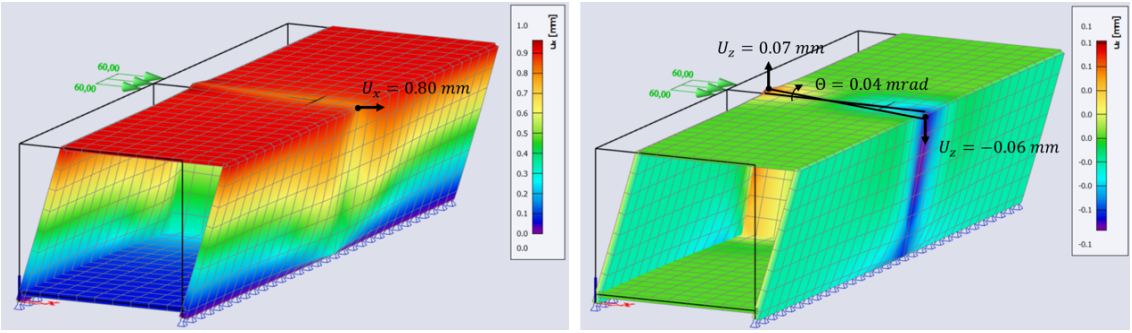

Figure 5.2: Deformation of module 0 (standard dimensions) with the horizontal displacement (left) and rotation (right)

The obtained relations between the height, width and force with the displacement and rotation are shown in black in Figure 5.3. For these relations, the trend line formula is given. Investigating the relations for the module width gives the black curves in Figure 5.3a and b. For several widths, the displacement and rotation is plotted. In the graphs the trend line formula is given which describes the relation mathematically. For the relation between the width and horizontal displacement, the formula is approximately $u = 3b^{-1}$ meaning that they are inversely related to the power 1. For the width and horizontal rotation relation, the trend line formula is approximately $\theta = 0.45b^{-2}$ which also means that they are inversely related, but to the power 2. From this is can be stated that for wider modules, the horizontal displacement and rotation decreases. The relations for the height are shown in graphs c and d of Figure 5.3 and are as follows: The height and displacement are related with the formula $u = 0.012H^2 + 0.13H + 0.3$. Having the formula as a 2^{ND} order polynomial makes it easier to use it when proposing the equation, because it has the same form as the starting equation. The height and rotation are related to each other by $\theta = 0.012H^1$. This means that for a higher module both the displacement and the rotation increases. Figure 5.7e and f show the relations for the force. For both the displacement and rotation, the relation is linear and is described with the formulas $u = 0.013F$ and $\theta = 0.0006F$ respectively.

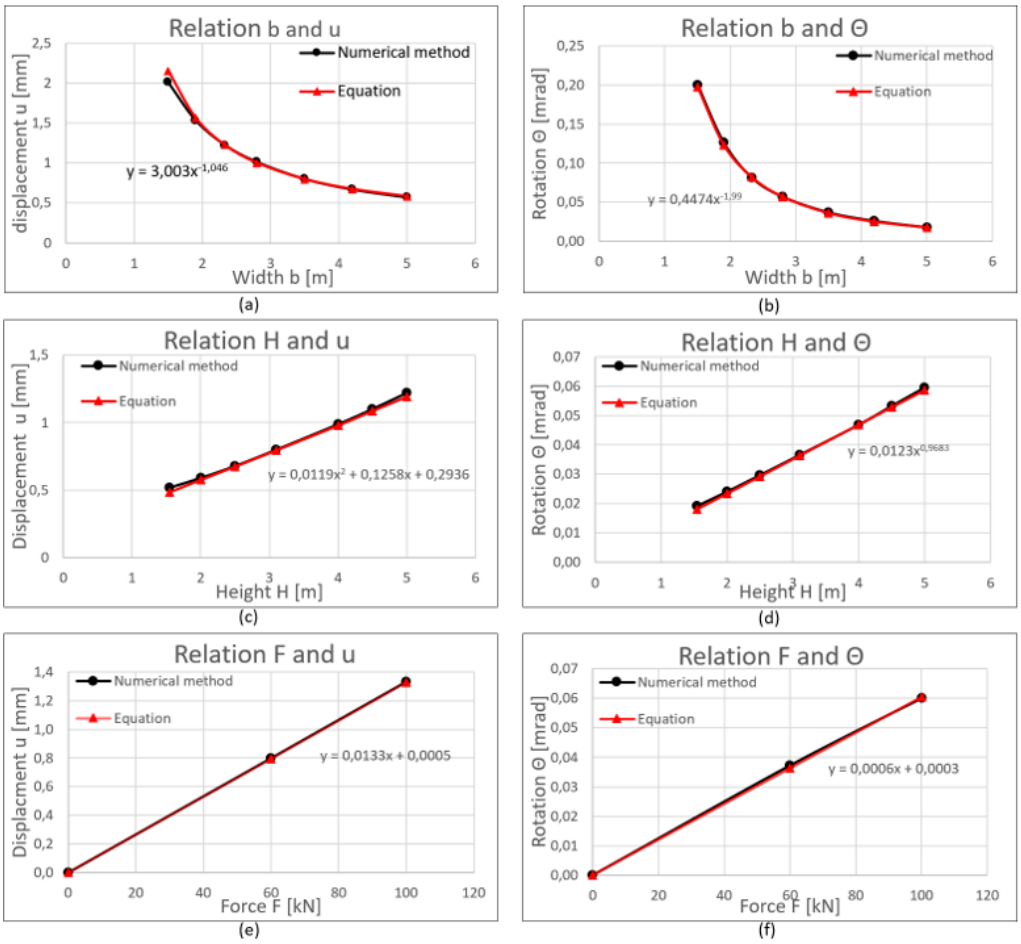

Figure 5.3: Module 0: a) relation width and displacement, b) relation height and displacement, c) relation force and displacement, d) relation width and rotation, e) relation height and rotation, f) relation force and rotation

At the beginning of this section, the shear and bending stiffness of the standard dimensioned modules were determined. The stiffnesses depend however on the dimensions of the module and should be adjusted for different heights and widths. As explained, the influence of the height is not separately investigated, but the relation between the width and the stiffnesses GA and EI is investigated. With the use of the discussed method, the stiffnesses are determined for varying values of b and subsequently the normalized stiffnesses $GA/(GA)_s$ and $EI/(EI)_s$ are plotted in Figure 5.4. These relations describe how GA and EI are related to the width and shows how it should be incorporated in the equations. For the shear stiffness GA the relation is linear, meaning that GA is obtained by multiplying $(GA)_s$ with $(0.34b - 0.156$ which can be simplified to $(\frac{b}{3} - 0.167)$. The bending stiffness EI for a certain width can be obtained by multiplying $(EI)_s$ with $0.13b^{1,6}$. These relations will be incorporated into the equation.

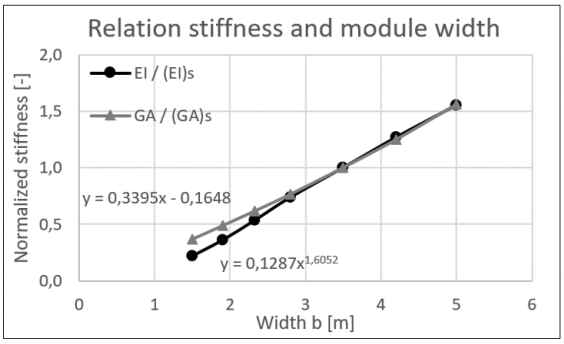

Figure 5.4: Relation stiffness and width for module 0

As mentioned, the basis of the proposed equations are the forget-me-nots (equation **??**). With the obtained relation for the shear and bending stiffness, the equation can be determined. First the best fitting equation for H, b and F are established separately, whereafter the best equation for the combined variables is defined. The same is done for the rotation θ, but because the rotation is not caused by shear deformation, only the bending term has to be considered. Appendix D contains the best fitting equations for H, b and F. Below the final proposed equations for u_{M0} and θ_{M0} are presented.

$$u_{M0} = \frac{FH^2b}{(EI)_s(b^{0.6})} + \frac{2.8FH}{(GA)_s((\frac{b}{3} - 0.167)H^{0.4})} \tag{5.3}$$

$$\theta_{M0} = \frac{22FHb}{(EI)_s(b^3)} \tag{5.4}$$

The proposed equations are plotted in red in the graphs of Figure 5.3 to see how they match the relations found by the numerical method. It can be seen that it has good correspondence with the found relations. At the end of this section, the equations will be tested for situations where all the parameters vary simultaneously to check whether the proposed equations also work in that case.

5.2.3. MODULE 1

The same approach is applied to module configuration 1. This module configuration Figure 5.5 shows the numerical model of module 1 for the standard dimensions. As the module width and height are adjusted to obtain the relations, the dimensions of the opening in the shear wall are relatively equal to the shear wall dimensions. The height of the door opening is 0.785 times the shear wall height and the width is 0.25 times the shear wall width.

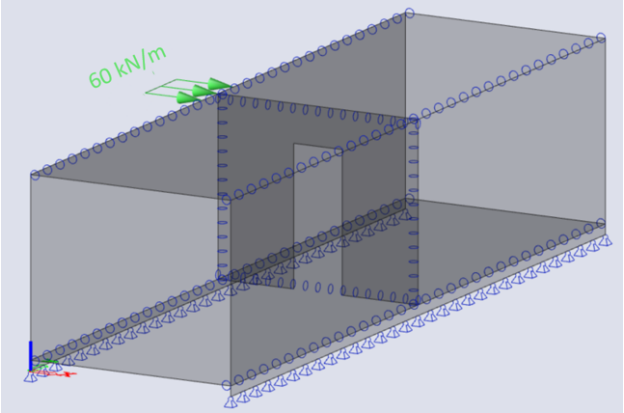

Figure 5.5: Numerical model of module 1

The analysis of the numerical model results in the values for the horizontal displacement and rotation, as shown in Figure 5.6. The horizontal displacement is 1.71 mm and the horizontal rotation is 0.03 mrad.

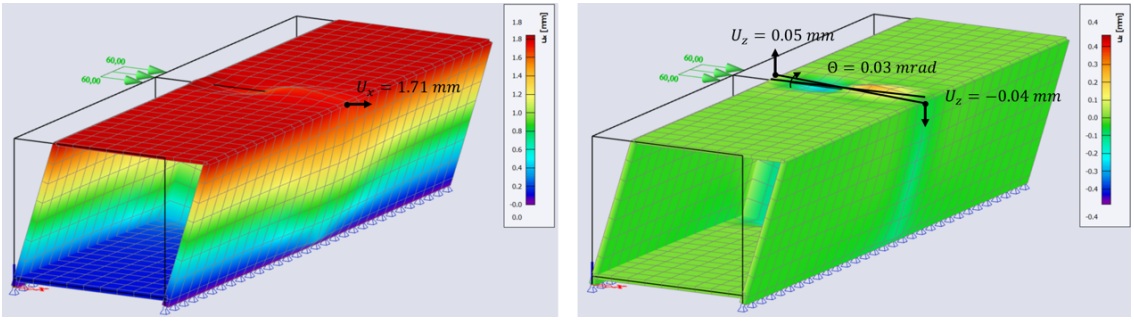

Figure 5.6: Deformation of module 1 with the horizontal (left) and vertical displacement (right)

The parameters are adjusted to obtain the relations for the displacement and rotation (see Figure 5.7). For the width of the module the following relations are found: $u = 6.9b^{-1}$ and $\theta = 0.24b^{-1.7}$ (Figure 5.7a and b). The width is therefore inversely related to the power 1 and 1,7 with the displacement and rotation respectively. For the height and displacement, the trend line formula is given as $u = 0.05H^2 + 0.25H + 0.46$. The height and rotation are related with $\theta = 0.019H^{0.32}$ as can be seen in Figure 5.7c and d. Finally, Figure 5.7e and f contain the relations for the force: $u = 0.029F$ and $\theta = 0.0005F$.

The normalized shear and bending stiffness are presented in Figure 5.8 and show how the width influences the stiffnesses. The shear stiffness relation is similar to the one of module 0, namely $(\frac{b}{3} - 0.167)$. The bending stiffness is related to the width by $EI = 0.093b^{1.86} * (EI)_s$. Using all the above-mentioned relations, the equations can be proposed. In appendix D the best fitting equations for the three parameters are given. Equations 5.5 and 5.6 are the final proposed equations for module 1.

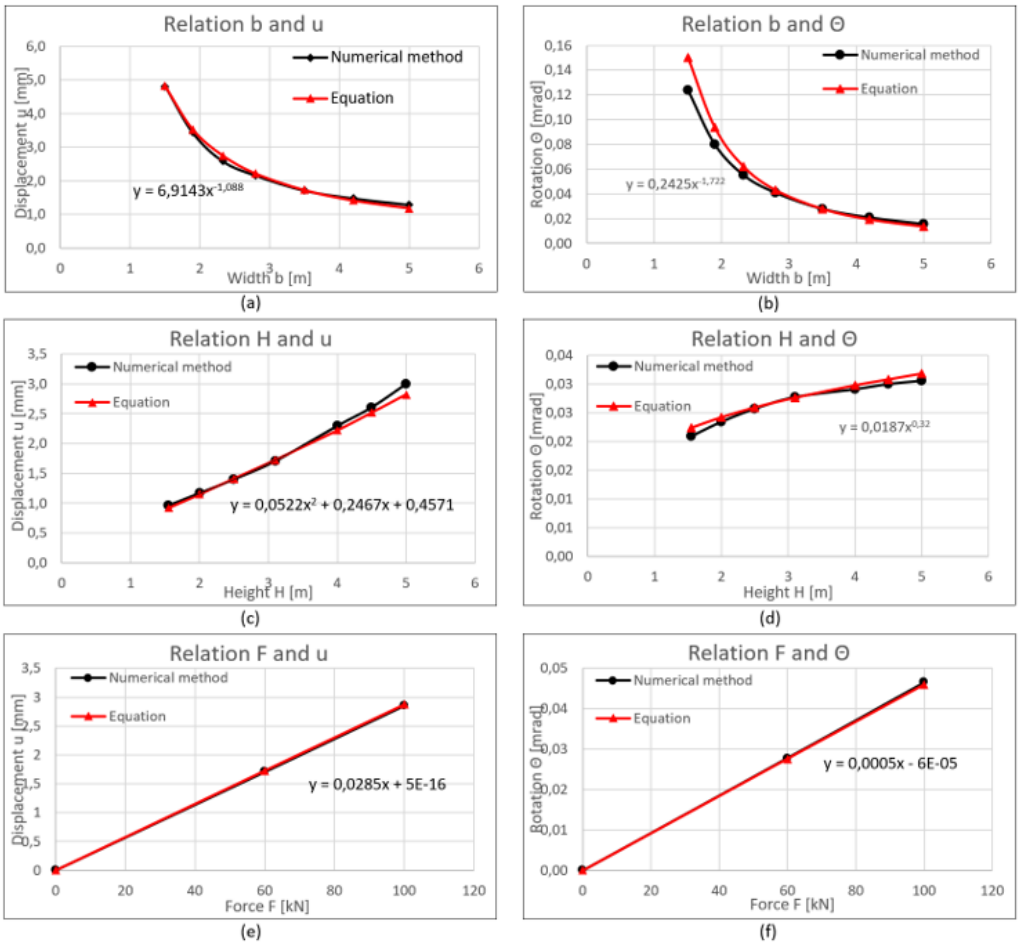

Figure 5.7: Module 1: a) relation width and displacement, b) relation height and displacement, c) relation force and displacement, d) relation width and rotation, e) relation height and rotation, f) relation force and rotation

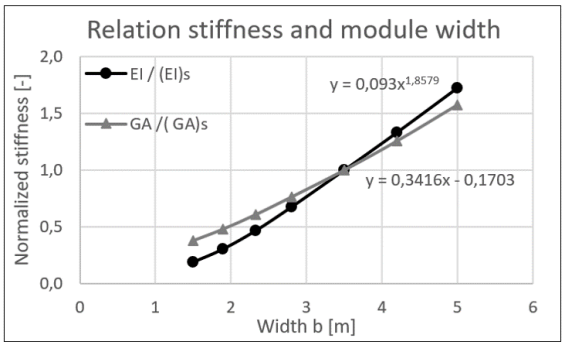

Figure 5.8: Relation stiffness and width for module 1

$$u_{M1} = \frac{10FH^2b}{(EI)_s(b^{1.9}H^{0.2})} + \frac{3.3FH}{(GA)_s((\frac{b}{3} - 0.167)H^{0.3})} \tag{5.5}$$

$$\theta_{M1} = \frac{14FHb}{(EI)_s(b^3H^{0.7})} \tag{5.6}$$

The proposed equations 5.5 and 5.6 are plotted in red in Figure 5.7 for comparison with the obtained relations in SCIA. Overall they show good agreement, but slight differences can be observed for the rotation in relation with the width and height.

5.2.4. MODULE 2

Module 2 with standard dimensions is modelled in SCIA as shown in Figure 5.9. Similar as for module configuration 1, the dimensions of the opening are kept relatively equal for all module dimensions. As such, the opening height is 0.785 times the shear wall height and the opening width is 0.5 times the shear wall width.

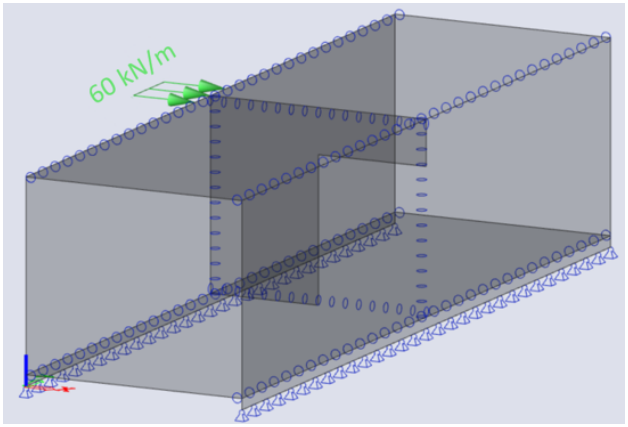

Figure 5.9: Numerical model of module 2

The performed analysis gives the deformed module as shown in Figure 5.10. The horizontal displacement at the shear wall is 4.12 mm and the horizontal rotation is 0.05 mrad.

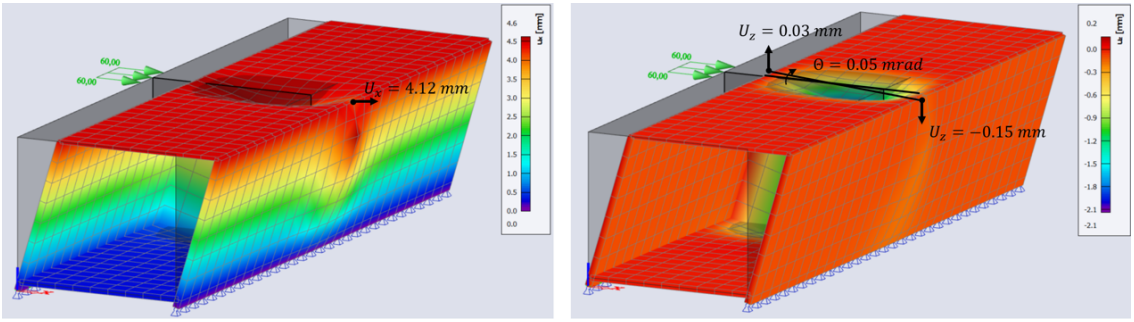

Figure 5.10: Deformation of module 2 with the horizontal (left) and vertical displacement (right)

The relations between the parameters and unknown displacements are obtained with this model and presented in Figure 5.11. The module width and height have the following relations with the displacement and rotation: $u = 9.5b^{-0.63}$, $\theta = 0.52b^{-1.85}$, $u = 0.1H^2 + 0.19H + 2.6$ and $\theta = 0.02H^{0.79}$, This means that for wider modules the displacement and rotation decreases, but increases for higher modules. The force and displacement are related by $u = 0.069F$ and the force and rotation by $\theta = 0.0009F$. With these relations and the relations for the normalized stiffnesses in Figure 5.16 the equations can be proposed. Appendix D contains the best fitting equations for the separate parameters. Equations 5.7 and 5.8 are the final proposed equations for the horizontal displacement and rotation.

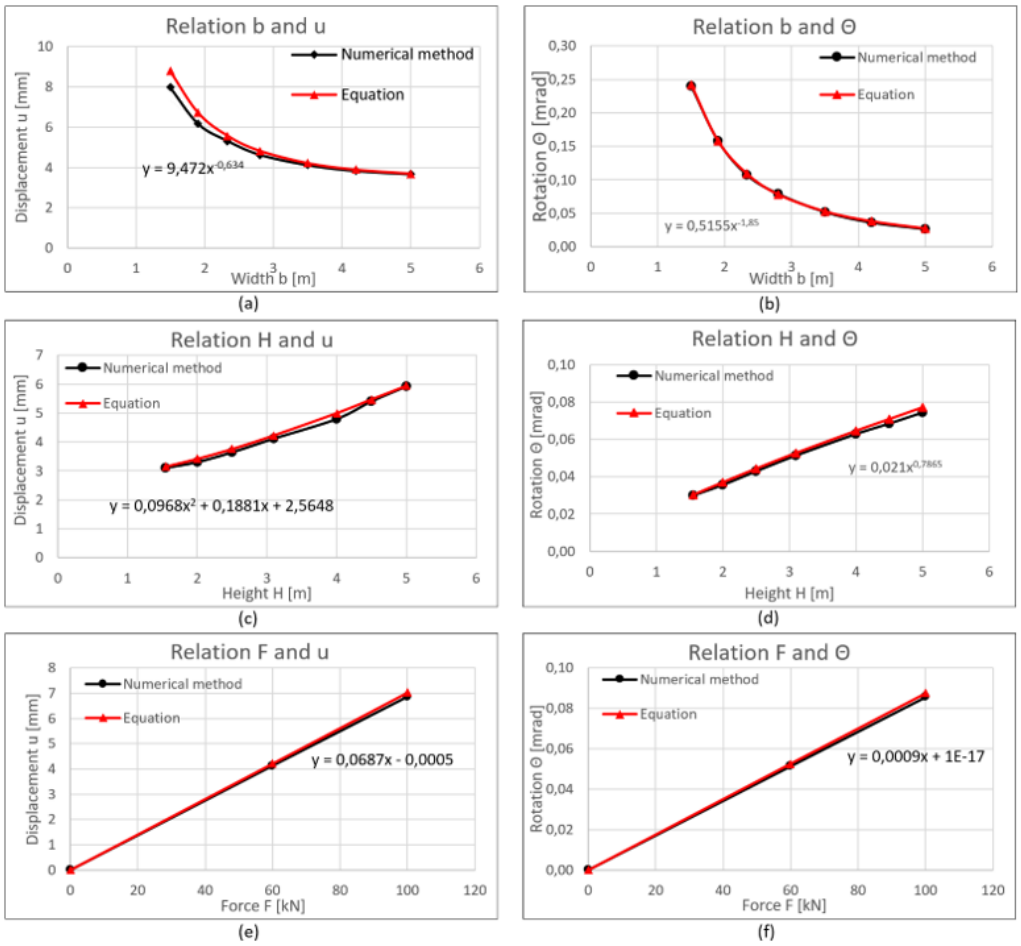

Figure 5.11: Module 2: a) relation width and displacement, b) relation height and displacement, c) relation force and displacement, d) relation width and rotation, e) relation height and rotation, f) relation force and rotation

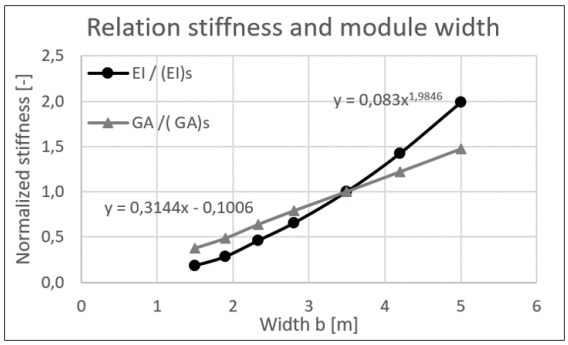

Figure 5.12: Relation stiffness and width for module 2

$$u_{M2} = \frac{8FH^2b}{(EI)_s(b^{0.5}H^{0.5})} + \frac{10FH}{(GA)_s(\frac{b}{3} - 0.167)H} \tag{5.7}$$

$$\theta_{M2} = \frac{10FHb}{(EI)_s(b^{2.8}H^{0.2})} \tag{5.8}$$

The final proposed equations are plotted in red in Figure 5.11. The proposed equations show good agreement with the relations from SCIA as can be seen in Figure 5.11. The red curve represent the proposed equations and match the found relations in SCIA (black line). Only for smaller values of b, the displacement u shows some deviating values, but those are small.

5.2.5. MODULE 3

The final module configuration is module 3. The numerical model is shown in Figure 5.13. The shear wall is for all module dimensions half the width of the module. The deformed modules from the numerical analysis are presented in Figure 5.14. The horizontal displacement is 60.4 mm and the horizontal rotation is 0.04 mrad.

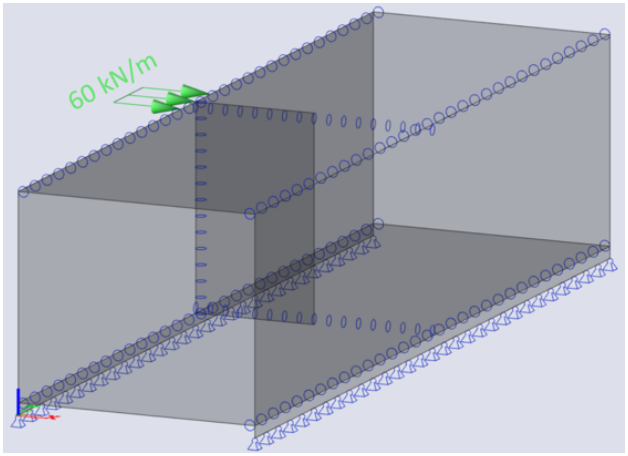

Figure 5.13: Numerical model of module 3

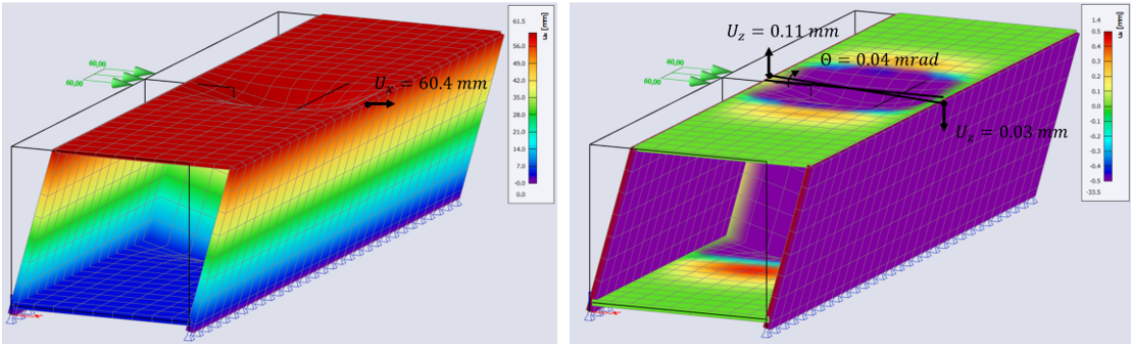

Figure 5.14: Deformation of module 3 with the horizontal (left) and vertical displacement (right)

The relations for the width, height and force are presented in Figure 5.15 and listed here: $u = 94.6b^{-0.35}$, $\theta = 0.57b^{-2.14}$, $u = 6.18H^2 + 0.28H + 0.24$, $\theta = 0.013H^1$, $u = F + 0.1$, $\theta = 0.0005F$. These relations together with the relation between the normalized stiffnesses and the width are used to propose the main equations for module 3. The best fitting equations are again listed in Appendix D. The final equations are equations 5.9 and 5.10.

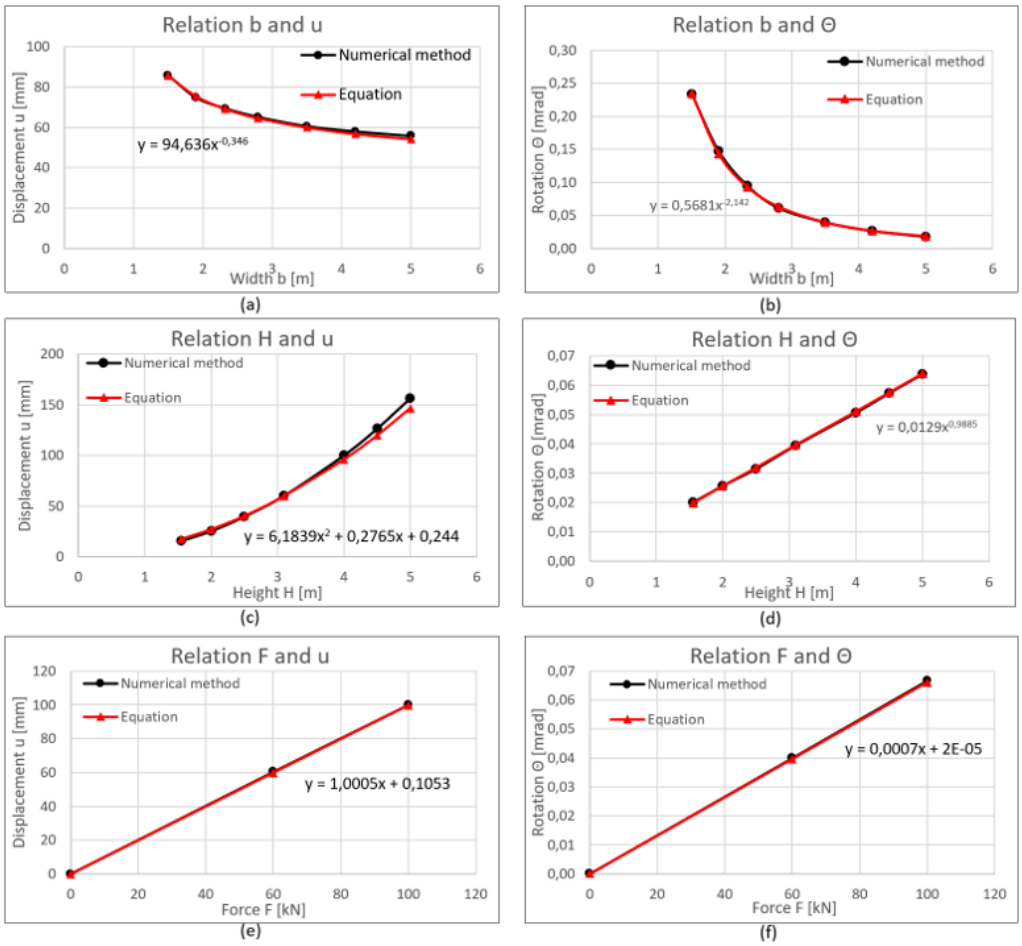

Figure 5.15: Module 3: a) relation width and displacement, b) relation height and displacement, c) relation force and displacement, d) relation width and rotation, e) relation height and rotation, f) relation force and rotation

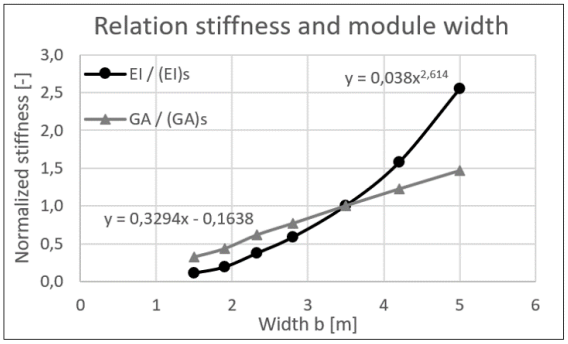

Figure 5.16: Relation stiffness and width for module 3

$$u_{M3} = \frac{150FH^2b}{(EI)_s(b^{1.15})} + \frac{10FH}{(GA)_s(\frac{b}{3} - 0.167)} \tag{5.9}$$

$$\theta_{M3} = \frac{4.2FHb}{(EI)_s(b^{3.1})} \tag{5.10}$$

The proposed equations are plotted in red in the graphs of Figure 5.15. There, it is possible to quickly see that the equations have good accuracy with the obtained relations. No significant deviations are visible.

5.2.6. SUMMARY AND VALIDATION OF THE EQUATIONS

The proposed main equations for the displacement u and rotation θ of the four module configurations are summarized below. They are established by adjusting one parameter at a time, but the equations should also provide good results when the three parameters are varied simultaneously. Therefore, they are tested for three situations where the parameters all vary. In SCIA these situations are modelled and the results for the displacement and rotation are compared with the outcomes of the proposed equations. The results for the displacement equations are presented in table 5.2 while the results of the rotation are given in table 5.3. The error in percentage is shown in brackets within the table.

Module 0:

$$u_{M0} = \frac{FH^2b}{(EI)_s(b^{0.6})} + \frac{2.8FH}{(GA)_s((\frac{b}{3} - 0.167)H^{0.4})}; \qquad \theta_{M0} = \frac{22FHb}{(EI)_s(b^3)}$$

Module 1:

$$u_{M1} = \frac{10FH^2b}{(EI)_s(b^{1.9}H^{0.2})} + \frac{3.3FH}{(GA)_s((\frac{b}{3} - 0.167)H^{0.3})}; \qquad \theta_{M1} = \frac{14FHb}{(EI)_s(b^3H^{0.7})}$$

Module 2:

$$u_{M2} = \frac{8FH^2b}{(EI)_s(b^{0.5}H^{0.5})} + \frac{10FH}{(GA)_s(\frac{b}{3} - 0.167)H}; \qquad \theta_{M2} = \frac{10FHb}{(EI)_s(b^{2.8}H^{0.2})}$$

Module 3:

$$u_{M3} = \frac{150FH^2b}{(EI)_s(b^{1.15})} + \frac{10FH}{(GA)_s(\frac{b}{3} - 0.167)}; \qquad \theta_{M3} = \frac{4.2FHb}{(EI)_s(b^{3.1})}$$

The values of the parameters force, height and width are shown in the tables. A wide range of values are chosen to check the accuracy for all possible situations. The results are considered sufficient if the error is below 10%. The equations for the displacement show an accuracy between 0 and 12% with the SCIA model. The largest deviation is for module 2 with 12 and 10%. The other module configurations all have an accuracy of 6% or lower. For the rotation, a larger deviation occurs for case 3 of module configuration 2 (13%). The rest of the accuracies are below 10%. It must be mentioned that because the values are very small and not too many decimals are presented, some results may be closer. These rounding errors can have an impact on the magnitude of the error.

Table 5.2: Validation of the displacement equations for three module designs

Force	**Dimensions**		**Module 0**		**Module 1**		**Module 2**		**Module 3**	
F	H	b	SCIA	equation	SCIA	equation	SCIA	equation	SCIA	equation
[kN]	[m]	[m]	u [mm]	u [mm]	u [mm]	u [mm]	u [mm]	u [mm]	u [mm]	u [mm]
50	2,5	2,8	0,71	0,71 (0%)	1,45	1,51 (4%)	3,28	3,68 (12%)	35,5	36,5 (3%)
60	3,1	3,5	0,80	0,79 (1%)	1,71	1,72 (1%)	4,12	4,22 (2%)	60,4	59,9 (1%)
20	4.0	4,2	0,27	0,28 (4%)	0,65	0,61 (6%)	1,43	1,58 (10%)	32,1	30,5 (5%)

Table 5.3: Validation of the rotation equations for three module designs

Force	**Dimensions**		**Module 0**		**Module 1**		**Module 2**		**Module 3**	
F	H	b	SCIA	equation	SCIA	equation	SCIA	equation	SCIA	equation
[kN]	[m]	[m]	$\theta[mrad]$	$\theta[mrad]$	$\theta[mrad]$	$\theta[mrad]$	$\theta[mrad]$	$\theta[mrad]$	$\theta[mrad]$	$\theta[mrad]$
50	2.5	2.8	0.039	0.038 (2%)	0.031	0.033 (6%)	0.057	0.055 (4%)	0.044	0.043 (2%)
60	3.1	3.5	0.037	0.036 (3%)	0.028	0.028 (0%)	0.051	0.053 (4%)	0.039	0.040 (3%)
20	4	4.2	0.001	0.011 (10%)	0.005	0.005 (0%)	0.017	0.015 (13%)	0.011	0.012 (9%)

5.3. MOMENT INDUCED DEFORMATION

The main equations proposed in the previous section describe the deformation due to horizontal wind load. When modules are stacked on top of each other, the horizontal load results in a bending moment. This bending moment leads to tension and compression forces in the lower module side walls. Consequently, these forces cause the module to rotate, because one side is extended due to tension forces, while the other side is compressed due to compression force. The difference in height of both sides leads to a tilt of the module. As the shear wall has to follow the deformation of the side walls, it will displace horizontally at the top. These mechanisms should be incorporated to determine the total deformation of the module.

5.3.1. MOMENT INDUCED ROTATION

The modules are stacked on top of each other at the side walls. The tension and compression force caused by the bending moment is transferred through the side walls. The force leads to an extension or compression of the side walls, which results in the rotation as visualized in5.17.

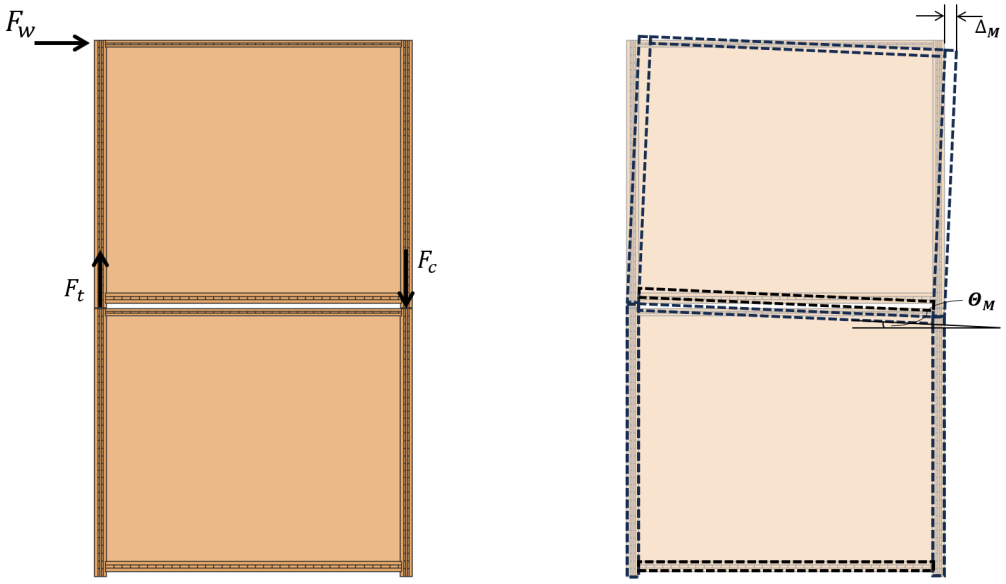

Figure 5.17: Deflection due to the bending moment: left) tension and compression force due to the horizontal load, right) deflection due to the tension and compression forces

The extension or compression of the side wall follows from the equation below:

$$\Delta_l = \frac{Fl}{EA} \tag{5.11}$$

where:

F = the compression or tension force

l = the height of the side wall

E = the modulus of Elasticity

A = the area of the side wall

The tension and compression force is determined with:

$$F_{t/c} = \frac{M}{b}, \quad with: \quad M = F_w H \tag{5.12}$$

where:

M = the bending moment at the top of the module
b = the width of the module
F_w = the horizontal wind load
H = the height of the module

Eventually, the rotation follows from trigonometry:

$$\theta_M = \frac{2\Delta_l}{b} \tag{5.13}$$

Now that the mechanism for the rotation is explained, the equation that can predict the rotation of the modules should be proposed. Since the compression and tension force is acting on the side walls, which are the same for every module configuration, the relations are valid for all module configurations. From literature, the equation for the rotation due to the moment is taken and adjusted with the standard bending stiffness and factor D and bH (see equation 5.14) [38].

$$\theta = \frac{\mathbf{D}MH}{(EI)_s(\mathbf{bH})} \tag{5.14}$$

The numerical model that is used is shown in Figure 5.18. A moment of 600 kNm is assumed. The corresponding tension and compression force at a module with standard dimensions is 171.4 kN. Similar as for the horizontal load, the force is modelled 1 meter around the shear wall. The found relations between the parameters b, H and M and the horizontal rotation are shown in black in the graphs of Figure 5.19.

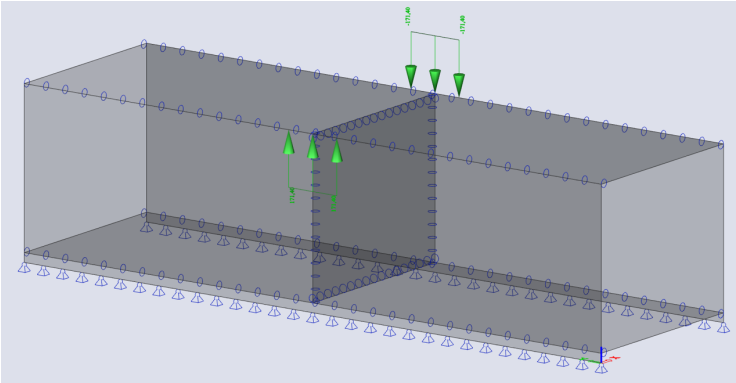

Figure 5.18: Numerical model for the moment induced rotation

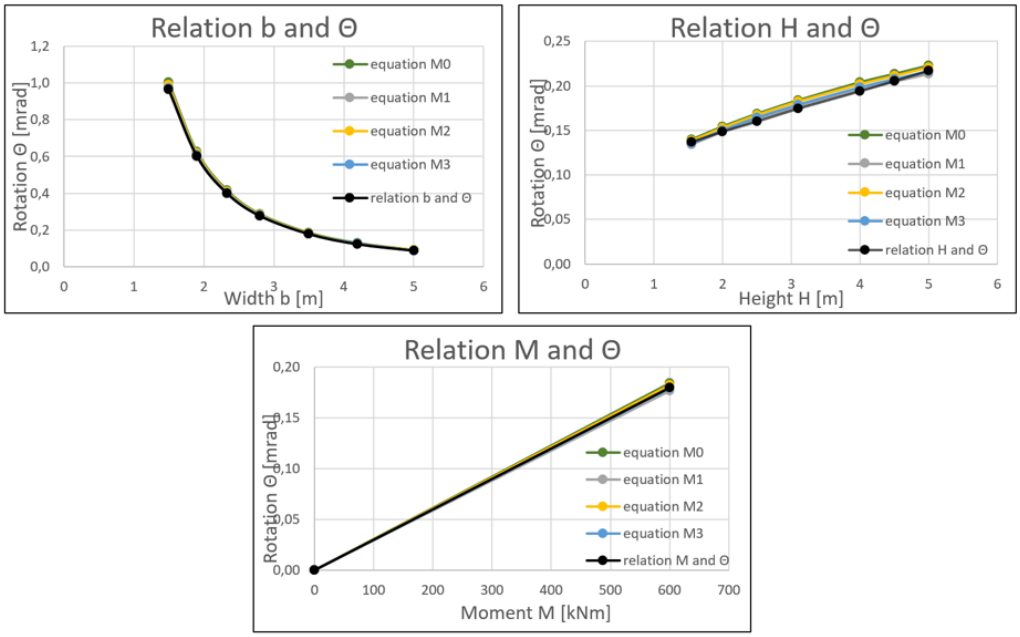

Figure 5.19: Equations for the modules plotted next to the numerical results

While the relations apply to all the module configurations, the bending stiffness differs. Therefore, the equations for the modules will be different. Just as for the main equations, the standard bending stiffness is used and adjusted for varying dimension with a constant bH. In these equations, this constant will be called λ. The equations for the four modules are presented below. They are plotted next to the found relations to compare the results (Figure 5.19). It can be seen that the equations for all four module configurations have good agreement with the numerical results.

$$\theta_{M0} = \frac{22MH}{(EI)_s(b^2H^{0.6})} \tag{5.15}$$

$$\theta_{M1} = \frac{8MH}{(EI)_s(b^2H^{0.6})} \tag{5.16}$$

$$\theta_{M2} = \frac{7MH}{(EI)_s(b^2H^{0.6})} \tag{5.17}$$

$$\theta_{M3} = \frac{3,3MH}{(EI)_s(b^2H^{0.6})} \tag{5.18}$$

Just as for the equations for the displacement and rotation due to the horizontal load, the equations should be correct when multiple parameters vary at the same time. Table 5.4 shows the results for the same three cases. It can be observed that the difference between the numerical and equation results are between 0 and 4%, from which can be concluded that the equations provide close results with the numerical model.

Table 5.4: Accuracy determination of the equations for varying parameters

Moment [kNm]	**Dimensions [m]**		**Rotation [mrad]**				
M	H	b	SCIA	M0	M2	M2	M3
200	2,5	2.8	0.086	0.088 (2%)	0.084 (2%)	0.087 (1%)	0.086 (0%)
350	3.1	3.5	0.180	0.184 (0%)	0.177 (4%)	0.182 (1%)	0.179 (3%)
100	4.0	4.2	0.024	0.024 (0%)	0.023 (4%)	0.023 (4%)	0.023 (4%)

5.3.2. MOMENT INDUCED DISPLACEMENT

The bending moment does not only cause a horizontal rotation of the module, but also a horizontal displacement. As explained, the tension and compressive force induced by the bending moment causes the side walls to extend and compress. Since the shear wall is attached to these walls, it has to follow this deformation, meaning that one side will extend and the other will compress. As a result, the shear wall will displace horizontally. Equation 5.19 describes this effect [38]. Again, the standard bending and shear stiffness are used and adjusted with a constant. For the moment induced displacement, this constant is chi.

$$u_M = \frac{\mathbf{E}MH^2}{(EI)_s(\mathbf{bH})} \tag{5.19}$$

In contrary of the moment induced rotation, the displacement is different for the module configurations. When the shear wall has to follow the deformation of the side walls, its design is of importance. The obtained relation between the width and height with the displacement is presented in Figure 5.20. The continuous line represents the found relation in SCIA and the dashed line represents the proposed equations as are listed below (eq. 5.20-5.23). As can be seen, the results of the proposed equations show good agreement with the found relations in SCIA.

$$u_{M,M0} = \frac{5.5MH^2}{(EI)_s(bH)} \tag{5.20}$$

$$u_{M,M1} = \frac{1.6MH^2}{(EI)_s(bH)} \tag{5.21}$$

$$u_{M,M2} = \frac{2.0MH^2}{(EI)_s(bH)} \tag{5.22}$$

$$u_{M,M3} = \frac{0.8MH^2}{(EI)_s(bH)} \tag{5.23}$$

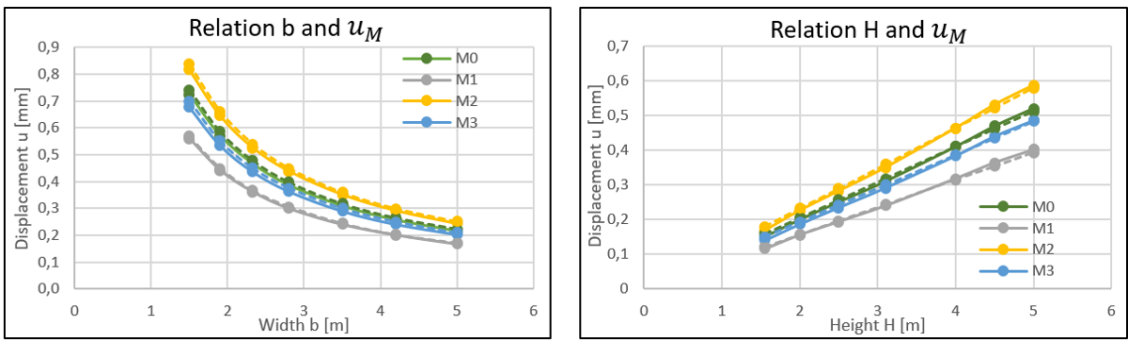

Figure 5.20: Equations for the module configurations (dashed curve) plotted next to the numerical results (continuous curve)

Again, the equations are tested for situations where the parameters vary simultaneously. Table 5.4 shows the results for three different cases. It can be observed that the difference between the results are between 0 and 20%. Even though this quite a big difference, it must be mentioned that the low accuracy can come from rounding errors. The majority of the results have an error less than 10%.

Table 5.5: Validation of the moment induced displacement equations for three module designs

Moment	**Dimensions**		**Module 0**		**Module 1**		**Module 2**		**Module 3**	
F	H	b	SCIA	equation	SCIA	equation	SCIA	equation	SCIA	equation
[kNm]	[m]	[m]	u [mm]	u [mm]	u [mm]	u [mm]	u [mm]	u [mm]	u [mm]	u [mm]
200	2,5	2.8	0.12	0.11 (9%)	0.09	0.08 (13%)	0.13	0.12 (8%)	0.11	0.10 (10%)
600	3.1	3.5	0.31	0.32 (2%)	0.24	0.24 (0%)	0.35	0.36 (2%)	0.29	0.30 (3%)
100	4.0	4.2	0.05	0.06 (20%)	0.04	0.04 (0%)	0.06	0.06 (0%)	0.04	0.05 (20%)

5.4. EXTENSION OF THE EQUATION

The proposed equations are established for the module design presented in Chapter 4.2. Because several module designs can be chosen for modular buildings, multiple design options should be given to broaden the applicability of the proposed equations. In this study, three design choices are included: intra-module connection stiffness, shear wall thickness and shear wall position. The design options are incorporated into the equations by certain factors. For the intra-module connection, a factor k_c is introduced. The shear wall thickness is included with factor k_t and the shear wall position by $u_{p,sw}$. How these factors are incorporated in the main equations for horizontal displacement and rotation can be seen in equations 5.24 and 5.25.

$$u = \frac{FH^2 b k_c}{k_{t,EI}(EI)_s \alpha} + \frac{FH k_c}{k_{t,GA}(GA)_s \beta} + u_{p,sw} \tag{5.24}$$

$$\theta = \frac{FHb k_c}{k_{t,EI}(EI)_s \gamma} \tag{5.25}$$

5.4.1. CONNECTION STIFFNESS

The intra-module connections can be designed in different ways, as discussed in chapter 2.4. Depending on the type and amount of connections, they have a certain stiffness, which is used to model the connections properly. This stiffness has influence on the deformation behaviour of the module and affects the lateral stiffness and thus the horizontal displacement. For the proposed equation, the intra-module connections were modelled as hinges with fixed translation in x/y/z-direction. To model the intra-module connections correctly, the translation should be modelled as springs with the corresponding stiffness. This section provides three design options for the intra-module connections: 'stiff', 'medium' and 'flexible'. They differ in the spacing between the screws. As explained, the influence of the connection is incorporated in the proposed equation with the factor k_c.

$$u = \frac{FH^2 b k_c}{k_{t,EI}(EI)_s \alpha} + \frac{FH k_c}{k_{t,GA}(GA)_s \beta} + u_{p,sw}; \qquad \theta = \frac{FHb k_c}{k_{t,EI}(EI)_s \gamma}$$

First, the design of the connections is explained. Figure 5.21 shows a cross-section of a module at the shear wall. The five locations where the intra-module connections are located are presented and Figure 5.22 shows the enlarged details. All the elements are connected through screws of 8 mm diameter, but the length and angle differs. Detail 1 and 2 are the connections between the side wall and ceiling/floor and will be done with ⌀8x240 mm screws placed at an 90 degrees angle. Connection 3 connects the side- and shear wall, with ⌀8x260 mm screws placed at 90 degrees. Details 4 and 5 consist of two screws placed at an angle of 45 degrees. For connection 4, which is between the ceiling and shear wall, ⌀8x240 mm screws are used, while for connection 5, which is between the floor and shear wall, ⌀8x260 mm

screws are used. The direction of placement is different for connections 4 and 5, because of manufacturing convenience. As discussed in chapter 2.4, the connections have a certain stiffness.

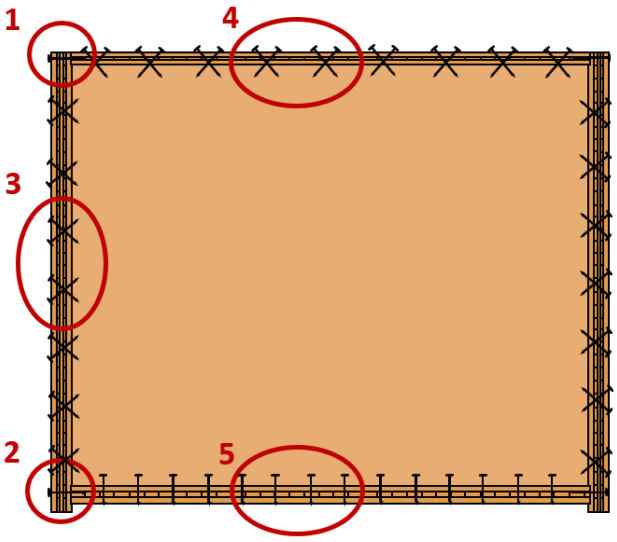

Figure 5.21: Cross-section of a module at the shear wall with the positions of the 5 intra-module connections

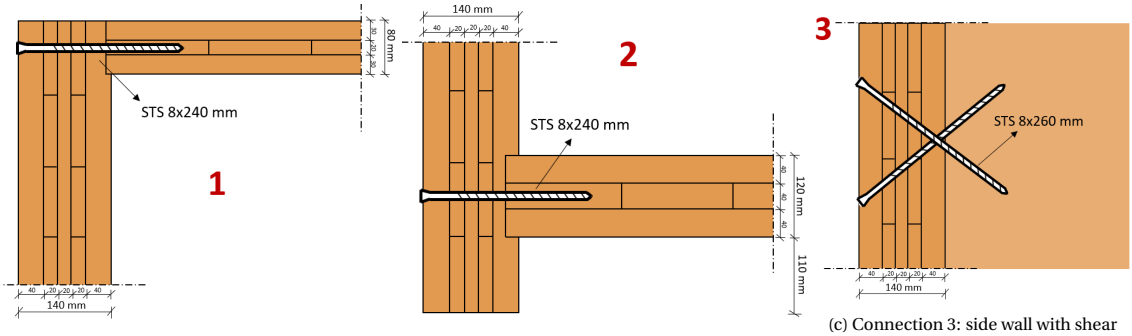

(a) Connection 1: side wall with ceiling

(b) Connection 2: side wall with floor

(c) Connection 3: side wall with shear wall

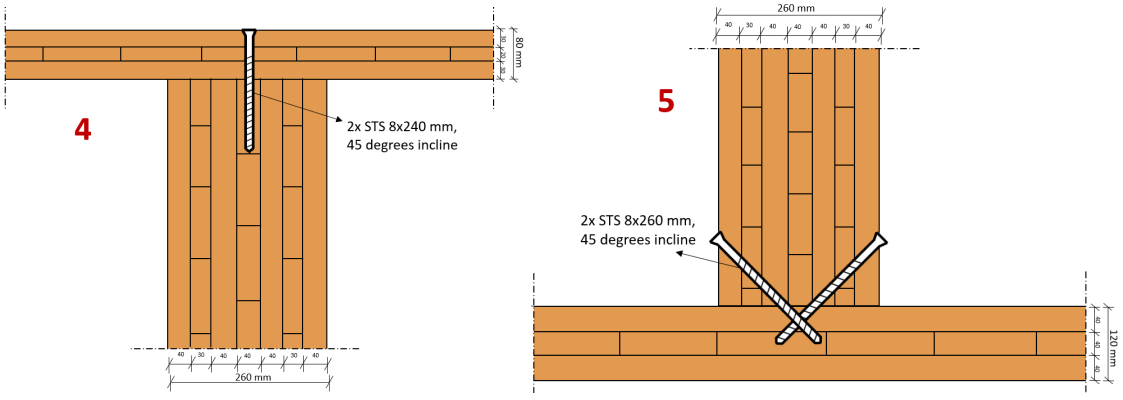

(d) Connection 4: Ceiling with shear wall

(e) Connection 5: Floor with shear wall

Figure 5.22: Details 1-5

The translational stiffness of the connections is listed in table5.6. Note that because the floor and ceiling are positioned slightly inside the side walls, additional stiffness arises. However, the value is difficult to

determine, so for simplification this additional stiffness is neglected. Only the stiffness from the screws is taken into account.

Table 5.6: Translation spring stiffness of the intra-module connections [29]

Connection	Kx [MN/m]	Ky [MN/m]	Kz [MN/m]
1	0.5	17.6	0.5
2	0.5	17.6	0.5
3	0.5	17.6	0.5
4	19.9	16.6	1.0
5	1.0	16.6	19.9

For the equation, three options will be presented. They differ in the spacing of the screws; the smaller the spacing, the stiffer the connection. Option A is the stiffest option, option B is the middle most and option C is the most flexible option. Table 5.7 presents the line-to-line spring stiffness that is used for modelling.

Table 5.7: Modelling line-to-line stiffness of the three options. Spacing in mm and stiffness in MN/m/m

Connection	Option A 'Stiff'				Option B 'Medium'				Option C 'Flexible'			
	spacing	Kx	Ky	Kz	spacing	Kx	Ky	Kz	spacing	Kx	Ky	Kz
1	100	5.0	176.0	5.0	200	2.5	88.0	2.5	300	1.7	58.7	1.7
2	75	6.7	234.7	6.7	150	3.3	117.3	3.3	225	2.2	78.2	2.2
3	125	159.2	140.8	4.0	250	79.60	70.4	2.0	375	53.1	46.9	1.3
4	100	199.0	166.0	10.0	200	99.5	83.0	5.0	300	66.3	55.3	3.3
5	100	10.0	166.0	199.0	200	5.0	83.0	99.5	300	3.3	55.3	66.3

The modelled springs have an equal tension and compression stiffness, which in most cases is correct. However, in some directions, elements will collide if compression occurs. That accounts for the y-direction for all five connections. This means that the compression should be rigid and the tension flexible, but SCIA gives no option to model that precisely. Therefore, non-linear springs are used with 10 times as stiff compression value compared to the tension. Figure 5.23 shows for connection 1, option A how that looks. This way the collision of the elements is modelled as accurate as possible. Using non-linear springs means that a non-linear calculation must be performed. The Newton-Raphson method is used, where the load is applied is five steps. The maximum number of iterations is 50. No geometric or physical non-linearities are considered.

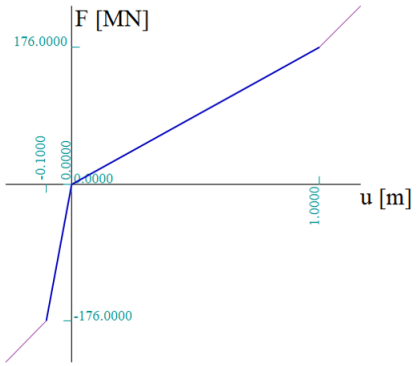

Figure 5.23: non-linear function of connection 1, option A

The factor k_c can now be determined for the four module configurations and the three connection

design options. In the numerical model, the connection stiffnesses are modelled and the linear elastic analysis is performed. Similar as for the main equations, the module height and width are adjusted to find the corresponding displacement and rotation. Plotting the results next to the found relations with the standard connection design (i.e. fixed translational stiffness), shows the influence of the three design options. Figure 5.24 shows for module 0 the found relations with the continuous curve. As can be seen, the displacement and rotation increase significantly for the three design options A, B and C. The factor k_c should account for this increase and will be in the form of $\frac{A}{bH}$. Adjusting these factors and incorporating them into the main equations results in the dashed lines in the graphs of Figure 5.24. Appendix D contains the results of all four module configurations.

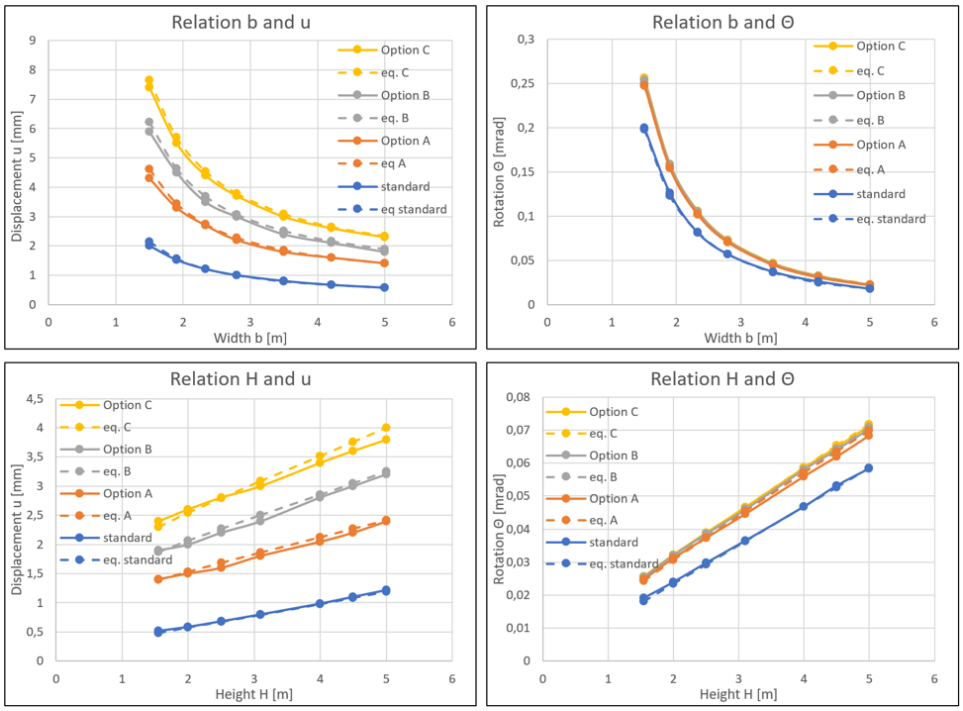

Figure 5.24: Relations for the connection design options of module 0

The values for k_c are chosen such that the equations show the best possible agreement with the found relations. Table 5.19 provides an overview of the factors $k_{c,u}$ and $k_{c,\theta}$ for the four module configurations and three connection design options.

Table 5.8: Factor k_c for the three connection design options

Module	$k_{c,u}$		
	A: 'stiff'	B: 'medium'	C: 'flexible'
0	$\frac{3.4}{b^{-0.1}H^{0.4}}$	$\frac{4.4}{b^{-0.1}H^{0.4}}$	$\frac{5.4}{b^{-0.1}H^{0.4}}$
1	$\frac{2.0}{b^{-0.1}H^{0.3}}$	$\frac{2.5}{b^{-0.1}H^{0.3}}$	$\frac{3.1}{b^{-0.1}H^{0.3}}$
2	$\frac{2,3}{b^{0.1}H^{0.2}}$	$\frac{2.9}{b^{0.1}H^{0.2}}$	$\frac{3.5}{b^{0.1}H^{0.2}}$
3	$\frac{2}{b^{0.4}}$	$\frac{2.1}{b^{0.4}}$	$\frac{2.3}{b^{0.4}}$

Module	$k_{c,\theta}$		
	A: 'stiff'	B: 'medium'	C: 'flexible'
0	$\frac{1.4}{b^{0.1}}$	$\frac{1.42}{b^{0.1}}$	$\frac{1.44}{b^{0.1}}$
1	$\frac{1}{b^{0.1}H^{-0.4}}$	$\frac{1.1}{b^{0.1}H^{-0.4}}$	$\frac{1.2}{b^{0.1}H^{-0.4}}$
2	$\frac{1.6}{b^{0.1}H^{0.1}}$	$\frac{1.7}{b^{0.1}H^{0.1}}$	$\frac{1.8}{b^{0.1}H^{0.1}}$
3	1.02	1.04	1.06

5.4.2. SHEAR WALL THICKNESS

The shear wall is the most important element for the transverse stiffness. Its dimensions determine the stiffness, because it influences the second moment of area I. The length of the wall is already incorpo-

rated separately in the proposed equation with the module width, but the shear wall thickness is not. The shear wall thickness will be included in the formula by the factor k_t. The values will be different for the bending and shear term of the equations.

$$u = \frac{FH^2bk_c}{k_{t,EI}(EI)_s\alpha} + \frac{FHk_c}{k_{t,GA}(GA)_s\beta} + u_{p,sw}; \qquad \theta = \frac{FHbk_c}{k_{t,EI}(EI)_s\gamma}$$

The standard thickness was chosen as 260 mm as discussed in Chapter 4.2. However, when designing a modular building, it could be necessary to choose a thicker or thinner shear wall to create a stiffer or less stiff module. Three shear wall design that are commonly used are therefore considered in this study. A thinner and a thicker design than the standard shear wall thickness [22]. Below, the build-up of the walls is listed:

- Smaller design: 200 mm 5-ply (40/40/40/40/40)
- Main design: 260 mm 7-ply (40/30/40/40/40/30/40)
- Larger design: 300 mm 7-ply (45/40/45/40/45/40/45)

Calculating the factor k_t will be done in two steps. First, the bending stiffness $(EI)_s$ and shear stiffness $(GA)_s$ must be determined again, because they are different for varying shear wall thicknesses. Table **??** provides an overview of the stiffnesses per module configuration and shear wall thickness.

Table 5.9: Standard stiffnesses for the three shear wall thicknesses

Module	$(EI)_s$ $[kNm^2]$			$(GA)_s$ $[kN]$		
	t=200	t=260	t=300	t=200	t=260	t=300
0	$8.26\cdot10^6$	$9.20\cdot10^6$	$1.02\cdot10^7$	$3.57\cdot10^5$	$4.79\cdot10^5$	$5.21\cdot10^5$
1	$2.91\cdot10^6$	$3.49\cdot10^6$	$3.72\cdot10^6$	$2.62\cdot10^5$	$3.37\cdot10^5$	$3.70\cdot10^5$
2	$2.51\cdot10^6$	$2.96\cdot10^6$	$3.16\cdot10^6$	$1.81\cdot10^5$	$2.34\cdot10^5$	$2.58\cdot10^5$
3	$1.18\cdot10^6$	$1.42\cdot10^6$	$1.54\cdot10^6$	$1.53\cdot10^5$	$1.98\cdot10^5$	$2.17\cdot10^5$

The second step is to determine the values for k_t. In the numerical model, the adjusted shear wall designs are modelled and the analysis is performed to find the corresponding horizontal displacement and rotation. Subsequently, the found results are divided by the results of the standard shear wall thickness of 260 mm. The factor that follows becomes the value for k_t. Tables 5.10 and 5.11 show the values for k_t.

Table 5.10: Values for $k_{t,u}$

Module	$k_{t,u,EI}$			$k_{t,u,GA}$		
	t=200	t=260	t=300	t=200	t=260	t=300
0	0.93	1.00	0.99	1.10	1.00	0.95
1	0.99	1.00	1.01	1.06	1.00	0.98
2	0.98	1.00	1.02	1.06	1.00	0.99
3	1.20	1.00	0.94	1.25	1.00	0.92

Table 5.11: Values for $k_{t,\theta}$

Module	$k_{t,\theta,EI}$		
	t=200	t=260	t=300
0	1.09	1.00	0.96
1	1.17	1.00	0.94
2	1.15	1.00	0.94
3	1.18	1.00	0.94

5.4.3. SHEAR WALL POSITION

In the proposed equations, the shear wall is located in the middle of the module. It could be possible however that the shear wall is placed more to the side. This asymmetric design will influence the lateral displacement because the horizontal load causes a torsional moment due to the eccentricity of the load. The additional displacement $u_{p,sw}$ that occurs should be added to the displacement of the module.

$$u = \frac{FH^2bk_c}{k_{t,EI}(EI)_s\alpha} + \frac{FHk_c}{k_{t,GA}(GA)_s\beta} + u_{p,sw}; \qquad \theta = \frac{FHbk_c}{k_{t,EI}(EI)_s\gamma}$$

The mechanism that cause the extra displacement is visualized in figure below, where 5.25a shows the deflection d_{sym} in the symmetric situation and 5.25b shows the extra displacement $u_{p,sw}$.

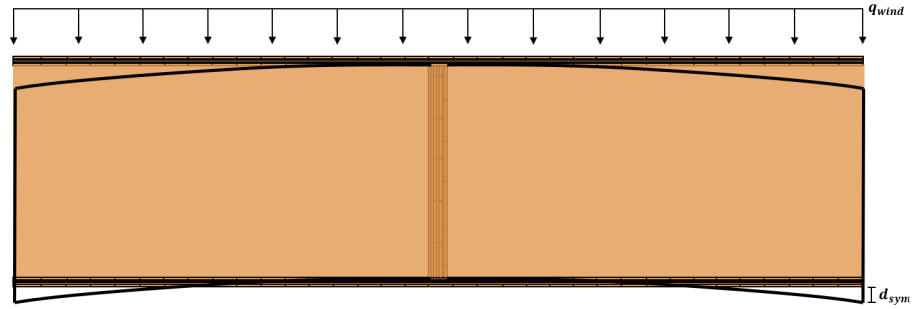

(a) Deflection of the diaphragm in a symmetric design

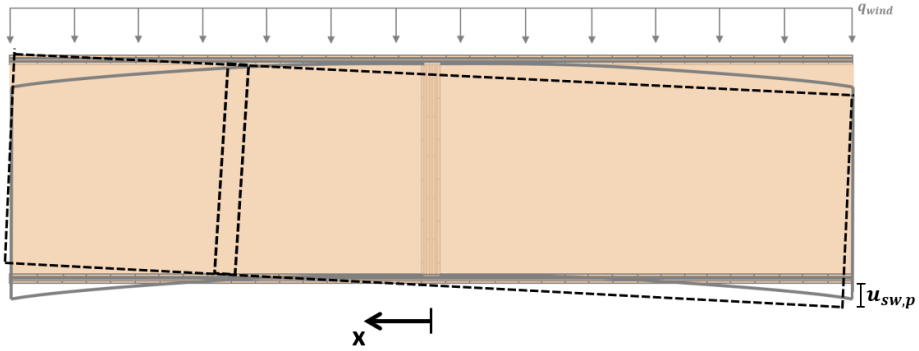

(b) Deflection of the diaphragm in an asymmetric design

Figure 5.25: Deflection of the diaphragm in symmetric and asymmetric designs

How large the additional displacement is, depends on different aspect. The formula for $u_{p,sw}$ is derived here. The eccentric wind load, relative to the shear wall position x of the building, determines the magnitude of the torsional moment. The distributed wind load is multiplied with the length to obtain the concentrated wind load that acts as a point load in the middle of the module (equation 5.26).

$$F = q_w * L \tag{5.26}$$

Multiplying this load with the eccentricity gives the torsional moment, see equation 5.27. This force is resisted by the side walls of the module who are positioned perpendicular to the wind load. To get the compression and tension force $F_{t/c}$ that acts on these walls, the torsional moment should be divided by the width of the module (equation (5.28)).

$$M_T = F * x \tag{5.27}$$

$$F_{c,t} = \frac{M}{b} \tag{5.28}$$

This force $F_{c/t}$ leads to the extension and compression of the side walls Δ_l. The relation between the force and Δ_l is obtained with SCIA and is shown in Figure 5.26. A distributed load of 5 kN/m (concentrated load F of 60 kN) is applied to a module with standard dimensions. Subsequently, the shear wall is translated along x, which gives the torsional moment, whereafter $F_{t,c}$ can be determined. This force is plotted against Δ_l in Figure 5.26. The relation can be described with the formula $\Delta_l = 0.004F$.

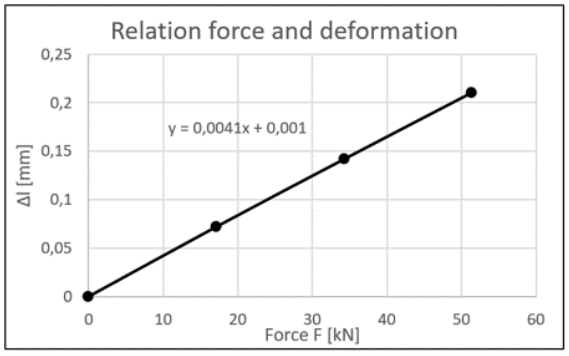

Figure 5.26: Relation between the concentrated wind load F and Δ_l

With the obtained compression or extension of the side walls, the rotation of the shear wall can be calculated. Hereafter, the torsion induced displacement can be calculated (equations 5.29 and 5.30).

$$\phi = \frac{2 * \Delta_l}{b} \tag{5.29}$$

$$u_{p,sw} = \phi * L \tag{5.30}$$

Substituting equations 5.26 - 5.30 gives the equation for $u_{p,sw}$.

$$u_{p,sw} = \frac{Fx}{125b^2}(x + \frac{L}{2}) \tag{5.31}$$

5.4.4. TEST OF THE EXTENSIONS

The extensions of the equations are established by only looking at one varying design option at a time, but the equation should also work when all three vary simultaneously. Therefore, three module designs are made and the numerical results are compared with the results of the proposed equations. The three design vary for the choice of the shear wall thickness, connection stiffness and shear wall position. Table 5.12 shows the design choices and the displacement results for all the module configurations. The equation results have an error between 0 and 8%. Table 5.13 presents the results of the rotation for the three designs.

Comparing the results shows that the difference between the proposed equation results and the numerical results are between 0 and 8%. For the rotation equation, the difference with the numerical results are between 0 and 3%. Again, it is assumed that the results have sufficient accuracy when the errors are below 10%. Therefore, it can be concluded that the proposed extensions of the equations do work when multiple design choices are adjusted.

Table 5.12: Validation of the displacement equations for three module designs

Design choices			Displacement u [mm]							
Shear wall thickness	Connection option	Shear wall position	Module 0		Module 1		Module 2		Module 3	
			SCIA	Equation	SCIA	Equation	SCIA	Equation	SCIA	Equation
t = 200 mm	A	1 m	2.4	2.6 (8%)	3.4	3.6 (6%)	8.6	8.6 (0%)	71.1	73.4 (3%)
t = 260 mm	B	2 m	2.9	3.1 (6%)	4.0	4.1 (3%)	9.8	9.3 (5%)	75.5	76.8 (2%)
t = 300 mm	C	3 m	3.8	4 (5%)	4.9	5.1 (4%)	11.3	10.5 (7%)	81.2	83.0 (2%)

Table 5.13: Validation of the rotation equations for three module designs

Design choices			Rotation θ [mrad]							
Shear wall thickness	Connection option	Shear wall position	Module 0		Module 1		Module 2		Module 3	
			SCIA	Equation	SCIA	Equation	SCIA	Equation	SCIA	Equation
t = 200 mm	A	1 m	0.045	0.046 (2%)	0.040	0.039 (2%)	0.067	0.068 (1%)	0.042	0.041 (2%)
t = 260 mm	B	2 m	0.046	0.045 (2%)	0.043	0.042 (2%)	0.069	0.070 (1%)	0.041	0.041 (0%)
t = 300 mm	C	3 m	0.043	0.043 (0%)	0.046	0.046 (0%)	0.072	0.074 (3%)	0.040	0.041 (3%)

5.5. WORKFLOW

Now that all the equations are established, a workflow is introduced to provide a guide on how to use the equations. When designing a timber modular building, this workflow can be used to calculate the horizontal displacement and rotation in the transverse direction of an individual module. The steps are here:

1. The first step is to choose the module configuration. This research provides four possible options: module 0, 1, 2 and 3.

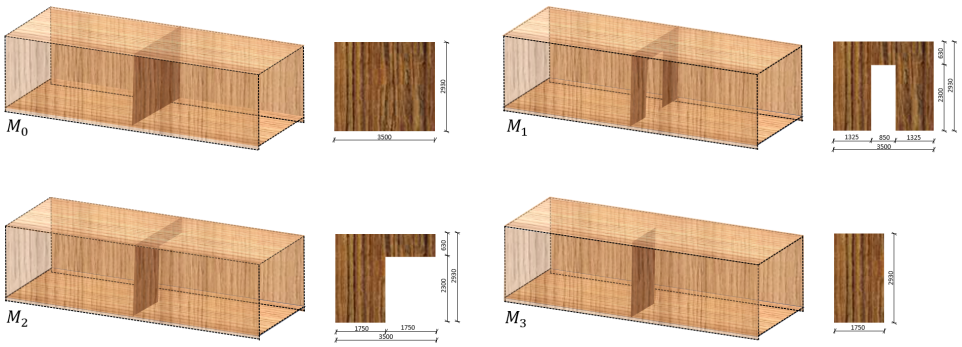

Figure 5.27: Design of the four module configurations

2. Consequently, the choice of the module configuration results in corresponding equations that predicts the displacement and rotation of the module (u_M and θ_M). These equations consist of various factors that depend on the dimensions of the module and of constants that depend on the design of the module. The dimensions are chosen in step 3, while the design is chosen in steps 5, 6 and 7.

Table 5.14: Equations for the module configurations

Module	Equation	
	Displacement	Rotation
0	$u_{M0} = \frac{FH^2bk_c}{k_{t,EI}(EI)_s\alpha} + \frac{2.8FHk_c}{k_{t,GA}(GA)_s\beta} + \frac{5.5MH^2}{(EI)_s\chi} + u_{p,sw}$	$\theta_{M0} = \frac{22FHbk_c}{k_{t,EI}(EI)_s\gamma} + \frac{22MH}{(EI)_s\lambda}$
1	$u_{M1} = \frac{10FH^2bk_c}{k_{t,EI}(EI)_s\alpha} + \frac{3.3FHk_c}{k_{t,GA}(GA)_s\beta} + \frac{1.6MH^2}{(EI)_s\chi} + u_{p,sw}$	$\theta_{M1} = \frac{14FHbk_c}{k_{t,EI}(EI)_s\gamma} + \frac{8MH}{(EI)_s\lambda}$
2	$u_{M2} = \frac{8FH^2bk_c}{k_{t,EI}(EI)_s\alpha} + \frac{10FHk_c}{k_{t,GA}(GA)_s\beta} + \frac{2MH^2}{(EI)_s\chi} + u_{p,sw}$	$\theta_{M2} = \frac{10FHbk_c}{k_{t,EI}(EI)_s\gamma} + \frac{7MH}{(EI)_s\lambda}$
3	$u_{M3} = \frac{150FH^2bk_c}{k_{t,EI}(EI)_s\alpha} + \frac{10FHk_c}{k_{t,GA}(GA)_s\beta} + \frac{0.8MH^2}{(EI)_s\chi} + u_{p,sw}$	$\theta_{M3} = \frac{4.2FHbk_c}{k_{t,EI}(EI)_s\gamma} + \frac{3.3MH}{(EI)_s\lambda}$

3. In this step, the decision on the module dimension is made. The length, height and width can be chosen. The standard dimensions are 12 x 3.1 x 3.5 m respectively. From the chosen dimensions, the shear wall height ($H_{sw} = H - 170$) and design follows.

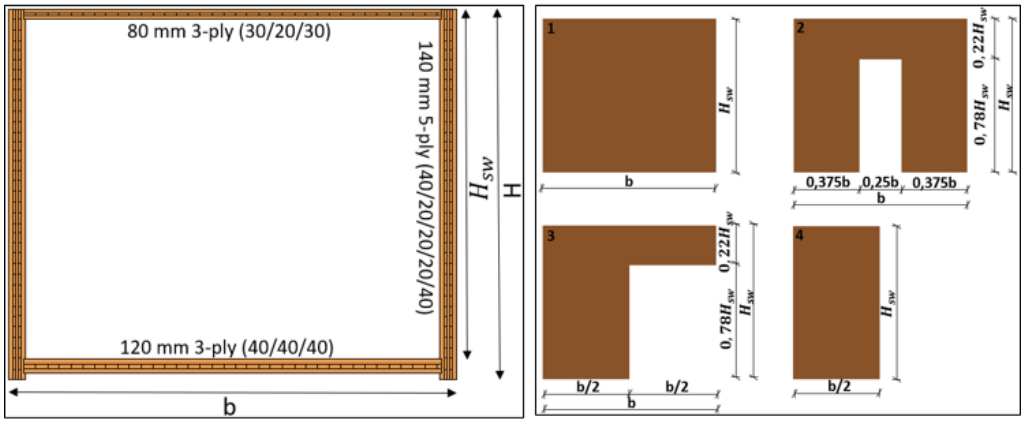

Figure 5.28: Module dimensions H, b and H_{sw} (left) and the corresponding shear wall design (right)

4. In step 4 the constants $\alpha, \beta, \chi, \gamma$ and λ are calculated based on the chosen dimensions. These factors adjust the standard shear and bending stiffness to account for varying dimensions

Table 5.15: Determination of the constants

Module	α	β	χ	γ	λ
0	$b^{0.6}$	$(\frac{b}{3} - 0.167)H^{0.4}$		b^3	
1	$b^{1.9}H^{0.2}$	$(\frac{b}{3} - 0.167)H^{0.3}$	bH	$b^3H^{0.7}$	$b^2H^{0.6}$
2	$b^{0.5}H^{0.5}$	$(\frac{b}{3} - 0.167)H$		$b^{2.8}H^{0.2}$	
3	$b^{1.15}$	$(\frac{b}{3} - 0.167)$		$b^{3.1}$	

5. Step 5 gives the option to choose the shear wall position x, where x=0 m is the center of the module and x increases as the shear wall translates along the module. For x=6 m the shear wall is at the end of the module. Choosing the position of the shear wall will give the value x after which the additional displacement $u_{p.sw}$ can be calculated with the following equation.

$$u_{p,sw} = \frac{Fx}{125b^2}(x + \frac{L}{2})$$

6. The thickness of the shear wall is chosen in step 6. The three options will lead to the standard bending and shear stiffness $(EI)_s$ and $(GA)_s$. Subsequently, the constants $k_{t,sw,EI}$ and $k_{t,sw,GA}$ follow.

Table 5.16: Standard stiffnesses for the three shear wall thicknesses

Module	$(EI)_s$ $[kNm^2]$			$(GA)_s$ $[kN]$		
	t=200	t=260	t=300	t=200	t=260	t=300
0	$8.26 \cdot 10^6$	$9.20 \cdot 10^6$	$1.02 \cdot 10^7$	$3.57 \cdot 10^5$	$4.79 \cdot 10^5$	$5.21 \cdot 10^5$
1	$2.91 \cdot 10^6$	$3.49 \cdot 10^6$	$3.72 \cdot 10^6$	$2.62 \cdot 10^5$	$3.37 \cdot 10^5$	$3.70 \cdot 10^5$
2	$2.51 \cdot 10^6$	$2.96 \cdot 10^6$	$3.16 \cdot 10^6$	$1.81 \cdot 10^5$	$2.34 \cdot 10^5$	$2.58 \cdot 10^5$
3	$1.18 \cdot 10^6$	$1.42 \cdot 10^6$	$1.54 \cdot 10^6$	$1.53 \cdot 10^5$	$1.98 \cdot 10^5$	$2.17 \cdot 10^5$

Table 5.17: Values for $k_{t,u}$

Module	$k_{t,u,EI}$			$k_{t,u,GA}$		
	t=200	t=260	t=300	t=200	t=260	t=300
0	0.93	1.00	0.99	1.10	1.00	0.95
1	0.99	1.00	1.01	1.06	1.00	0.98
2	0.98	1.00	1.02	1.06	1.00	0.99
3	1.20	1.00	0.94	1.25	1.00	0.92

Table 5.18: Values for $k_{t,\theta}$

Module	$k_{t,\theta,EI}$		
	t=200	t=260	t=300
0	1.09	1.00	0.96
1	1.17	1.00	0.94
2	1.15	1.00	0.94
3	1.18	1.00	0.94

7. Step seven gives the option for the connection stiffness. Three options are given, which leads to the constant k_c.

Table 5.19: Factor k_c for the three connection design options

Module	$k_{c,u}$		
	A: 'stiff'	**B: 'medium'**	**C: 'flexible'**
0	$\frac{3.4}{b^{-0.1}H^{0.4}}$	$\frac{4.4}{b^{-0.1}H^{0.4}}$	$\frac{5.4}{b^{-0.1}H^{0.4}}$
1	$\frac{2.0}{b^{-0.1}H^{0.3}}$	$\frac{2.5}{b^{-0.1}H^{0.3}}$	$\frac{3.1}{b^{-0.1}H^{0.3}}$
2	$\frac{2.3}{b^{0.1}H^{0.2}}$	$\frac{2.9}{b^{0.1}H^{0.2}}$	$\frac{3.5}{b^{0.1}H^{0.2}}$
3	$\frac{2}{b^{0.4}}$	$\frac{2.1}{b^{0.4}}$	$\frac{2.3}{b^{0.4}}$

Module	$k_{c,\theta}$		
	A: 'stiff'	**B: 'medium'**	**C: 'flexible'**
0	$\frac{1.4}{b^{0.1}}$	$\frac{1.42}{b^{0.1}}$	$\frac{1.44}{b^{0.1}}$
1	$\frac{1}{b^{0.1}H^{-0.4}}$	$\frac{1.1}{b^{0.1}H^{-0.4}}$	$\frac{1.2}{b^{0.1}H^{-0.4}}$
2	$\frac{1.6}{b^{0.1}H^{0.1}}$	$\frac{1.7}{b^{0.1}H^{0.1}}$	$\frac{1.8}{b^{0.1}H^{0.1}}$
3	1.02	1.04	1.06

8. When all steps are completed, the equation for the displacement and rotation is obtained with all values for the parameters, factors and constants. Below, the workflow is presented.

6

Calculation method for multi-storey modular buildings

The previous chapter proposed equations for the horizontal displacement and rotation of individual modules. These equations can be used to calculate the deflection of multi-storey modular buildings. This chapter describes the calculation procedure to determine the lateral deflection in transverse direction of multi-storey modular buildings. First, the deformation mechanisms that are taken into account in this research are elaborated on in Chapter 6.1. The modelling method for connected modules is discussed in Chapter 6.2. Next, the calculation method is described in Chapter 6.3 and a workflow is presented in Chapter 6.4. Finally, two examples are considered in Chapter 6.5 to check the calculation method against the numerical results.

6.1. INDIVIDUAL MODULE DEFORMATION

Chapter 3 described the deformation mechanisms of multi-storey modular buildings. In this study, the focus is only on the deformation of the module itself. Rotation and sliding of the modules is ignored, because inter-module connections are not studied specifically. The earlier stated assumption, that the resultant vertical force is negative, means there is no uplift of the modules and therefore no rotation can occur. Ignoring this term will therefore not result in incorrect calculations. Sliding of the modules occurs if the horizontal force is larger than the friction between the modules. By ignoring this deformation mechanism, the assumption arises that the friction between the modules is larger than the force, meaning that the modules stay in place. This will be taken as true and further investigation is outside the scope of this research. Since only the deformation of the module is taken into account, the proposed equations describe all necessary deformation mechanisms that are needed to calculate the deflection of multi-storey modular buildings. To summarize, four module deformation mechanisms were observed: horizontal displacement due to horizontal force u_V, horizontal rotation due to horizontal force θ_V, horizontal displacement due to bending moments u_M and horizontal rotation due to bending moment θ_M (see Figure 6.1). The proposed equations of Chapter 5 include terms for these deformations and will be integrated in the calculation of multi-storey modular buildings.

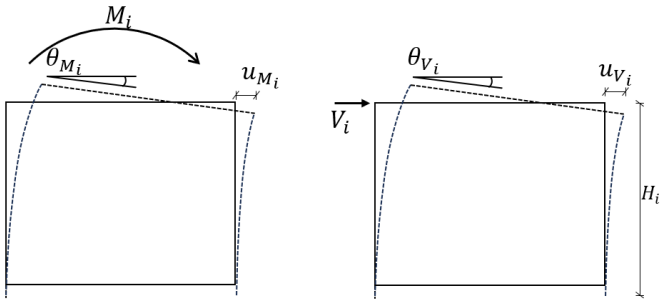

Figure 6.1: The four deformation contributions θ_M, u_M, θ_V and u_V

6.2. MULTI-STOREY DEFORMATION

Expanding from single module deformation to multi-storey deformation is explained here. Figure 6.2 shows for a six-storey building, with horizontal wind loading, the shear force and bending moment distribution. Also, the deformation behaviour is presented. To calculate the deformation, the displacement of the module itself is added with the displacement due to the cumulative effect that is caused by the module rotation. As explained, four terms lead to the deformation, where u_v and u_M cause the module displacement and θ_V and θ_M cause the cumulative effect.

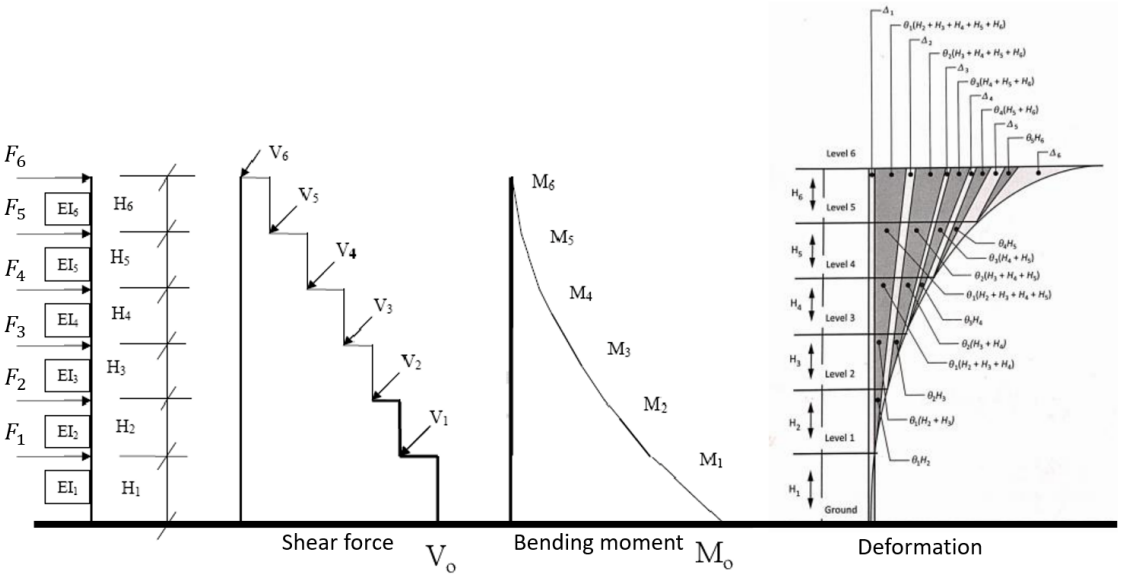

Figure 6.2: Force distribution and deformation behaviour of a six-storey building [37][38] (adjusted)

To begin with, it must be noted that the horizontal rotation due to the shear force is much smaller than the rotation due to the bending moment. Especially for higher structures, this difference is significant, meaning that θ_V can be neglected. This results in three remaining contributions. The total building displacement is the sum of the storey displacements. The lateral displacement of the i-th storey consists of the contribution due to the shear force, the bending moment at the top of the storey and the cumulative effect due to rotation of the lower storeys. For all three terms, an equation is proposed in the previous chapter. Substituting V and M in the proposed equations will give θ_M, u_M and u_V. For u_M the bending moment at the top of the storey is used. Summing u_M and u_V gives displacement of the module at the storey. Additionally, the displacement due to the cumulative effect should be calculated. The rotation calculated at a lower storey is multiplied with the height of the modules times the number of modules. Doing this for all lower modules gives the cumulative effect, as visualized in Figure 6.2. The

explained deflection calculation of multi-storey modular buildings with the proposed equation must be checked with results from the numerical simulations to see whether the results show good agreement. Therefore, the modelling of vertical and horizontal stacked modules is explained in the next section.

6.3. MODELLING OF VERTICAL AND HORIZONTAL STACKED MODULES

As a modular structure is considerably more complex than a traditional structure owing to the existence of inter-module connections, it is necessary to introduce a few assumptions for simplification. The calculation assumptions in this study are as follows:

- The vertical inter-module connection is a combination of vertical, horizontal and rotational springs. The vertical and horizontal spring stiffness is taken as infinite, meaning that the axial deformation is not considered. For the rotational spring, a stiffness of zero is used, resulting in a hinged connection.
- The horizontal inter-module connection, between adjacent modules on the same storey, is equivalent to a rigid connection ($k = \infty$). From this follows that the displacement of each module on the same storey is equal.
- The modules and inter-module connections stay in the elastic state.

From the above listed assumptions, the models for vertical and horizontal stacked modules can be constructed. Figure 6.3 contains these models, with on the left the vertical and on the right the horizontal stack. A modular building consists of m x n modules. In vertical direction, the modules are denoted from 1 to the i-th module and ends with module m. In horizontal direction, they also start with 1 and goes via the j-th module to the final n-th module. The modules have dimensions H x b. The lateral wind load that acts on the facade of the building is transferred through the side walls to the ceiling and floor of the modules. There, it will act as a distributed line load q on the ceiling. For simplification, the line load that acts on the floor is modelled at the ceiling of the module below. Multiplying this line load with the length gives the point load F as is shown in Figure 6.3.

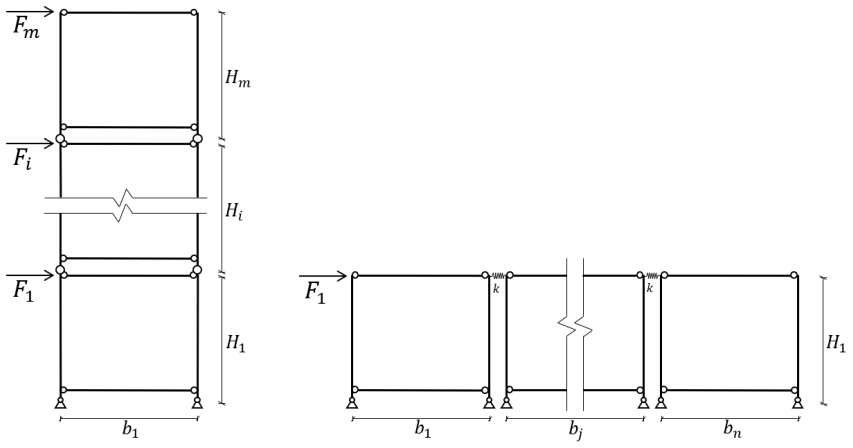

Figure 6.3: Simplified model of vertical (left) and horizontal (right) stacked modules

At the location where modules come together, a 2D connection scheme is presented in Figure 6.4. The intra- and inter-module hinges are visible, as well as the horizontal inter-module connection. The horizontal inter-module connections are modelled with a rigid 1d-element at the top of the modules.

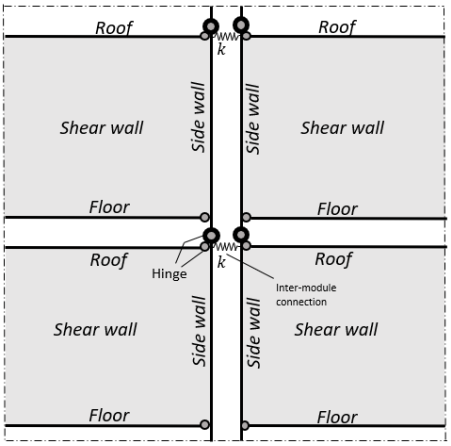

Figure 6.4: Modelling detail of horizontal and vertical connected modules

6.4. CALCULATION METHOD

The calculation method integrates the proposed equations with the theory. To do so, the equation results are compared with the numerical results of stacked modules. Stacking modules on top of- and next to each other creates a multi-storey modular building. The translation from the individual module equations to the calculation method of the total building deflection will take place in this section. First, the horizontal stacking is discussed, whereafter the focus shifts to vertical stacking.

6.4.1. HORIZONTAL STACKING

Positioning modules next to each other results in a distribution of force F, which is dependent on the stiffness of the modules. Having for example two modules, where one is twice as stiff as the other, leads to a force distribution of 2:1. However, because the assumption is that the displacement of each module at the same storey is equal and the system acts in series, the combined stiffness of the storey determines the storey displacement. In the case where the same module configurations are used in the entire storey, the force F can be divided by the number of modules n. When different configurations are situated in a storey, the force should be divided by the equivalent number of modules that can be calculated with the module stiffnesses. However, in this study it is assumed that all the modules on a storey have the same configuration. In building designs this is often the case and therefore the assumption is valid.

The theory that is described above is checked with the numerical model of module configuration 0. For the situation with a distributed q-load of 50 kN/m the displacement of 1, 2, 4 and 8 horizontally connected modules are compared. The distance between two modules is 80 mm and they are connection with five inter-module connections located at the edges, in the middle and in between the edge and middle. They are modelled as rigid bar, because it was assumed that $k = \infty$. The displacements are 8.4, 4, 1.9 and 0.9 mm respectively. This shows that with double the amount of modules, the displacement decreases by just over half (approximately 2.1). The reason for this is that at the location of the applied load, compression of the shear wall occurs, which results in part of the force going directly to the supports. A smaller force is therefore transferred to the next module. The reaction force at the support of the first module is thus higher than that of the others. If, for example, the force is applied at one of the other modules, that module would have higher reaction forces. To account for this, a factor k_n is introduced. It is found that when doubling the number of modules in a storey n_i, the displacement is 2,1 times lower, meaning 5% extra reduction. Since linear analysis is used, doubling the amount of modules is equal to dividing the force by two. Therefore, dividing the force by the number of modules will give a conservative result. Concretely, this means that for the proposed equations, the shear force V is divided by the number of modules at the storey: V_i / n_i. Besides, the bending moment due to the horizontal load is also divided by the number of modules n, because the tension and compression force due to the bending moment M is divided over the whole storey: M_i / n_i. At the end, a reduction factor k_n

is applied which is 1 for n = 1 and is subtracted with 0.05 every time n gets doubled. In between, linear interpolation can be applied. This approach reduces the m x n building to a m x 1 building, simplifying the calculations.

6.4.2. VERTICAL STACKING

Chapter 6.4 described the calculation method to predict the lateral deflection of a multi-storey modular building. In this section, the calculation with the proposed equations for vertical stacked modules is checked against numerical results. The proposed equations determine θ_M, u_M and u_V and with the explained calculation the deflection of the building can be calculated. The results are compared with the results from the numerical model. This is done for a building of m x 1 modules, with m having values of 2, 4, 6, 8 and 10. The modules have the standard dimensions (L x b x H = 12 x 3.5 x 3.1 m) and a distributed horizontal line load of 5 kN/m is applied at the top of every module. Figure 6.5 shows the numerical models of the four configurations for a 6 x 1 building. Figure 6.6 presents the deflected structures, the mesh size is again chosen as 400 mm. The deflection at every storey is taken at the top of the module at the location of the shear wall.

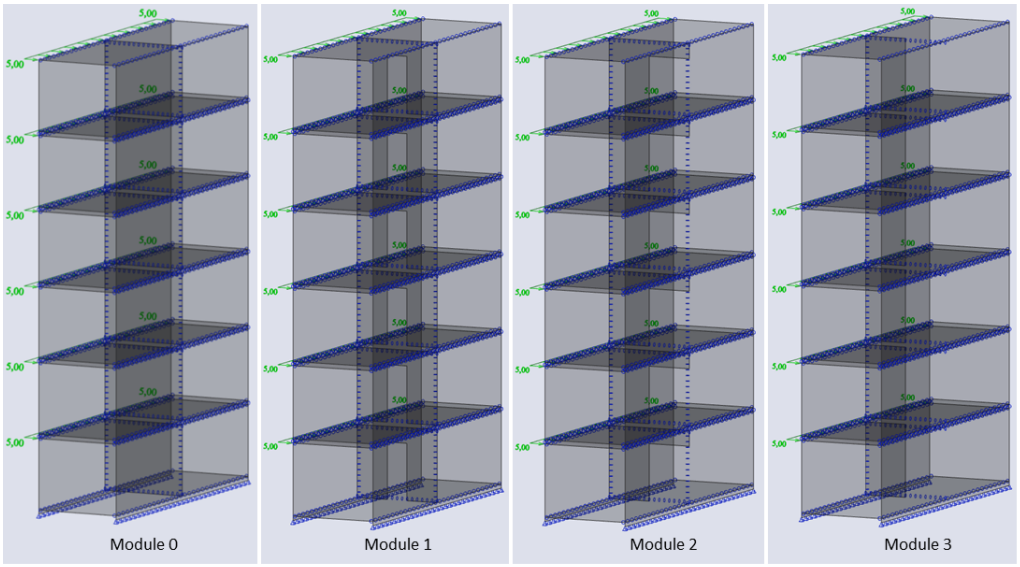

Figure 6.5: Numerical models of the four module configurations for a 6 x 1 building

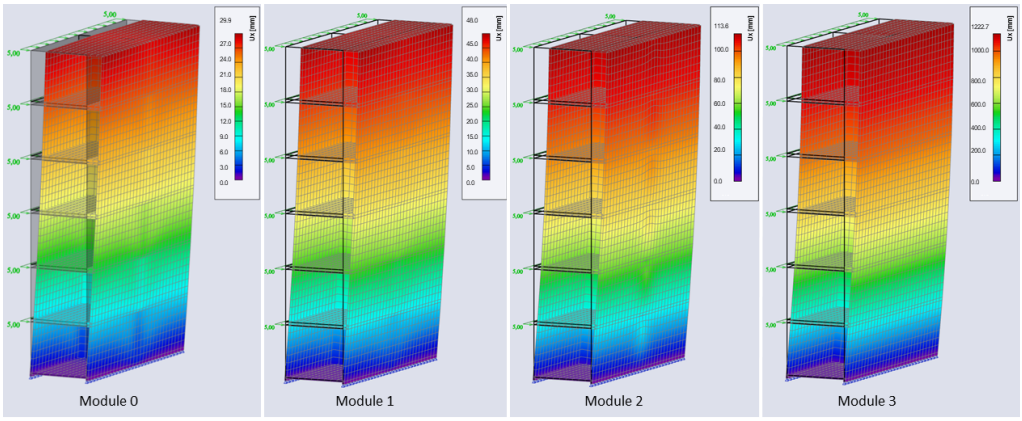

Figure 6.6: Lateral displacements of the four module configurations for a 6 x 1 building

The results are shown in Figure 6.7, where the displacement versus the storey number is plotted. The continuous curves are the numerical results and the dashed lines are the calculation results. Graphs a to d represent the module configurations 0 to 3 respectively.

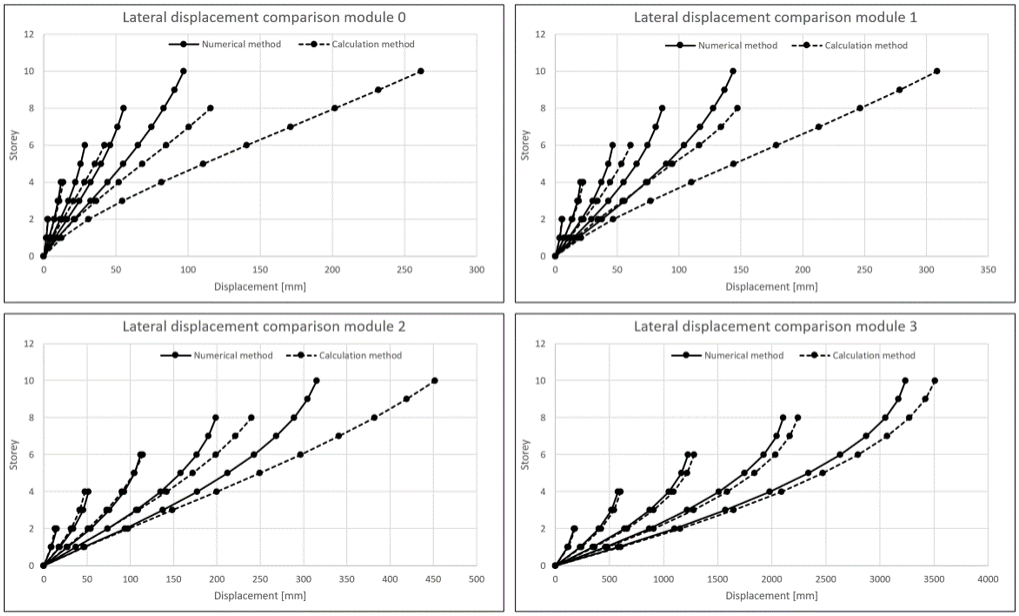

Figure 6.7: Lateral deflection of an m x 1 modular buildings

In the graphs it can be seen that the for all module configurations, the 2 and 4 storey building results show good agreement. However, when the height increases, the curves show significant different behaviour. A building with 10 storeys shows the biggest difference for module configuration 0 and 1 (170 and 115% respectively), for configuration 2 the difference is 43% and for module 3 this the lowest (8%). It can be concluded that the cumulative effect gets dominant for higher buildings and is overestimated. This can be assigned to the made assumptions when the equations were proposed and will be explained hereafter.

6.4.3. FORCE SPREAD FACTOR

When the equations were proposed, an assumption was made for the width of the acting force. As explained in chapter 4.4, the wind load that acts as a distributed load on the whole width of the facade is transferred through the shear walls to the lower modules. Therefore, the horizontal force on the lower module is concentrated around this shear wall. In the assumption, the load was spread over 1 meter. For the horizontal load this is a valid assumption since the load has to travel constantly through the shear walls and thus remains at this width. However, the compression and tension force in the side walls, caused by the bending moment, can spread over a larger width. The force is not transferred via the shear wall but through the continuous side walls. Consequently, the force spreads over a larger area. In Figure 6.8 this is visualised. For a 8-storey modular building with a distributed horizontal load of 1 kN/m at the top, the internal normal force is presented. It can be seen that going down the structure the force gets larger (because the bending moment increases) and also spreads. This means that for lower modules the force is acting over a larger width and this results in smaller deformations, because a larger part of the wall contributes in absorbing the force.

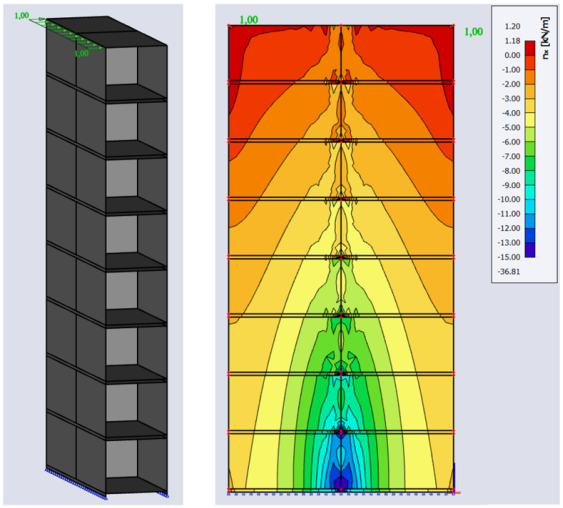

Figure 6.8: Visualization of the normal force spreading in a multi-storey modular building due to an applied lateral load at the top.

To incorporate this effect, a factor is introduced at every storey to account for the spreading of the load and the corresponding reduction of the deformation. First, it is investigated how much the reduction is for a certain force spread. In the initial situation, a width of 1 meter was assumed, meaning half a meter at both sides of the shear wall. Table 6.1 shows for a load of 1000 kN, that is applied at a certain width, the corresponding vertical and horizontal displacement of the side wall. Comparing the results with the initial width gives the reduction factor. It shows that the reduction factor is equal for the vertical and horizontal displacement and that for the first meters the reduction is large and after that slowly decreases.

Table 6.1: Displacement due to spreading of the force

q [kN/m]	**width [m]**	$U_z[mm]$	$U_x[mm]$	**Factor**
1000	1	1.8	1.8	1.00
500	2	1.1	1.1	0.61
333.3	3	0.8	0.8	0.44
250	4	0.6	0.6	0.33
200	5	0.5	0.5	0.28
166.7	6	0.4	0.4	0.22
142.9	7	0.35	0.35	0.19
125	8	0.3	0.3	0.17
111.1	9	0.25	0.25	0.14
100	10	0.23	0.23	0.13
90.9	11	0.21	0.21	0.12
83.3	12	0.19	0.19	0.11

The factor that has to be used per storey can now be determined. Important to mention is that because a horizontal load is applied on every storey, all spreading along the height of the building, every storey should have a factor for all the individual horizontal loads. However, this makes it complicated and therefore for simplification it is chosen to only apply one factor per storey that incorporates the force spread of all the horizontal loads.

Determining the exact spreading of the force over the building height is difficult. Therefore, numerical results are used and compared with the calculation results. By applying a force spread factor at every storey, the calculation results can be matched with the results from SCIA. The factors are chosen such

that for every storey, the force spreads equally. Or in other words, for every storey you go down, the load is spread over an equally increased width. The objective is to follow the deformation behaviour of the numerical model, meaning that the results do not have to match exactly, but the displacement curve should be parallel. This is done because there are other aspects that can cause deviations, but not the deformation shape. Figure 6.9 shows the results for the same models as in the previous analyses, but with the force spread factor per storey as is presented in table 6.5. The top storey does not have a factor, because the force does not start to spread yet. The factor is multiplied with θ_M to reduce the overestimation of the cumulative effect. For a building with m storeys, the load spread factor is applied as follows: for the top storey, the factor for storey m is used. Subsequently, the factor for storey m-1 is used for the second-highest storey and so on until the ground module is reached.

Table 6.2: Force spread factor per storey

Storey	**m-9**	**m-8**	**m-7**	**m-6**	**m-5**	**m-4**	**m-3**	**m-2**	**m-1**	**m**
force spread factor k_f	0.14	0.17	0.19	0.22	0.28	0.33	0.44	0.61	1.00	-

The graphs show again the displacement versus the storey number for the different module configuration. In the graphs, it is visible that the calculation method curves follow the numerical method curves. Although they have no perfect agreement, the introduced load spread factor results in a matching deformation behaviour.

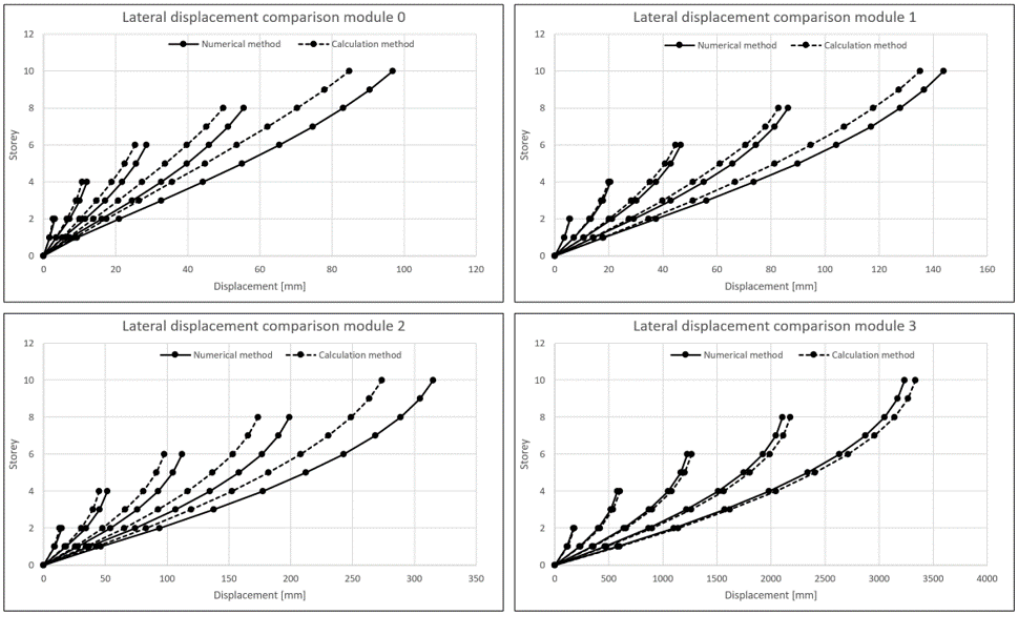

Figure 6.9: Lateral displacements of an m x 1 modular buildings. Situation with the force spread factor

6.4.4. CORRECTION FACTOR

Finally, to get a better agreement between the results, a correction factor k_{cor} is introduced. They are chosen such that the calculation method results show the best possible agreement with the numerical results for all values of m. In the process of proposing the equations, several simplifications and assumptions were made. For example, the rotation due to the bending moment was taken as equal for all module configurations. In reality however, there will be some small differences. Another assumption was that in the equation proposal, the load was applied at one meter width to simulate the force transfer to a lower module. In the stacked modules the load is modelled over the total length and the FEA determines how the load is transferred. The one meter is a simplification, how much the load really spreads can be different. The correction factor incorporates these effects.

Table 6.3: Correction factor

Module	k_{cor}
0	1.17
1	1.04
2	1.15
3	0.98

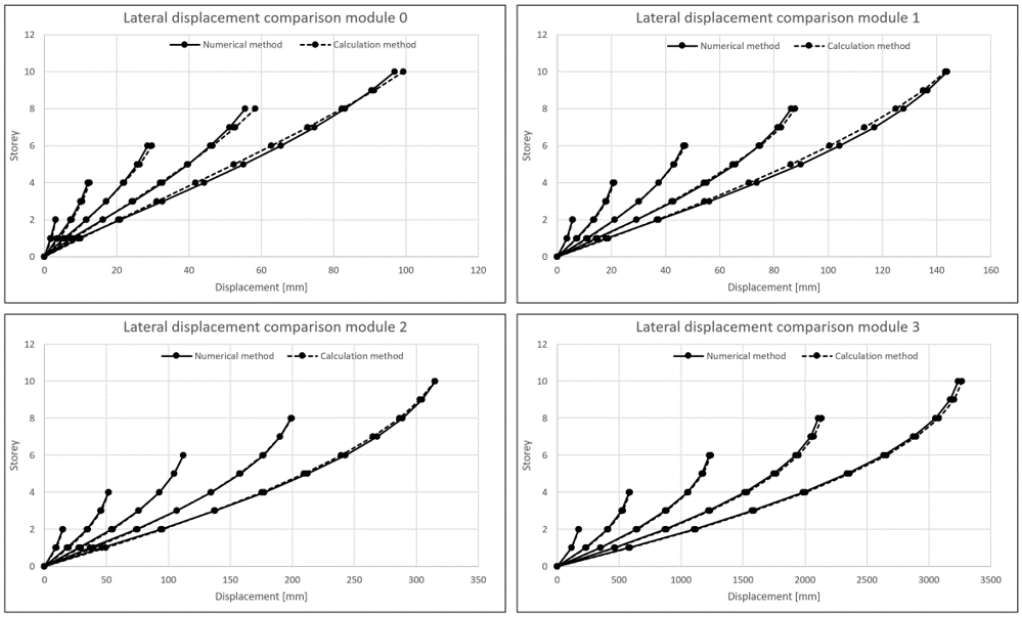

Figure 6.10: Lateral displacements of an m x 1 modular buildings. Situation with the force spread- and correction factor

After this correction factor is applied, the results are plotted in Figure 6.10. Now the calculation results show good agreement with the SCIA results. The deviations at the top of the buildings are listed in table 6.4. The accuracy lies between 0 and 5% which is lower than 10%, meaning the calculation method results in good prediction of the lateral deflection of modular buildings in transverse direction.

Table 6.4: Results of the numerical analysis and hand calculation

number of storeys	2		4		6		8		10	
Module	SCIA	calc.	SCIA	calc.	SCIA	calc.	SCIA	calc.	SCIA	calc.
0	3.1	3.1 (2%)	12.0	12.5 (5%)	28.5	29.8 (4%)	55.5	58.3 (5%)	96.9	99.3 (2%)
1	5.7	5.8 (1%)	20.6	21.1 (2%)	46.6	47.3 (2%)	86.4	87.7 (2%)	143.8	143.3 (0%)
2	14.8	14.9 (1%)	51.6	51.8 (0%)	112.0	112.2 (0%)	198.8	199.5 (0%)	315.3	314.8 (0%)
3	173.3	176.3 (2%)	579.5	589.4 (2%)	1227.4	1240.6 (1%)	2107.0	2132.9 (1%)	3234.0	3267.2 (1%)

6.5. WORKFLOW

A workflow is presented to have a brief overview on the calculation procedure. First, the applied assumptions are listed, whereafter the specific steps for determining the lateral deflection of a multi-storey modular building using the proposed method are given.

Assumptions:

- One module configuration is applied in the entire building.
- Local effects at the storeys are not considered.

• Vertical loads are not taken into account.

Specific steps:

1. Choose the building dimensions m × n.
2. Choose the module configuration that will be used. Design the module with workflow 1 that is presented in chapter 5.5 and determine the corresponding equations for u_V, u_M, θ_V and θ_M. Remove the term for θ_V.
3. Determine the wind load that acts on the building and calculate F per storey. Calculate the shear force and bending moment distribution along the building. Divide V and M by the number of modules n.
4. Calculate u_V, u_M and θ_M for every storey.
5. Reduce θ_M with the force spread factor. For the top storey, use the factor according to storey 10. The second-highest storey gets the factor for storey 9, and so on until the lowest module is reached.

Table 6.5: Force spread factor per storey

Storey	**m-9**	**m-8**	**m-7**	**m-6**	**m-5**	**m-4**	**m-3**	**m-2**	**m-1**	**m**
force spread factor	0.14	0.17	0.19	0.22	0.28	0.33	0.44	0.61	1.00	-

6. Calculate the cumulative effect per storey due to θ_M.
7. Sum the three displacements to obtain the inter-storey drift per storey.
8. Reduce the displacement with k_n. For n = 1, k_n = 1, and for doubling the number of modules n, 0.05 is subtracted. In between, linear interpolation can be applied.
9. Accumulate the storey displacements to obtain the total building displacement.
10. Multiply with k_{cor} to find the deflection of the building..

Table 6.6: Correction factor

Module	k_{cor}
0	1.17
1	1.04
2	1.15
3	0.98

6.6. EXAMPLES

Two examples are evaluated in this study: a four storey, four span building with module configuration 1 (Example 1) and a eight by eight building with module configuration 3, which is based on hotel Jakarta (Example 2). Based on the workflow for the calculation method as described above, the lateral deflection is calculated. The results are compared with the numerical results.

6.6.1. EXAMPLE 1

This example consists of a four storey, four span building designed with module configuration 1. Table 6.7 shows the design characteristics of the building. The modules have dimensions L x b x H of 3.3 x 3.7 x 12 m. As for the design choices, shear wall thickness 300 mm, connection design B and shear wall position x=2 m are chosen. A horizontal distributed load q of 6 kN/m is applied at the top of every

storey. As discussed earlier, the horizontal stiffness of the inter-module connections are modelled as rigid ($k = \infty$). The mesh size is 400 mm. The numerical model is shown in Figure 6.11(a).

Table 6.7: Design characteristics example 1

			Building design		**Module dimensions**				**Module design**	
Characteristic	m	n	Module configuration	q_w	H	b	L	Shear wall thickness	Connection design	Shear wall position
Value	4	4	1	6 kN/m	3.3 m	3.7 m	12 m	300 mm	B	x = 2 m

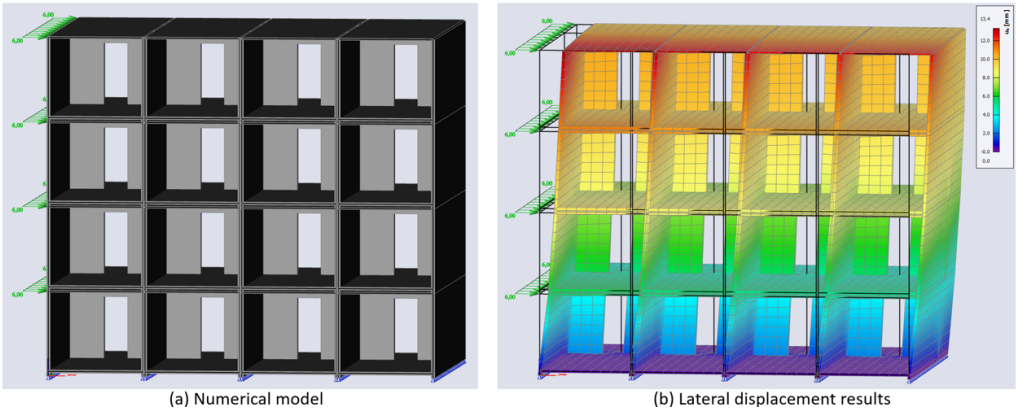

(a) Numerical model (b) Lateral displacement results

Figure 6.11: Numerical analysis of Example 1

The results of the numerical model are shown in Figure 6.11b. Note that the maximum displacement occurs at the edge due to local effects, while the proposed equations predict the displacement at the location of the shear wall. The displacement of the numerical model at the shear wall (u_{SCIA}) is given in table 6.8. They are compared with the calculation results, which consist of the module displacement due to shear force u_V and bending moment u_M plus the displacement due to the cumulative effect u_{θ_M}. Summing these displacements gives the inter-storey drift Δ_s and by accumulating the total displacement u_T is obtained. The last step is to include the correction factors k_{cor} (=1.06) and k_n (=0.9) to find $u_{T,f}$. The results of the numerical model and calculation method indicate that the difference is in the range between 0 and 8.7%. Thus, the errors are below 10% meaning the calculation method results are in good agreement with the numerical results. As the obtained values are larger, the results are safe. Comparison of the lateral deflection obtained by the proposed method and the numerical simulations are shown in Figure 6.12.

Table 6.8: Lateral displacement of Example 1

Storey	u_V **[mm]**	u_M **[mm]**	u_{θ_M} **[mm[**	Δ_S **[mm]**	u_T **[mm]**	$u_{T,f}$ **[mm]**	u_{SCIA} **[mm]**	**Error [%]**
4	1.13	0	0.3	1.43	12.09	11.2	10.3	8.7
3	2.25	0.02	0.25	2.52	10.66	9.9	9.2	7.6
2	3.38	0.06	0.15	3.59	8.14	7.6	7.1	7.0
1	4.5	0.04	0	4.55	4.55	4.3	4	7.5

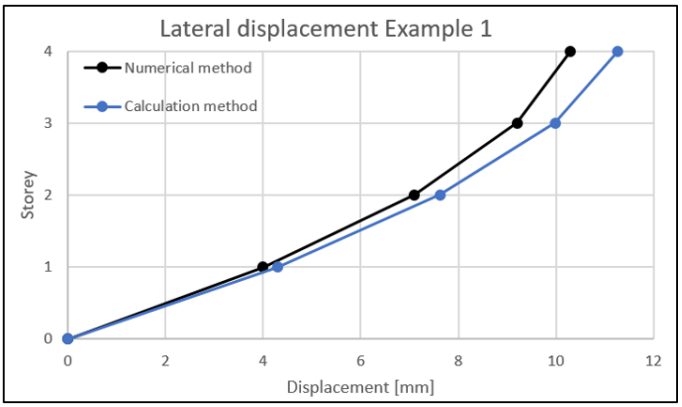

Figure 6.12: Lateral displacement of Example 1

6.6.2. EXAMPLE 2

An eight-storey, eight-span timber modular building is evaluated in Example 2. The example is inspired on Hotel Jakarta, which is evaluated in the study of R. Gijzen [3]. Within the design choices that are given in this study, the design of Hotel Jakarta will be approached. The relevant model parameters and details are provided in table 6.9.

Table 6.9: Design characteristics example 2

			Building design		**Module dimensions**				**Module design**	
Characteristic	m	n	Module configuration	q_w	H	b	L	Shear wall thickness	Connection design	Shear wall position
Value	8	8	3	kN/m	2.9 m	3.5 m	9 m	200 mm	A	x = 0.5 m

Figure 6.13a shows the numerical model of the building. Module configuration 3 is chosen with module dimensions of L x b x H of 9 x 3.5 x 2.9 m. The design choices are as follows: shear wall thickness t=200 mm, connection design A and shear wall position x=0.5 m. The horizontal wind load differs per storey and can be seen in Figure 6.13a. From top to bottom the values for q are: 2.18, 4.36, 4.36, 4.36, 3.79, 3.60, 3.38 and 3.10 kN/m respectively. Subsequently, the shear force V and bending moment M over the building can be calculated.

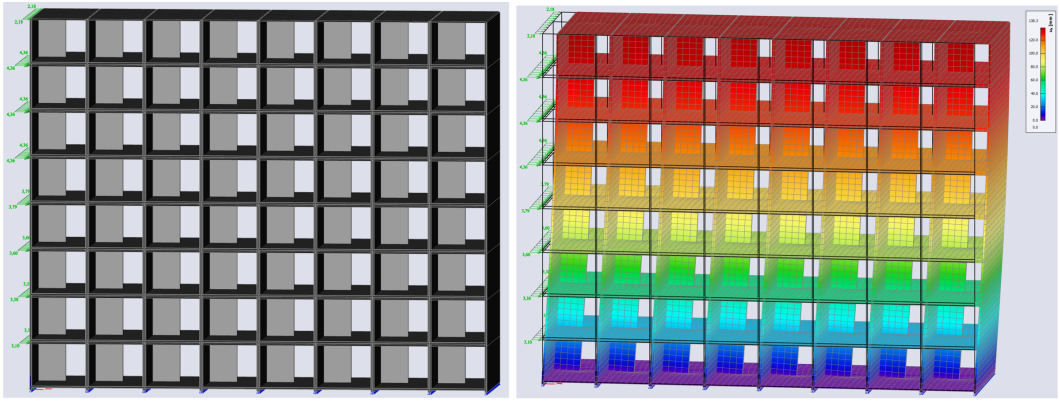

(a) Numerical model of Example 2

(b) Results of Example 2

Figure 6.13: Numerical analysis of Example 2

The deformation of the numerical model is shown in Figure 6.13b where the horizontal displacement is presented. Per storey, the displacement value u_{SCIA} is listed in table 6.10. In the table, the inter-storey

drift is given as a result of the three terms u_V, u_M and u_{θ_M}. Accumulating and incorporating the factors $k_{cor} = 0.98$ and $k_n = 0.85$ results in the total building displacement. Comparing the calculation method results and the numerical results show an error between 0 and 9.5%. The curves in graph 6.14 show good agreement and because the error is below 10% it can be concluded that sufficient accurate results were obtained. As the calculated values are larger, the results are safe.

Table 6.10: Lateral displacement Example 2

Storey	u_V **[mm]**	u_M **[mm]**	u_{θ_M} **[mm[**	Δ_S **[mm]**	u_T **[mm]**	$u_{T,f}$ **[mm]**	u_{SCIA} **[mm]**	**Error [%]**
8	2.70	0.00	1.79	4.49	169.88	141.5	137.9	2.6
7	7.96	0.03	1.74	9.73	165.39	137.8	133.9	2.9
6	13.22	0.06	1.62	14.90	155.66	129.7	125.6	3.2
5	18.47	0.11	1.42	20.00	140.76	117.3	113.1	3.7
4	23.19	0.14	1.16	24.50	120.76	100.6	96.4	4.3
3	27.50	0.18	0.82	28.51	96.26	80.2	76.1	5.3
2	31.55	0.21	0.44	32.19	67.75	56.4	52.6	7.3
1	35.32	0.24	0.00	35.56	35.56	29.4	26.8	9.5

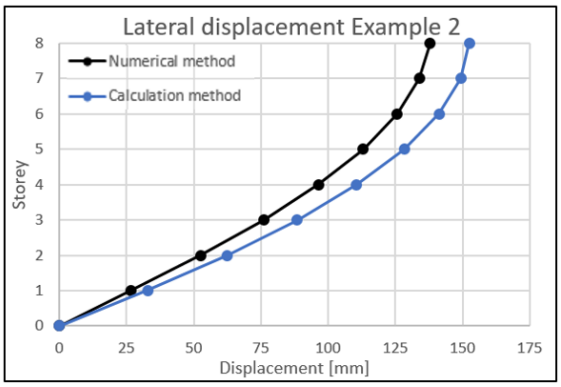

Figure 6.14: Lateral displacement of Example 2

7

Case study verification

This chapter contains a verification for the proposed calculation method. A case study is used to verify if the method provides an accurate prediction of the transverse lateral deflection of multi-storey modular buildings. The case study is explained in Chapter 7.1. Hereafter, Chapter 7.1 calculates the lateral deflection of the modular structure. Finally, the calculation method results are compared with the official results in Chapter 7.3.

7.1. POPPIES

The case study that is used is the building Poppies, which is located in Amsterdam and constructed by the company Van Rossum Raadgevende Ingenieurs. It is a timber modular building that is divided in four blocks: block A to D. Block A is a self-supporting modular structure that is stabilized by timber shear walls in both directions. For the transverse direction, the shear walls inside the module have to provide the lateral stability. In this case study, block A is analysed. The lateral deformation in transverse direction is calculated with the proposed equations and calculation method. The results are subsequently compared with the results of the internal documents of the company. These results will be referred to as the Van Rossum results. By verifying the calculation method with the practical case study, it can be investigated whether the method is applicable to the company's calculation process.

Figure 7.1: Cross section of Poppies with block A indicated [41]

7.1.1. STRUCTURAL DESIGN

Block A is a four-storey, six-span building that consists of CLT modules. The structure is 23.1 m wide and 12.3 m deep. The height of the four storeys is 12.4 meter. It is supported by a concrete podium construction that consist of beams and columns. Between the modules, a cavity of 80 mm is present and four steel plates connect the horizontal aligned modules. In vertical direction the modules are separated by sound bearing strips and no vertical connections are needed because no tension forces

occur. Fire safety is provided by gypsum boards.

MODULE DESIGN

The modules have a length of 12.3 m, a width of 3.58 m and a height of 3.1 m. The shear wall in transverse direction has an opening at one side of 1.625 x 2.232 m. It is located 2.82 m from the center. The build-up of the CLT elements is as follows:

- Side walls: 140 mm thick 5-ply (40-20-20-20-40)
- Roof: 80 mm thick 3-ply (30-20-30)
- Floor: 120 mm thick 3-ply (40-40-40)
- Shear wall: 260 mm thick 7-ply (40-30-40-40-40-30-40)

MODEL AND DEFORMATION

The numerical model used for the Van Rossum calculation is shown in Figure 7.2. The assumptions that correspond to the model are as follows:

- The bottom modules are supported with pinned supports
- Floor and ceiling are connected with hinges to the side walls
- The floor and ceiling are not connected to the shear wall
- Between vertical stacked modules, sound bearing strips are modelled with a E-modulus of 5 MPa.
- No tension between the module arises.

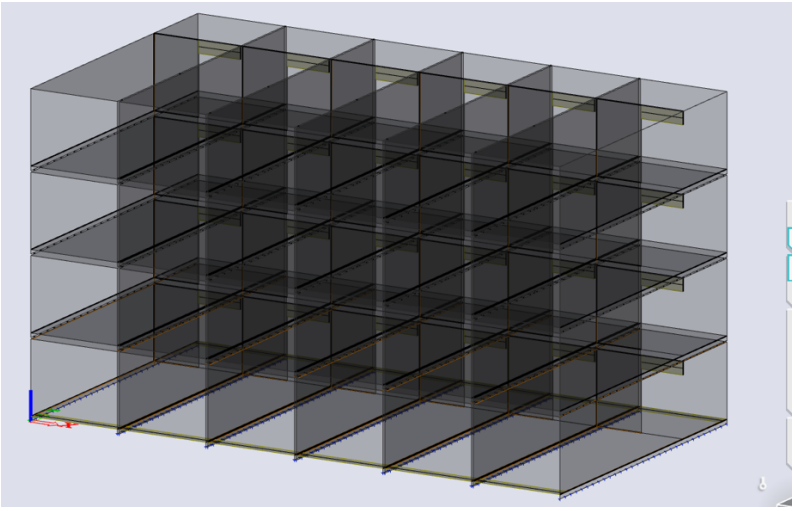

Figure 7.2: Van Rossum model of Poppies [41]

The horizontal wind load acting on the building is calculated in the documents. For block A, the wind load has a magnitude of 0.92 kN/m^2. The pressure and suction coefficients are 0.8 and 0.6 respectively. A reduction factor of 0.85 may be used because pressure and suction will not act simultaneous. As a result, the wind load is $1.095 kN/m$. Figure 7.3(a) shows how the load is applied on the building. The deformation corresponding to the loading is shown in Figure 7.3(b). The results are taken at the location of the shear wall and are compared later with the proposed calculation method.

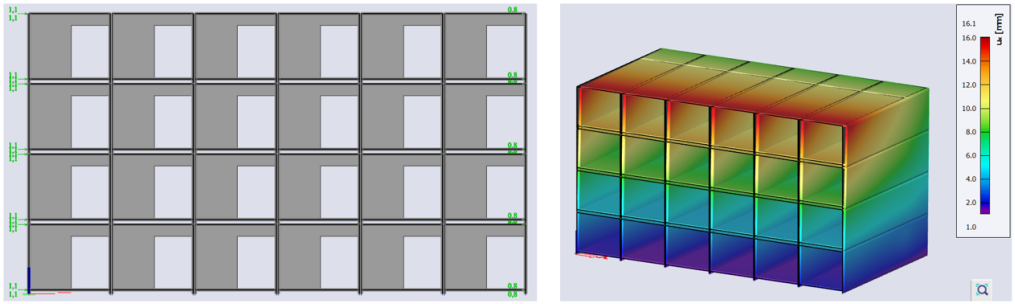

Figure 7.3: Numerical analysis of Van Rossum [41]

7.2. PREDICTING THE LATERAL DEFLECTION

The structural design as described above can now be used to predict the lateral deflection of the building. The proposed equations and calculation method is used to calculate the lateral deflection in transverse direction. Within the possibilities of the design options that are given in the study, the design of Poppies will be approached as good as possible. These design choices are determined first, whereafter the calculation based on the workflows as presented in chapter 5.5 and 6.5 is performed.

7.2.1. DESIGN

To match the design of Poppies block A, the following design choices that lie within the possibilities of the proposed equations are made. The building size m x n is 4 x 6 modules. The module design is in good correspondence with module configuration 2. The module dimensions are: L x b x H = 12.3 x 3.58 x 3.1 m. The CLT elements have equal dimensions except for the floor, which is 20 mm thicker in the design of Poppies. For the shear wall a thickness of 260 mm is taken, equal to the design of Poppies. Its position is 2.82 m from the center. In the analyses of Poppies the connection stiffness is not considered, so this won't be taken into account in the calculation as well. An overview of the design is given in table 7.1. Overall, the Poppies design can be matched closely with the design choices of the proposed equations.

Table 7.1: Design characteristics Poppies

	Building design			**Module dimensions**			**Module design**		
Characteristic	m	n	Configuration	H	b	L	Shear wall thickness	Connection design	Shear wall position
Value	4	6	2	3.1 m	3.58 m	12.3 m	260 mm	-	x = 2.82 m

7.2.2. CALCULATION

To begin with, the workflow from chapter 5.5 is followed to obtain the equations for the deformation of the module. The first step is to pick the module configuration, which is M2. The corresponding equation for the displacement and rotation is found in step 2 (equation 7.1 and 7.2).

$$u_{M2} = \frac{8FH^2bk_c}{k_{t,EI}(EI)_s\alpha} + \frac{10FHk_c}{k_{t,GA}(GA)_s\beta} + \frac{2MH^2}{(EI)_s\chi} + u_{p,sw} \tag{7.1}$$

$$\theta_{M2} = \frac{10FHbk_c}{k_{t,EI}(EI)_s\gamma} + \frac{7MH}{(EI)_s\lambda} \tag{7.2}$$

The third step is to set the module dimensions, after which the shear wall dimensions follow. The dimensions L x b x H are 12.3 x 3.58 x 3.1 m, this means that the height of the shear wall is 3.1 - 0.17 = 2.93 m. The opening in the shear wall is 0.5*3.58 = 1.79 m wide and 0.78*2.93 = 2.29 m high. Now that the dimensions are known, the constants $\alpha, \beta, \chi, \gamma$ and λ in equations 7.1 and 7.2 can be determined in

step 4. From b = 3.58 and H = 3.1 their values can be calculated: α = 3.33 β = 3.18 χ = 25.27 γ = 44.58 and λ = 11.10.

Step 5 calculates $u_{p,sw}$. Since x = 2.82, the additional displacement $u_{p,sw} = 0.19\,mm$. Then in step 6, the shear wall thickness is chosen, which is 260 mm. This gives $(EI)_s = 2.96 * 10^6\,kNm^2$ and $(GA)_s = 2.34 * 10^5\,kN$. Also $k_{t,u,EI} = 1$, $k_{t,u,GA} = 1$ and $k_{t,\theta,EI} = 1$ follow. The last step is to choose the connection design. Since the connections are not considered in the analyses of Poppies, $k_{c,u}$ and $k_{c,\theta}$ are equal to 1.

All factors and constants for the equations of a individual module are now known, except for the forces V and M. That will be determined when the calculations on the global structure is performed. Chapter 6.5 gives the specific steps for determining the lateral displacement of a multi-storey timber modular building using the method proposed in this study. First, the building size m x n is chosen. Block A of Poppies is a four-storey, six-span building, as such m = 4 and n = 6. The next step is to calculate the horizontal wind load F that acts on the top of every storey. The distributed wind load q is multiplied by the length of the module to obtain force F. For Poppies, wind load F for storey 4 to 1 is 23.4, 46.7, 46.7 and 23.4 kN respectively. Subsequently, the shear force and bending moment distribution along the building can be calculated. V and M are then divided by the n, which is 6. The force distribution is presented in table 7.2. By substituting V and M in the obtained equations from the first part (7.1 and 7.2), the values for u_V, u_M and θ_M are obtained. The term θ_V can be neglected. For θ_M the force spread factor must be applied, whereafter the displacement per storey due to the cumulative effect can be calculated. The penultimate step is to collect the individual displacement contributions per storey and accumulate them to find the lateral displacement at the top. Finally, k_{cor} and k_n are multiplied with the displacement. In this case k_{cor} = 1.15 and k_n = 0.875. Below, table 7.2 shows all the outcomes.

Table 7.2: Lateral deflection prediction of Poppies

Storey	**V** [kN]	**M** [kNm]	u_V [mm]	u_M [mm]	θ_M [mrad]	u_{θ_M} [mm]	Δ_S [mm]	u_S [mm]	u_T [mm]
4	23.37	0	0.47	0.00	0.000	0.08	0.55	5.09	5.12
3	70.11	72.45	1.01	0.01	0.004	0.07	1.08	4.54	4.57
2	116.85	289.79	1.55	0.02	0.009	0.04	1.61	3.46	3.48
1	140.22	652.02	1.82	0.03	0.014	0.00	1.85	1.85	1.86

Note: V and M are not yet divided by n, u_{θ_M} denotes the cumulative effect displacement, Δ_S denotes the total displacement per storey, u_S denotes the displacement at every storey and u_T is the final displacement including k_{cor} and k_n.

7.3. RESULTS

The results are compared with the Van Rossum results. Figure 7.4 shows the graph with the plotted deflections. The black curve represents the Van Rossum results and in blue the results from the proposed calculation method are displayed. The displacement at the top are 9.2 and 5.1 mm respectively. The results have a difference of 45%, with the calculation method having smaller values.

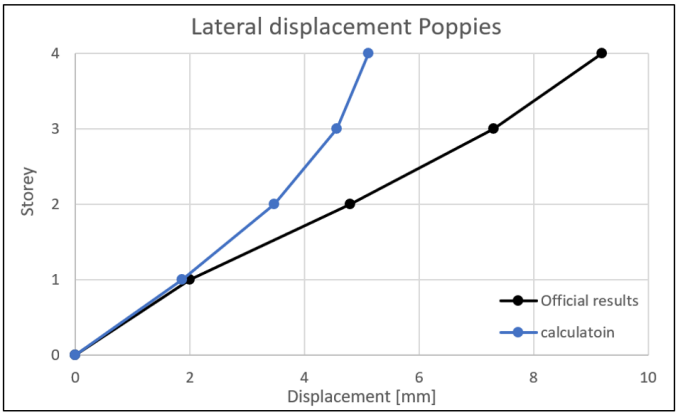

Figure 7.4: Lateral deflection of Poppies

The large difference can be assigned to different aspects. The most important difference between the models is the existence of soundproofing bearing strips. In the Van Rossum analysis these are included, while they are not incorporated in the calculation method. These strips have a very low stiffness and therefore deform significantly. Especially in vertical direction, it can cause an extra rotation of the module, which subsequently leads to extra cumulative effects and thus additional deflections. That is also the reason why at higher storeys the results have less agreement. At the first storey the results only have a deviation of 7.5%, because the influence of the mentioned extra rotation is not present. At higher storeys, this additional rotation gives the extra deflection and that is why the results show more deviating results. Another aspect is that the shear walls were not connected to the roof and floor of the modules. This reduces the stiffness and therefore larger deformations can occur.

Everything considered, the results do have significant differences, but those are explainable. This means that in hindsight, it is not possible to verify the calculation method with this case study. At the same time, it can also not be rejected, because the different results can be explained.

8

Discussion

The outcomes of this research provided equations for the horizontal displacement and rotation of individual modules, which were integrated in a calculation method that predicts the lateral deflection of multi-storey timber modular buildings in transverse direction. The results indicated that the proposed equations provide accurate results of the horizontal displacement and rotation of the designed modules. Two examples demonstrated that the calculation method is capable of predicting the lateral deflection of modular buildings. A case study verification investigated the practical application of the calculation method. Because deviating results were found, shortcomings of the method were revealed. In this chapter, the results, modelling approaches, implications of certain assumptions and limitations are discussed.

RESULTS

The proposed equations showed overall sufficient accurate results, because errors lower than 10% were found. Several design choices were integrated, increasing their applicability. The extensive validation of the numerical simulations proved the reliability of the model. The extended equations showed sufficient results as well, as errors were below 4%. Only the main equation test of module configuration 2 showed an error of 12%. Even though this is larger than 10%, the results are considered as sufficient because of the small exceedance being for one test only. The equation for the moment induced displacement showed for 3 out of 12 results errors between 10 and 20%. Although these are too large, they could be explained by the confined use of decimals, that resulted in rounding errors. Presenting them with more decimals would have lowered the errors. In addition, a notion must be made on the number of tests. Every proposed equation was tested for three situations. The input parameters were chosen such that a wide variety of designs were tested. The three situations can however not represent all module designs. Even though practical applicable input parameters were chosen, errors of other designs are not known. However, it can be stated, that since the three cases showed sufficient accurate results, other designs will show accurate results as well.

The calculation method was validated with two examples. The lateral deflection of two created buildings was compared with numerical results. Results showed sufficient accurate results, with the errors being below 10% (9.5 and 7.0% for example 1 and 2 respectively). Additionally, the calculation method results were on the safe side, because larger deflections were obtained than those from the numerical results. It was shown that deflections of modular buildings that are designed within the scope of the study could be predicted accurately with the calculation method.

A case study was performed to investigate whether the calculation method could be applied to a practical example. A building constructed by the company Van Rossum Raadgevende Ingenieurs was chosen to verify if the method would be applicable for their calculations. The significant difference in results (45%) between the calculation method and the Van Rossum calculation can be explained by the design differences. The existence of sound proofing bearing strips and the lack of connection between

the shear- and side walls in the case study results in a higher deflection. Because the difference can be explained, this specific case study can not confirm or reject the practical applicability of the calculation method. However, it can be discussed that in practice, the sound proofing bearing strips are almost always applied. As such, the calculation method will not provide accurate results if the cumulative effect of the soundproofing bearing strips is not included. The calculation method results were smaller than the Van Rossum results, meaning that no safe results were found as well. It could be argued however that a company has the aim to design safe buildings. By doing so, a conservative approach is used to ensure a safe building and also be able to tackle possible future changes and setbacks. Therefore, it is unsure whether the Van Rossum calculations provide results that represent reality closely. Investigating this would be interesting for a future study.

As the calculation method shows sufficient accurate results for buildings within the design boundaries, but not for practical constructed buildings, it can be stated that the method is not applicable for later design stages. In early design stages, when exact calculations and numerical models are not yet made, the calculation method could provide a reference for engineering design. It gives quick insight in the consequences of certain design choices. Although it does not provide accurate results for buildings out of the boundary conditions, it can be used to make design decisions. Existing methods to explore module designs are not available, which makes a thorough calculation necessary in the early design stages. The significance of this research lies in the applicability in early design stages and the ease of use. Comparing the equations of this thesis to for example the study of Wang (2022), who proposed complex equations for the lateral displacement of steel column-supported modules, the relative simplicity of the equations stand out.

MODELLING

Modelling is done to represent reality as close as possible. In the study, a comprehensive validation was done on the modelling methods. However, capturing reality exactly is almost impossible. Therefore, a discussion on the model used and its weaknesses is necessary.

• The equations were proposed based on numerical analyses. Therefore, it was crucial that the numerical model represent reality as close as possible. No experiments that investigate the deformation of timber modules were found in literature. As a result, the numerical model could only be validated against comparable structures. Although the validation demonstrated that the model produced realistic results, it would be preferable to validate it with experiments on actual modules.
• Since the mesh size had significant influence on the results, an optimal mesh size was studied. Finding the optimal mesh size was based on an estimation. This leaves room for errors and by choosing a different mesh size, smaller or larger results could have been found. On the total results, it would have had a lower impact, because the correction factor would have tackled the differences.

ASSUMPTIONS

In the process, several assumptions and simplifications were made. The correctness and influence of them is discussed below.

• An important boundary condition for the use of the method was that the resultant vertical force must be negative. This means that uplift due to horizontal wind loading is prevented. The assumption is introduced to neglect the rocking deformation and making the results valid for wind loading in both directions. In practice, this boundary condition proves to be plausible, because self-supporting modular buildings are often low-rise buildings with more modules next to each other than on top of each other. Therefore, the resultant vertical force is in most situations negative and thus the equations can be applied.
• Local deformation effects were not considered. The maximum displacement was taken at the location of the shear wall and if necessary added with the torsion induced displacement. As the wind load is applied as a distributed load along the length of the module, additional displacement would occur at the edges. At the top storey, the additional displacement gives the maximum building displacement. In practice, often a middle value between the edge and shear wall is chosen to incorporate some local effects. However, local effects are mainly of importance at the top storey and therefore only slightly higher deflections would be obtained.

LIMITATIONS

The proposed equations and calculation method have several limitations, which are discussed here.

• For this research, a general applicable design was made for the modules. However, not all buildings are constructed with this design. For example, concrete floors are often applied, although the trend is to switch to timber floors. As it is one design only, the design freedom is restrained. To overcome this, several frequently used design choices were incorporated.
• Only buildings with one type of module configuration were examined. The proposed calculation method is therefore verified for those types of buildings only. The aim was to make the calculations possible for a modular building with various types of modules so that design freedom was achieved. Due to time constrains, this was not achieved.
• The focus of the study was specifically on the serviceability limit state. No calculations for the ultimate limit state were performed. That means that if the lateral deflection prediction fulfils the code requirements, no conclusions can be drawn on the strength of the structure.

9

Conclusions and recommendations

In this research, it was investigated if a calculation method can be developed to calculate the deflection of multi-storey timber modular buildings in transverse direction. In the final chapter of this thesis, the main findings are stated in Chapter 9.1. Hereafter, recommendations for future research based on the results and discussion are provided in Chapter 9.2.

9.1. CONCLUSIONS

This thesis dealt with research on lateral deflections of multi-storey timber modular buildings. The main objective was to propose a calculation method that is able to predict the lateral deflection in transverse direction of multi-storey modular buildings. By proposing equations for the deformation of individual modules and integrating them in multi-storey deflection calculations, a calculation method was established.

First of all, it was found that superposition of bending and shear deformation does not result in the total deformation of a module. The possibility of the shear wall to compress at the supports results in an additional deformation term. Equations are therefore proposed to incorporate this effect. On global scale, the lateral deflection of multi-storey timber modular buildings includes the lateral displacement of the module itself and the cumulative effect caused by the rotation of lower modules. Horizontal wind load results in both deformation due to shear forces and bending moments. Therefore, four deformation terms were included: horizontal displacement and rotation due to shear force and horizontal displacement and rotation due to the bending moment. It was found that the rotation due to the shear force was negligible, as it is substantial small compared to bending moment induced rotation.

In addition, the research showed that the proposed equations for the deformation of individual modules give sufficient accurate results for calculating the horizontal displacement and rotation of a module with a general applicable design. Equations for four different module configurations were established based on numerical models. Results showed errors less than 10%. The extension of the equations includes various design options such as intra-module connection design, shear wall thickness and shear wall position. Including them with factors into the equations makes it possible to use the formulas in a variety of designs. Accurate results for the extensions were obtained as well. Besides the lateral displacement of the module itself, the cumulative effect due to rotation of lower modules must be added to obtain the buildings' deflection. The proposed calculation method includes those terms. Based on two examples, the accuracy of the proposed calculation method has been demonstrated. Example 1 showed the maximum error of 8.7% at the top. Example 2 resulted in a maximum error of 9.5%, which was on the lowest storey. At the top, a difference of 2.6% was found. Both errors were lower than 10% and on the safe side, meaning they were sufficient accurate and safe. The excellent agreement between the predicted deflection and that obtained from a detailed finite element analysis suggests that the proposed calculation method is suitable for use by design engineers. Calculating the lateral deflections of

multi-storey timber modular buildings designed within the design conditions of the method is therefore possible.

A case study was performed to verify if the method is applicable in practice. The building design was outside the design conditions, mostly due to the existence of soundproofing bearing strips. Also, the lack of connections between the shear wall and ceiling was a notable difference. The results showed significant different results (45%). Even though these can be assigned to the mentioned deviating designs, the case study can not confirm or reject the practical applicability of the calculation method. However, because soundproofing bearing strips are often applied in practice, the calculation method is not suited.

This thesis aimed to answer the main research question stated in this research: *Is it possible to predict the lateral deflection in the transverse direction of multi-storey timber modular buildings with a calculation method based on proposed equations?*. The research showed that the proposed calculations can predict the lateral deflection of buildings that are within the design boundaries of the method. At the other side, the case study results show that for practical applicability, the method is not yet suited. The limitations of the method make detailed calculations, that are necessary in later design stages, not possible. For more detailed calculations, it is recommended to use finite element software. However, in early design stages where quick hand calculations are performed, the method shows its value. Compared to a parametric model that can be useful when a finite element software is needed in the early design stages, it provides quick insight in the effect of certain design choices on the building's deflection.

9.2. RECOMMENDATIONS

Based on the discussion and conclusion presented in this thesis, further recommendations can be proposed to enhance and expand the current research. Potential areas for future exploration and improvements are given here.

• The equations could be extended with many other design options. For example, concrete floors and different element sizes for the ceiling and floor could be added. Also, different connections types can be applied. For the included design choices in this research, the most common options were chosen. These reflect however not all possible options. Expanding the options will increase the design freedom and thus the applicability of the equations.

• The influence of soundproofing bearing strips was not considered. However, as they are common practice, including them in the analysis would increase the practical applicability and closer results to the reality will be found. The induced rotation can be calculated based on known equations. The cumulative effect can subsequently be calculated, resulting in the extra deflection.

• Analyses were performed on buildings with one module design applied in the whole building. It would be interesting to check the calculation method if buildings with multiple module configurations are used within the building. Would the proposed calculation method give accurate results in that case as well? The freedom of building design would increase drastically in that case.

• This research did not specifically examine inter-module connections. This led to neglecting two deformation mechanisms corresponding to this connection type: rocking and sliding. More realistic results could be obtained for the lateral deflection of multi-storey modular buildings when these mechanisms are included. This would have as a consequence that the vertical load should be added to the analysis, making it more complex.

• In the research, several aspects that contribute to the deflections of modular buildings are not considered, because they were outside the scope. For example, the inter-module connections, the second order effect and the notional loads influence the total building's deflection. A Finite Element software can perform exact calculation that include all aspects. An investigation in the benefits of parametric Finite Element Models could provide insight if such a model would offer a solution for detailed calculations in combination with early design choices.

Bibliography

[1] M. Lawson, R. Ogden, and C. Goodier, *Design in modular construction*. CRC Press, 2014.

[2] Rijksoverheid. "900.000 nieuwe woningen om aan groeiende vraag te voldoen." (n.d.), [Online]. Available: https://www.rijksoverheid.nl/onderwerpen/volkshuisvesting/nieuwe-woningen#:~:text=In%202021%20steeg%20het%20woningtekort,die%20een%20woning%20nodig%20hebben.. (accessed: 15-08-2023).

[3] R. Gijzen, "Modular cross-laminated timber buildings," M.S. thesis, TU Delft, Feb. 2017.

[4] M. F. Musa, M. R. Yusof, M. F. Mohammad, R. Mahbub, S. Alam, and F. Com, "Characteristics of modular construction: Meeting the needs of sustainability and innovation," in *Colloquium on Humanities, Science and Engineering*, 2014, pp. 216–221.

[5] L. F. Carvalho, L. F. C. Jorge, and R. Jerónimo, "Plug-and-play multistory mass timber buildings: Achievements and potentials," *Journal of Architectural Engineering*, vol. 26, no. 2, p. 04 020 011, 2020. DOI: 10.1061/(ASCE)AE.1943-5568.0000394. eprint: https://ascelibrary.org/doi/pdf/10.1061/\%28ASCE\%29AE.1943-5568.0000394. [Online]. Available: https://ascelibrary.org/doi/abs/10.1061/%5C%28ASCE%5C%29AE.1943-5568.0000394.

[6] F. E. Boafo, J.-H. Kim, and J.-T. Kim, "Performance of modular prefabricated architecture: Case study-based review and future pathways," *Sustainability*, vol. 8, no. 6, 2016, ISSN: 2071-1050. [Online]. Available: https://www.mdpi.com/2071-1050/8/6/558.

[7] D. Dovolis. "Assessing the financial feasibility of modular construction." (2023), [Online]. Available: https://www.woodworks.org/resources/assessing-the-financial-feasibility-of-modular-construction/. (accessed: 12-07-2023).

[8] N. Bertram, S. Fuchs, J. Mischke, R. Palter, G. Strube, and J. Woetzel, "Modular construction: From projects to products," *McKinsey & Company: Capital Projects & Infrastructure*, vol. 1, pp. 1–34, 2019.

[9] V. R. R. Ingenieurs. "Amsterdam poppies." (2022), [Online]. Available: https://www.vanrossumbv.nl/projecten/poppies/. (accessed: 12-06-2023).

[10] J. Knuppee, "Robustness of modular timber buildings," M.S. thesis, TU Delft, Dec. 2022.

[11] K. Zutt, "Connection optimisation for robustness in a timber modular building," M.S. thesis, TU Delft, Feb. 2024.

[12] S. Srisangeerthanan, M. J. Hashemi, P. Rajeev, E. Gad, and S. Fernando, "Review of performance requirements for inter-module connections in multi-story modular buildings," *Journal of Building Engineering*, vol. 28, p. 101 087, 2020.

[13] A. W. Lacey, W. Chen, H. Hao, and K. Bi, "Structural response of modular buildings–an overview," *Journal of building engineering*, vol. 16, pp. 45–56, 2018.

[14] H.-T. Thai, T. Ngo, and B. Uy, "A review on modular construction for high-rise buildings," *Structures*, vol. 28, pp. 1265–1290, 2020, ISSN: 2352-0124. DOI: https://doi.org/10.1016/j.istruc.2020.09.070. [Online]. Available: https://www.sciencedirect.com/science/article/pii/S2352012420305476.

[15] Z. Li and K. D. Tsavdaridis, "Limited-damage 3d-printed interlocking connection for timber volumetric structures: Experimental validation and computational modelling," *Journal of Building Engineering*, vol. 63, p. 105 373, 2023.

[16] Getzner. "Innovative sound control with sylodyn® for the timber construction sector." (n.d.), [Online]. Available: https://www.getzner.com/en/products/construction-products/sylodyn-bearing-strips. (accessed: 26-10-2023).

[17] S. Enso. "Building systems by stora enso." (2016), [Online]. Available: https://www.storaenso.com/-/media/Documents/Download-center/Documents/Product-brochures/Wood-products/Design-Manual-A4-Modular-element-buildings20161227finalversion-40EN.pdf. (accessed: 01.11.2023).

[18] J. van Daalen, "Timber-glass shear wall stabilisez timber modules," M.S. thesis, TU Delft, Feb. 2024.

[19] K. Voulpiotis, "Robustness of tall timber buildings," Ph.D. dissertation, ETH Zurich, 2021.

[20] R. Brandner, R. Tomasi, T. Moosbrugger, E. Serrano, and P. Dietsch, "Properties, testing and design of cross laminated timber," *A State-Of-The-Art Report by COST Action FP1402/WG2*, 2018.

[21] V. De Araujo, F. Aguiar, P. Jardim, *et al.*, "Is cross-laminated timber (clt) a wood panel, a building, or a construction system? a systematic review on its functions, characteristics, performances, and applications," *Forests*, vol. 14, no. 2, 2023, ISSN: 1999-4907. [Online]. Available: https://www.mdpi.com/1999-4907/14/2/264.

[22] Derix. "Houten modules." (2022), [Online]. Available: https://derix.de/nl/producten/houtmodulebouw/. (accessed: 01.11.2023).

[23] M. Wallner-Novak, J. Koppelhuber, and K. Pock, "Cross-laminated timber structural design–basic design and engineering principles according to eurocode," *ProHolz: Innsbruck, Austria*, p. 181, 2014.

[24] P. Aondio, P. Glaser, and H. Kreuzinger, "Fe-berechnung von geklebtem brettsperrholz – teil 1: Theorie/fe calculation of glued cross laminated timber – part 1: Theory," *Bauingenieur*, vol. 95, pp. 22–25, Jan. 2020. DOI: 10.37544/0005-6650-2020-01-46.

[25] F. Janssens, "Influence of a timber outrigger system on cross laminated timber core buildings," 2023.

[26] A. M. P. G. Dias, "Mechanical behaviour of timber-concrete joints.," 2005.

[27] M. Hamelijnck, "Parametric hybrid modular timber construction: Computational design approach for modular construction to discover different building typologies based on global and local structural requirements," 2021.

[28] R. Jockwer and A. Jorissen, "Stiffness and deformation of connections with dowel-type fasteners," *Design of Connections in Timber Structures, A State-of-the-Art Report by COST Action FP1402/WG3, Ed. Sandhaas, Munch-Andersen, Dietsch*, pp. 95–126, 2018.

[29] G. Flatscher, K. Bratulic, and G. Schickhofer, "Screwed joints in cross laminated timber structures," in *Proceedings of the WCTE2014—World Conference on Timber Engineering, Quebec City, QC, Canada*, 2014, pp. 10–14.

[30] D. K. Tran and G. Y. Jeong, "Design of geometric variables of hold-down and angle bracket connections for lateral resistance enhancement of cross-laminated timber (clt) walls considering the influence of wood species, load-grain angles, and floor conditions," in *Structures*, Elsevier, vol. 48, 2023, pp. 1003–1017.

[31] M. Shahnewaz, S. Alam, and T. Tannert, "In-plane strength and stiffness of cross-laminated timber shear walls," *Buildings*, vol. 8, no. 8, p. 100, 2018.

[32] Rothoblaas. "Fastening." (n.d.), [Online]. Available: https://www.rothoblaas.com%5Cproducts%5Cfastening. (accessed: 30-10-2023).

[33] Delta-L. "Straviwood modulink." (n.d.), [Online]. Available: https://delta-l.nl/oplossingen/straviwood-modulink/. (accessed: 31-10-2023).

[34] S. Sendanayake, D. Thambiratnam, N. Perera, T. Chan, and S. Aghdamy, "Enhancing the lateral performance of modular buildings through innovative inter-modular connections," *Structures*, vol. 29, pp. 167–184, 2021, ISSN: 2352-0124. DOI: https://doi.org/10.1016/j.istruc.2020.10.047. [Online]. Available: https://www.sciencedirect.com/science/article/pii/S2352012420306032.

[35] I. Lukacs, A. Björnfot, and R. Tomasi, "Strength and stiffness of cross-laminated timber (clt) shear walls: State-of-the-art of analytical approaches," *Engineering Structures*, vol. 178, pp. 136–147, 2019, ISSN: 0141-0296. DOI: https://doi.org/10.1016/j.engstruct.2018.05.126. [Online]. Available: https://www.sciencedirect.com/science/article/pii/S0141029617338130.

[36] Y. Duan, W. Pan, T. Ping, B. Mou, and B. Young, "Effects of module-to-module connection rotational stiffness on the structural performance of high-rise steel modular buildings," *Journal of Building Engineering*, vol. 82, p. 108 187, 2024.

[37] T. Leung, A. Asiz, Y. H. Chui, L. J. Hu, and Mohammad, "Predicting lateral deflection and fundamental natural period of multi-storey wood frame buildings," 2010. [Online]. Available: https://api.semanticscholar.org/CorpusID:139087729.

[38] M. M. Bagheri, "Study of deflection of single and multi-storey light frame wood shear walls," Ph.D. dissertation, Université d'Ottawa/University of Ottawa, 2018.

[39] R. M. Lawson and J. Richards, "Modular design for high-rise buildings," 2010. [Online]. Available: https://api.semanticscholar.org/CorpusID:110962808.

[40] T. Gunawardena and P. Mendis, "Prefabricated building systems—design and construction," *Encyclopedia*, vol. 2, no. 1, pp. 70–95, 2022.

[41] V. R. R. Ingenieurs. "Internal documents." (2023), [Online]. Available: https://www.vanrossumbv.nl. (accessed: 30-05-2024).

[42] D. Casagrande, S. Rossi, T. Sartori, and R. Tomasi, "Proposal of an analytical procedure and a simplified numerical model for elastic response of single-storey timber shear-walls," *Construction and Building Materials*, vol. 102, pp. 1101–1112, 2016, SHATIS 2013 : Research on Timber Materials and Structures, ISSN: 0950-0618. DOI: https://doi.org/10.1016/j.conbuildmat.2014.12.114. [Online]. Available: https://www.sciencedirect.com/science/article/pii/S0950061815000021.

[43] M. Shahnewaz, "Performance of cross-laminated timber shear walls for platform construction under lateral loading," Ph.D. dissertation, University of British Columbia, 2018.

[44] E. Ruggeri, G. D'Arenzo, M. Fossetti, and W. Seim, "Investigating the effect of perpendicular walls on the lateral behaviour of cross-laminated timber shear walls," in *Structures*, Elsevier, vol. 46, 2022, pp. 1679–1695.

[45] E. M. Ruggeri, G. D'Arenzo, D. L. Cavoli, R. D. Cottonaro, and M. Fossetti, "Experimental investigation on the lateral performance of clt shear walls connected to perpendicular walls," *Procedia Structural Integrity*, vol. 44, pp. 464–471, 2023.

[46] J. van den Berkmortel, "Hoogbouwsysteem in hout," M.S. thesis, TU Eindhoven, Jun. 2010.

[47] J. Penners, "Timber terraced housing," M.S. thesis, TU Delft, Feb. 2024.

Appendix A: Numerical validation

This appendix contains the validation of the numerical modelling methods by comparing horizontal deflections of the numerical models in SCIA with experimental and analytical results. The methods to model the CLT, connections, supports and loads are first described. After that, three validations are done. To start, a basic CLT shear wall under lateral load is checked. Hereafter, a coupled CLT shear wall and a CLT shear wall connected to a floor and perpendicular wall is validated. Finally, a validation is made for a one-storey CLT building with all modelling methods coming together. Validation of these three numerical models will confirm if the modelling methods result in accurate models.

MODELLING METHODS

The Finite Element Software used is SCIA, which is a comprehensive finite element software for structural analysis and design. Modelling of a structure is always a representation of reality captured as good as possible in the model to approach real behaviour of a structure. When modelling, choices have to be made to model the behaviour of the CLT panels, connections, supports and loads in the software. These modelling choices result in the following methods.

CROSS-LAMINATED TIMBER

As CLT is an orthotropic material, It is important to model this correctly by incorporating the right stiffness matrix. SCIA has an option to select cross-laminated when creating the build-up of a 2D element, that calculates the stiffness matrix automatically. As input parameters it needs a material, which is generated separately, and information on the layup of the CLT. The material can be selected from the database, while the following layup parameters should be entered: plate thickness, number of layers, thickness of each layer and board width. Based on the German and Austrian National code (ÖNÖRM B 1995-1-1) the stiffness matrix is determined. The stiffness matrix is verified by the use of the software "CLT designer".

To ensure that the stiffness matrix coincides with the intended direction in the models, the local coordinate system of the CLT elements needs to follow the correct convention as can be seen in Figure 2.9: the x-axis is the 'main' longitudinal direction, the y-axis in the transverse direction and the z-axis is the out-of-plane direction.

CONNECTIONS

Modelling of the connections can be done as rigid, free, flexible or non-linear depending on the connection type. Most connections are modelled correctly as flexible, simplifying the connection as a spring with a certain stiffness. Connecting elements is done in SCIA by applying a hinge between the members. The degrees of freedom, as shown in Figure 9.1, can be constrained when required. Some connections should be modelled as supports, the same constrains can be given to the degrees of freedom as for a hinge.

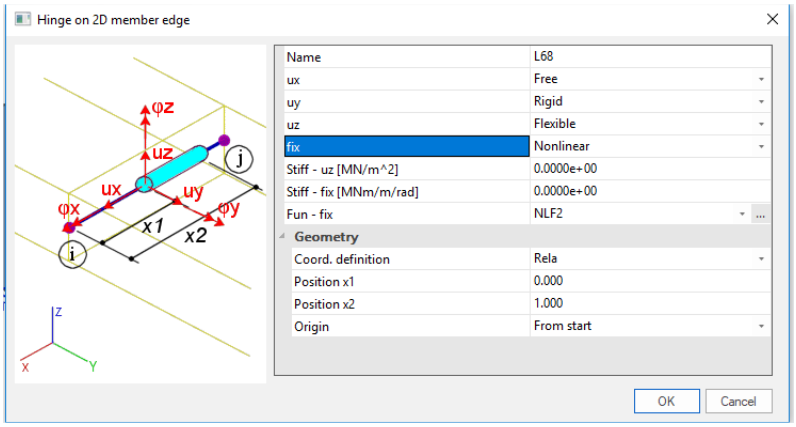

Figure 9.1: Orientation joint with degrees of freedom in SCIA

LATERAL LOAD

The lateral loads are modelled as line loads acting on the floors of the modules. Since the facades are not included in the structural design, it is assumed that the facade of a module is supported at the bottom and top of a module and not on the sides. This results in the lateral forces acting on the floor and ceiling of the module. Dead and live loads are modelled as distributed loads on the floor.

SIMPLE CLT SHEAR WALL

To start simple, a validation is made for a basic cross-laminated timber shear wall. The paper of Lukacs et al. [35] describes the state of the art of the analytical approaches to calculate the strength and stiffness of such shear walls. The results of the analytical calculations are compared with experimental results. The validation done in this paragraph will compare the results of the numerical model with both the analytical and experimental results.

DESCRIPTION OF THE EXPERIMENTAL MODEL

The shear wall which is discussed in the paper of Lukacs et al. is shown in Figure 9.2. It is a square wall with a height and width of 2500 mm which is anchored to a concrete foundation with hold-downs (HD) and angle brackets (AB). In this experiment, the connectors are named HD620 and AB200. The locations are shown in the figure as well and are only placed on one side of the shear wall. At the top of the wall a distributed load of 20 N/mm is placed while the lateral load is attached in the top left corner. The CLT wall consists of a 90 mm thick three-ply (30/30/30) panel with a ply width of 150 mm. Table 9.1 lists the material properties of the timber and the other characteristics of the experiment.

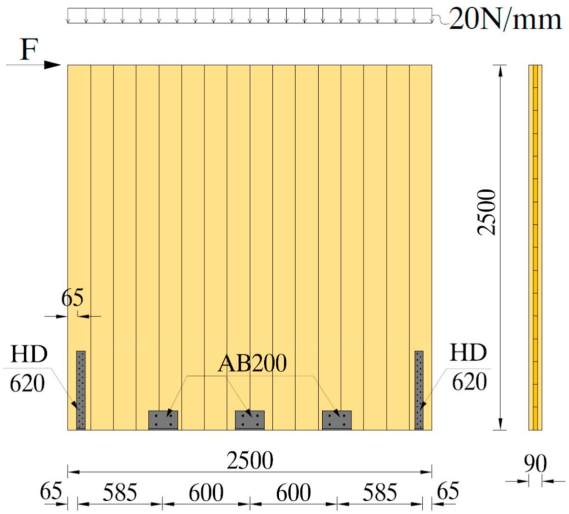

Figure 9.2: Shear wall with geometry [35]

Table 9.1: Properties of CLT shear wall

property	h	w	t	a	q	n_{AB}	$k_{H,HD}$	$k_{h,AB}$	$k_{v,AB}$	G	E	f_c
value	2500 mm	2500 mm	90 mm	150 mm	20 N/mm	3	9.07 kN/mm	6.07 kN/mm	6.07 kN/mm	650 MPa	11600 MPa	21 MPa

DESCRIPTION OF THE NUMERICAL MODEL

For the numerical analysis, the experimental setup is modelled in SCIA. This section describes the modelling methods and assumptions used for the numerical validation model.

An overview of SCIA model is shown in Figure 9.3 where the panel, connections and loads are visible. In the next paragraphs these are discussed and an explanation is given on how these are modelled and why it is done that way.

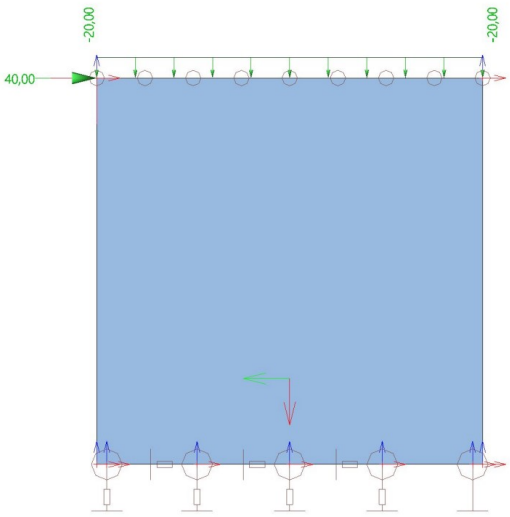

Figure 9.3: Numerical model

CLT
Modelling the CLT is one of the most important aspects to correctly capture the timber behaviour. Because of the orthotropic material that CLT is, a stiffness matrix has to be computed to assign the right structural behaviour to the panel. SCIA has a built-in option to calculate the stiffness matrix for a CLT panel. It needs some input parameters, which are the thickness of the panel and plies, as well as the width of these plies. Furthermore, the elastic modulus and shear modulus should be entered. Important for the CLT panel is that the local coordinate system coincides with the intended direction of the CLT panel. For SCIA this means that the strong direction of the panel corresponds with the x-direction. Finally, the timber material properties can be automatically computed from the Austrian code. The input fields of SCIA with the right values taken from table 9.1.

CONNECTIONS
The connections are two hold downs and three angle brackets, all anchored to the concrete foundation. This means that only tension can occur and that the panel can not move to negative z values. The connections can be modelled as springs to capture the behaviour in the proper way. In table 9.1 the spring stiffnesses are given for both the HD's and AB's. For the HD's only a vertical stiffness (9.07 kN/mm) is considered, while for the AB's both a horizontal (6.07 kN/mm) and vertical stiffness (6.07 kN/mm) is applied. Important to note is that for the right hold down, a rigid support is used to represent the concrete foundation on which the wall is supported. Lastly, all the modelled supports at the bottom restrict translation in y-direction and to prevent the wall from falling over a line support with the same restriction is placed at the top.

LOADS
A vertical load of 20 kN/m is applied at the top of the wall representing a vertical load coming from higher storeys. The horizontal load is applied in the top left corner of the wall representing a lateral load like wind. This lateral load is increased to analyse the displacement for different forces.

RESULTS AND DISCUSSION
Running a linear analysis in SCIA gives the displacements in x-direction for the given load. Doing this for different lateral loads and plotting this in a graph results in the load-displacement curve (figure9.4). In the same graph, the curves for the experimental and analytical analysis are plotted. The curves can be compared to validate the outcomes of the numerical model. It must be noted that the experimental results showed a non-linear behaviour when the lateral force was above 130 kN, because the analytical and numerical analysis was linear it is chosen to compare only the linear stage.

The analytical analysis was based on the study of Casagrande et al. [42], where a simplified method was proposed for the load-carrying capacity. The experimental results were taken from the study from Lukacs et al. [35]. Looking at the graph, it can be noticed that the three lines start relatively close to each other and that the results from SCIA and the experiment stay close to each other. The analytical results follow a slightly different slope after the kink. It can be stated that the numerical model gives trustworthy results and that the model is validated.

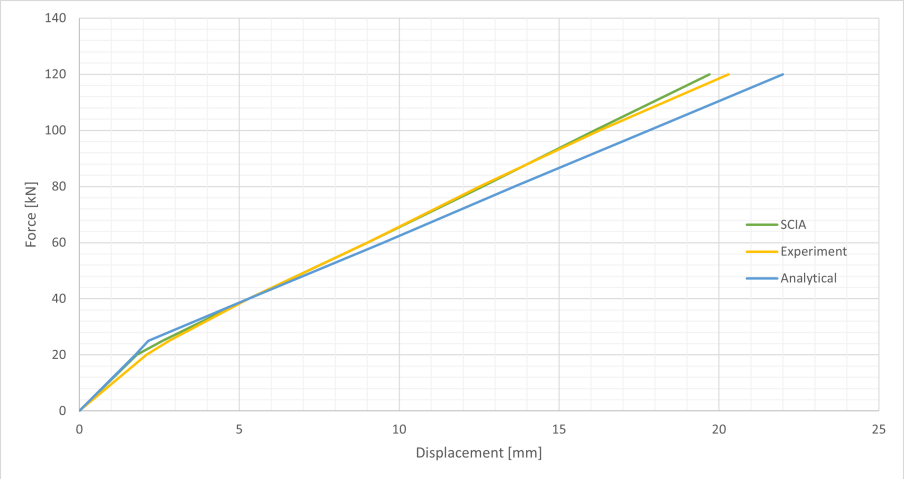

Figure 9.4: Load displacement curves

SIMPLIFICATION TECHNIQUES

Now that it is known that the results from SCIA correspond well with the experimental results and thus the modelling method works, it is interesting to see whether modelling simplification affect the results. For future modelling of larger structures, it can be a time-consuming task to model all the connections independent and at exactly the right spot. Easier would be to simplify the numerical model and save time. It must be checked however if the results are not significantly influenced by these simplifications. Table 9.2 gives an overview of simplification methods for the basic shear wall and the influence on the lateral displacement.

Table 9.2: Influence of simplification in modelling

Simplification		Standard model	HD's at corners	$k_{h,AB}$ at one point (bottom left)	$k_{h,AB}$ at one point (bottom right)	HD's in corners + $k_{h,AB}$ at bottom right	AB's as line support
Displacement U_x [mm]	40 kN	5.3	6.1 (+15.1%)	6.0 (+13.2%)	5.6 (+5.7%)	5.8 (+9.4%)	5.0 (-5.7%)
	100 kN	15.8	17.6 (+11.4%)	17.6 (+11.4%)	16.7 (+5.7%)	17.1 (+8.2%)	15.5 (-1.9%)
Average deviation [%]		-	13.25	12.3	5.7	8.8	-3.8

It can be concluded that simplification has influence on the outcomes. All the simplifications resulted in a higher displacement meaning a more conservative approach, except when the angle brackets are modelled as distributed spring.

MORE COMPLEX CLT SHEAR WALLS

Now that the numerical model for a basic shear wall is validated, the shear wall can be made more complex to check whether the results still match with experimental and analytical analyses. This paragraph looks into three different CLT shear walls discussed in the study from Shahnewaz [43]. The study proposes advanced analytical calculation methods to determine the resistance and deformation of different CLT shear wall configurations under lateral load. The analytical analyses are based on advanced equations for determining the lateral displacement of a shear wall. These analytical calculation methods are verified with experimental tests on CLT shear walls and numerical finite element analysis. It was concluded that the proposed equations describe the CLT shear wall behaviour accurately and that they can be used to determine the horizontal displacement of different shear wall set-ups. [43].

DESCRIPTION OF THE ANALYTICAL MODEL

As mentioned, there are three shear wall configurations which are validated in this section. First of all, a basic shear wall is checked to see whether the standard wall results match, after that the shear wall can be made more complex in terms of configurations and connections. Figure 9.5 shows the three analysed

models where a) is the basic shear wall, b) is a coupled shear wall and c) is a shear wall connected to a perpendicular wall and floor. Input parameters are the same for all of them and are listed in table 9.3 or mentioned in Figure 9.5. Important to note is that self-weight is not included in the analytical analysis.

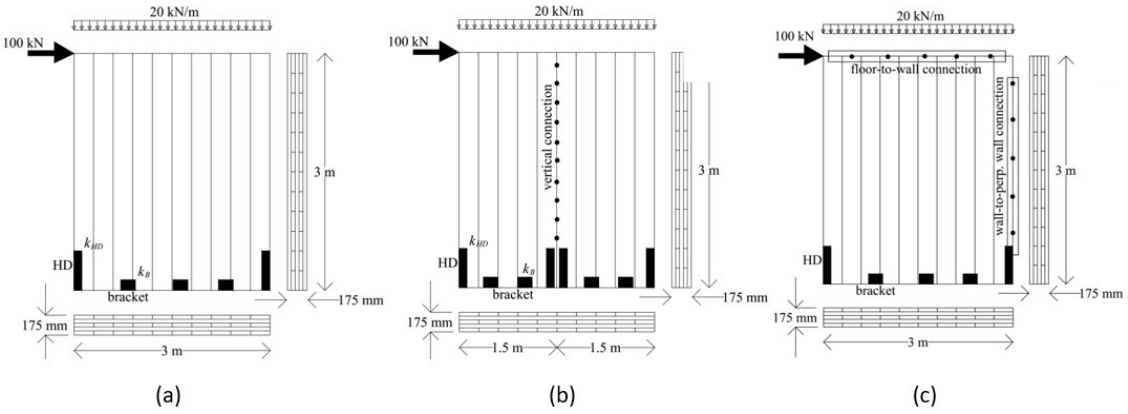

Figure 9.5: Analytical models of the CLT shear walls with: (a) basic shear wall, (b) coupled shear walls and (c) shear wall connected to a perpendicular wall and floor

Table 9.3: Properties of the CLT shear walls

Parameters	**value**	**Parameters**	**value**
Length	3000 mm	Vertical loading, q	20 kN/m
Height	3000 mm	Stiffness of CLT wall-to-floor above connections, k_{fi}	0.5 kN/mm
Stiffness of bracket, k_{AB}	5 kN/mm	Stiffness of CLT wall-to-perp. wall connections, k_{wi}	0.5 kN/mm
Stiffness of hold-downs, k_{HD}	6 kN/mm	Tensile stiffness of brackets in perpendicular wall, $k_{t,p}$	1 kN/mm
Elastic modulus E_0	12000 MPa	Shear stiffness of brackets in perpendicular wall, $k_{s,p}$	1 kN/mm
Shear modulus, G_{CLT}	250 MPa	No. of brackets in perp. wall, n_p	3
No. of layers in CLT panel, n	5	Spacing of STSs in CLT shear wall-to-perp. wall connections	500 mm
Thickness of CLT panel, t_{CLT}	175 mm	Spacing of STSs in CLT shear wall-to-floor connections	500 mm

DESCRIPTION OF THE NUMERICAL MODEL

The numerical models created in the finite element software SCIA are based on the analytical models as described before. The hold-downs are modelled with a spring support in vertical direction and the angle brackets as a horizontal spring support. STSs are modelled as spring supports in vertical and horizontal direction for the floor-to-wall connection, while the wall-to-wall connection was modelled as a continuous spring in vertical and horizontal direction. Stiffnesses of these connections are according to table 9.1 so equal to the values of the analytical method. The same applies for the CLT panel, a 175 mm thick 5-ply panel is modelled with the corresponding parameters as described in the analytical model. For the load, a line load of 20 kN/m is applied and the 100 kN horizontal load is modelled in the top left corner.

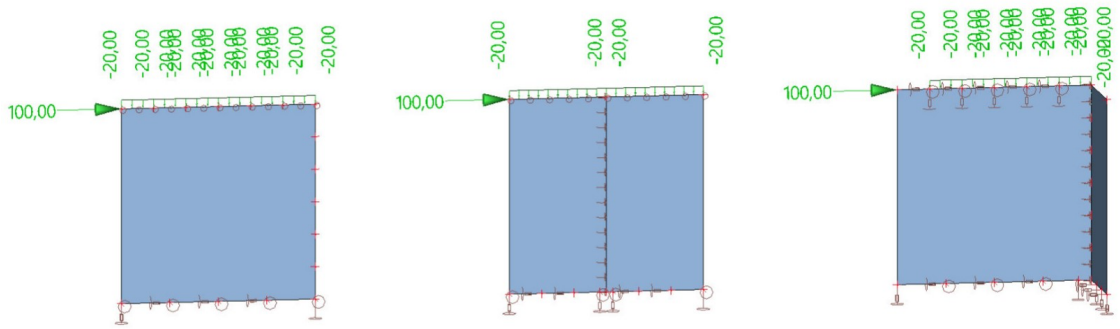

Figure 9.6: Numerical models of the CLT shear walls with: (a) basic shear wall, (b) coupled shear walls and (c) shear wall connected to perpendicular wall and floor

RESULTS AND DISCUSSION

To validate the numerical models, the results have to be compared with the analytical results. The results of both methods are listed in table 9.4. Comparing these results gives information on the accuracy of the numerical model.

Looking at the basic shear wall the analytical calculations resulted in a displacement of 21.1 mm, the numerical calculations resulted in 23.9 mm displacement. Even though the results are quite close, they do not match exactly and results in a deviation of 13%.

The coupled shear wall results show a 40.8 mm displacement for the analytical analysis versus a 40.1 mm displacement for the numerical model. This difference of 1.5% shows that the numerical model represents the analytical model very well and that a coupling of two shear walls can be modelled as described.

Finally, the shear wall that is connected to a perpendicular floor and wall shows a good agreement in the results. The displacement of the analytical and numerical analysis are 14.8 and 14.6 respectively.

Table 9.4: Displacement results

Analysis	**Basic shear walll**	**Coupled shear wall**	**Shear wall with perp. floor and wall**
Analytical	21.1 mm	40.8 mm	14.8 mm
Numerical	23.9 mm	40.2 mm	14.6 mm

ONE-STOREY CLT STRUCTURE

For the final validation, a one-storey CLT structure with shear walls connected to perpendicular walls and floors is modelled and checked with a load-displacement curve from a numerical analysis performed in the study from Ruggeri et al. [44]. This structure is a complete representation of a lateral load resisting building in terms of elements, connections and supports. Validating this structure will give all the tools to model the proposed modules and perform the study of this thesis.

DESCRIPTION OF THE NUMERICAL REFERENCE MODEL

The three-dimensional model that is analysed in [44] is shown in Figure 9.7a. It considers six shear walls connected with perpendicular walls and floors together with their hold downs and angle brackets, the wall-to-wall connections, and the floor-to-wall connections. For the wall-to-wall connections, a 2-joint multilinear elastic links with elastic-plastic behaviour was modelled in the vertical direction. The floor-to-wall connections were modelled as a series of 2-joint linear elastic links characterized by elastic behaviour in the x and y plane. The CLT shear walls are modelled assuming a high elastic modulus, which had the function to act as a diaphragm and distribute the load to the walls. The load was applied as a horizontal point load acting on the roof in the middle of the short side, as can be seen in image

9.7a. Calculations were performed with a nonlinear static analyses to reproduce the elastic plastic behaviour of the model. Figure 9.7b shows a floor plan of the one-storey CLT building together with the distribution of its base connections. All shear walls have a length of 2,5m and the building has a height of 3m. Every shear wall is anchored to the foundation with two hold downs located at the extremity of the walls and three angle brackets divided along the wall. The stiffness of these connections are listed in table 9.5. Out-of-plane behaviour of these connections was neglected, because this information is generally not available. For the wall-to-wall connections self-tapping screws 10x180 mm are used inclined at 90 degrees. The spacing of these STS is 300 mm and the stiffness is 1,5 kN/mm. Floor-to-wall connections are identical to the wall-to-wall connections.

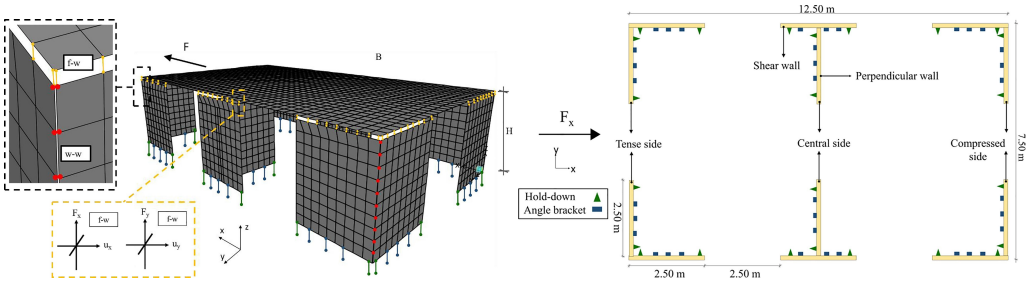

(a) Numerical model

(b) Top view with connection locations

Figure 9.7: 3D view and top view of the one-storey CLT structure [45]

Table 9.5: Geometrical and mechanical parameters of the building

Geometry	**Wall base connections**		**Wall-to-wall connections**		**Wall-to-floor connections**	
h	$k_{h,AB}$	$k_{v,HD}$	$k_{w-w,y}$	$k_{w-w,x}$	$k_{w-f,y}$	$k_{w-f,x}$
3 m	10.8 kN/mm	4.6 kN/mm	1.5 kN/mm	1.5 kN/mm	1.5 kN/mm	1.5 kN/mm

DESCRIPTION OF THE NUMERICAL VALIDATION MODEL

The numerical validation model is created in SCIA and is based on the numerical reference building as described before. It can be seen in Figure 9.8 where the connections, supports and load is shown. The way of modelling this structure is discussed in the following paragraphs.

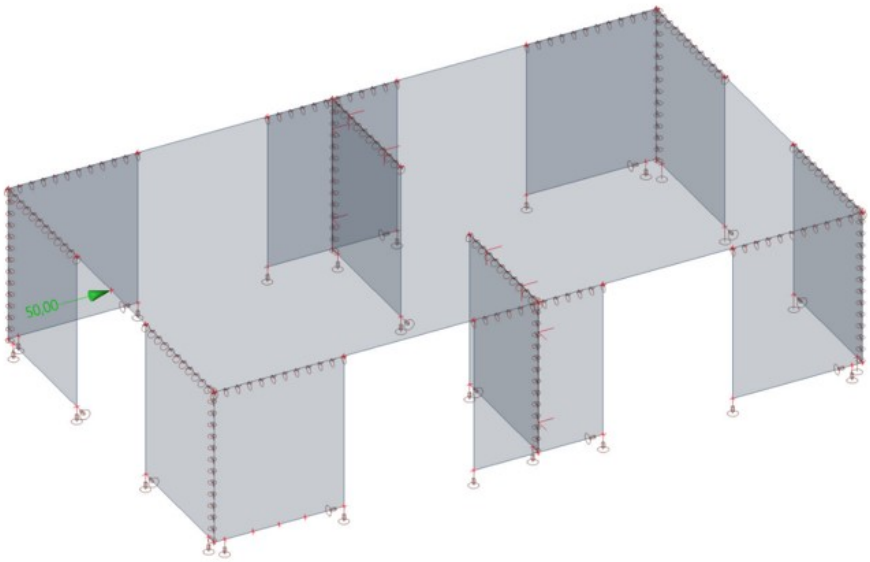

Figure 9.8: SCIA model of the 3D building

Information on the thickness of the shear walls is not given, but because the elastic modulus is considered as infinitely high, the thickness does not matter as the wall behaves as a stiff panel. SCIA needs however input parameters for the CLT material and therefore a 5-ply 100 mm thick (20/20/20/20/20) is chosen with a ply width of 80 mm. For the elastic modulus, a value of 10^{10} MPa is used, while the shear modulus is taken as 650 MPa.

The connections are modelled as springs but different to the reference model the angle brackets are modelled as one horizontal spring combining the three horizontal stiffnesses and the wall-to-wall and floor-to-wall connections are modelled as distributed line connections. This latter is calculated by multiplying the stiffness of one STS with the number of screws per meter, which is 1000/300 = 3.33 for the given spacing of 300 mm. All the connection stiffnesses used in the model are stated in table 9.6. For the HDs, a distinction is made for tension and compression, as the reference model does this as well.

The load is modelled as a point load acting on the roof in the middle of the short side of the building. Additionally, self weight of the structure is turned on and a combination of the two loads is made having both a load factor of 1.

Table 9.6: Stiffness of the connections used in the numerical validation model

Connections	HD tension	HD compression	AB	total stiffness of AB	Wall-to-wall	spacing	W-w per meter	Floor-to-wall	spacing	F-w per meter
symbol	$k_{v,HD,t}$	$k_{v,HD,c}$	$k_{h,AB}$	$n * k_{AB}$	$k_{w-w,x/y}$	s	$k_{w-w,x/y}$	$k_{w-w,x/y}$	s	$k_{w-w,x/y}$
value	4.6 kN/mm	9.2 kN/mm	10,8 kN/mm	32,5 kN/mm	1.5 kN/mm	300 mm	5 kN/mm	1.5 kN/mm	300	5 kN/mm

RESULTS AND DISCUSSION

Validation of the numerical model is carried out by considering the overall response of the reference building in terms of lateral stiffness. This is done based on the load-displacement curve of the 3D model of the building. Next to the described building configuration, there is also a configuration where the shear walls are not connected to the perpendicular walls. The results of that analysis are also used for validation. From these curves, the stiffness of the structure can be determined. In the study of Ruggeri et al. [44] this lateral stiffness is determined and compared with a analytical analysis. These results will be used to validate the numerical model analysed in SCIA.

Despite the fact that a nonlinear elastic analysis was performed in the paper of Ruggerti et al. the analysis that is done for the validation model is a linear elastic analysis. This is possible if the connections

don't reach the plastic phase and validation is done in the linear phase of the structure. From the paper it can be seen that the elastic phase of the 3D model with perpendicular walls (SW + PW) is until a lateral load of approximately 260 kN and for the shear wall only configuration (SW) until 200 kN. Testing the validation models proves that for a maximum load of 250 kN for the SW + PW configuration, the base connections did not reach their elastic stage. The same applies for a maximum load of 200 kN for the SW configuration.

With the parameters as discussed in the previous section, the values reported in table 9.7 were found for the lateral stiffness for the cases of shear wall plus perpendicular walls (SW+PW) and the shear wall only (SW) configurations. From table 9.7it is possible to see that the results show similar results. The reference and analytical stiffness shows a maximum of 1% difference, while the validation model shows a maximum of 3% difference. This reveals a good accuracy of the validation model, meaning that the modelling method is a proper way to model the structure. Figure 9.7a shows the load displacement curves of the two configurations obtained from the numerical models. As is clear, the curves of the reference (paper) and validation (SCIA) for both the SW+PW and SW configurations follow each other closely until the plastic range and the validation curve is stopped. This confirms the validation of the numerical model used in the finite element software SCIA.

Table 9.7: Lateral stiffness of the models

	SW+PW			SW		
model	Analytical	Reference	Validation	Analytical	Reference	Validation
$K_{building}$ [kN/mm]	22,23	22.22	22.47	17.42	17,43	16.94

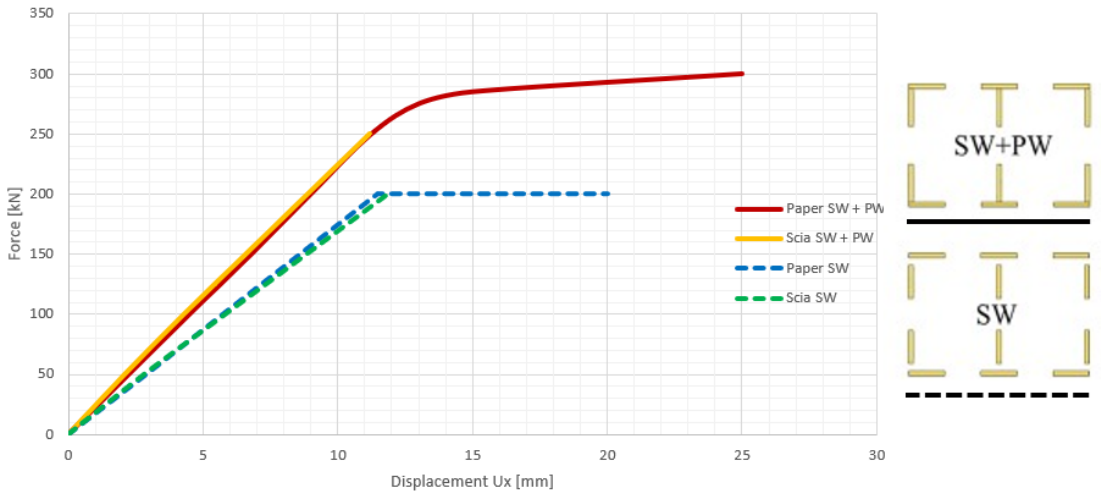

Figure 9.9: Load displacement curve of the 3D reference (paper) and validation (SCIA) model for both building configurations

Although the numerical model is validated and the results are close, they do no match exactly. As mentioned before, the analysis done for the reference model was non-linear, while the validation model is linear. Even though the results are only monitored in the elastic range and the base connections do not exceed the elastic strength. For the wall-to-wall and floor-to-wall connections this is unclear and it could be the case that they exceed their elastic strength. Another factor for the slight difference could be the inaccuracy. The SCIA outcomes were rounded to one decimal, while the reference study reported outcomes with two decimals. Slight rounding errors could therefore explain the minimal differences. Finally, the values of the load displacement curves were not exactly mentioned in the paper and therefore they were estimated with the global stiffness values which were given. However, it is unclear whether the stiffness is an average or determined from the end of the elastic phase.

Appendix B: Mesh size influence

In Finite Element Analysis, the accuracy of the result obtained is determined by the size of the mesh. Besides, the mesh size heavily influences the computational time. According to the theory, small elements results in higher accuracy compared to larger elements. However, a smaller mesh means that forces are more concentrated, which can lead to overestimated output values. This is for example the case for point loads and supports, who are modelled at a very small surface, or where elements intersect. By adjusting the mesh size, the force will be spread over a smaller or larger area.

The numerical model of the modules has some of these difficulties. The horizontal load acting on the roof is concentrated, while in reality will act on a larger area. The same holds for the supports, which are modelled at a very small area, leading to increased concentrated forces. Finally, the intersection of the shear and side wall is a place where forces are transferred, meaning concentrated forces will occur. It is important for realistic results that these mentioned points are observed and the right mesh is chosen to accommodate for the concentrated forces. For module 3 the maximum displacement increased when a smaller mesh was used. For example, a mesh of 200, 400 and 600 mm had a displacement of respectively 66.4, 60.4 and 56.4 mm.

It can be concluded that the mesh should be smaller for better results, but because of stress concentration should not be too small. Thus, an optimum should be found. To come to an optimum mesh size, a CLT shear wall loaded at the top is investigated. The wall is supported by two pinned supports, which is similar to the modules in this thesis. Five different mesh sizes were analysed, focusing on the maximum lateral displacement and vertical displacement due to the compression at the supports. Table **??** shows the summarized results for the different mesh sizes. Figure 9.10 shows their deformation behaviour. The analysis with a mesh size of 400 mm shows the most realistic behaviour, because the concentration at the supports is not too large and at the location of the load the local effect is only just notable, But still sufficient accurate results are obtained.

Table 9.8: Total deflection and local deflection for varying mesh sizes.

Mesh size [mm]	**50**	**100**	**200**	**400**	**600**
U_x^{top} [mm]	119.7	108.5	97.4	86.1	80.0
U_z^{bottom} [mm]	7.5	6.6	5.7	4.8	3.6

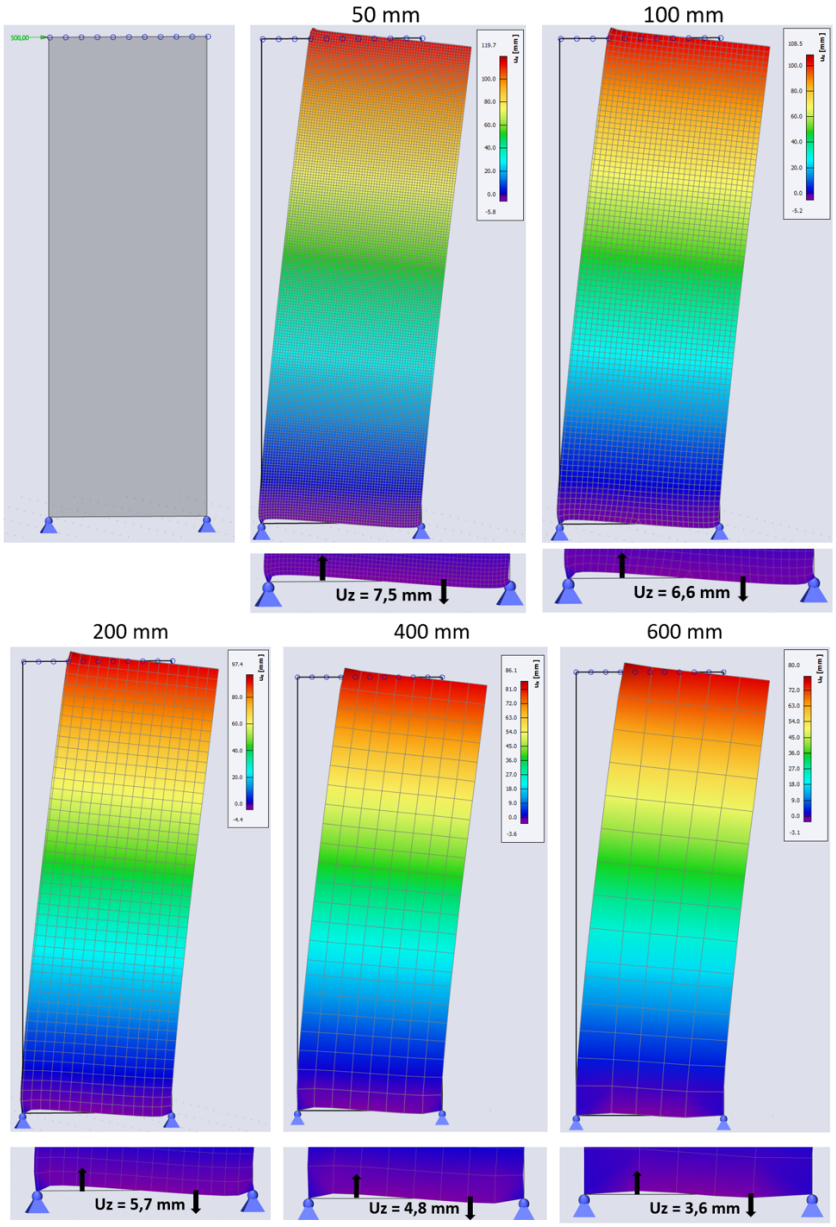

Figure 9.10: Deformation for different mesh sizes, with the focus on compression at the supports

Appendix C: Bending and shear stiffness determination

The shear and bending stiffness GA and EI respectively are determining factors for the module deflection. In simple structures calculating GA and EI is relatively easy, but for more complex structures that have not straightforward dimensions it will become much more difficult to calculate them by hand. Looking at the modules, it is obvious that they belong to the latter category, where calculating the shear and bending stiffness is not so easy. Therefore, a different approach is used to calculate them. This approach uses two equations to solve the two unknowns GA and EI [46].

The approach to determine the shear and bending stiffness is by creating two equations with two unknowns, which can then be solved for the two unknowns. With the use of the forget-me-nots for cantilevers this can be done. However, as explained before, the superposition of the bending and shear deformation is not possible for the modules as they are modelled on two supports. Nevertheless, GA and EI are values that are dependent on the design and dimensions of a structure and independent of the support conditions. Therefore, the stiffnesses can be determined by adding a rigid support along the width of the module which then corresponds to the cantilever model. Then the superposition can be used to calculate GA and EI.

METHOD AND CHECKING

The equation for the deformation of a cantilever with a point load at the top or a distributed load consist of a shear and bending part and are as follows:

Point load at top:

$$u = \frac{F * H^3}{3 * EI} + \frac{F * H}{GA} \tag{9.1}$$

Distributed load:

$$u = \frac{q * H^4}{8 * EI} + \frac{q * H^2}{2 * GA} \tag{9.2}$$

The force, height and displacement are knowns when modelling the structure, leaving only GA and EI as unknowns. Because H has a different power in the two parts, adjusting it results is two equations with two unknowns. This can be solved to obtain GA and EI.

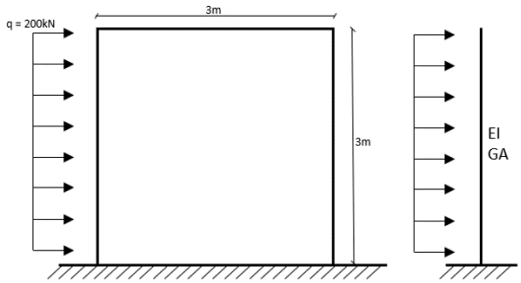

Figure 9.11: Dimensions of the wall and the corresponding cantilever model

Before using this method to compute the shear and bending stiffness of the modules, it should be tested for a more simple structure to verify that it works. This is done with a simple shear wall of 3 x 3 m consisting of an isotropic timber C24 plate of 100 mm thick. The E-modulus is 11000 MPa and the shear modulus is 5500 MPa. The q-load is 200 kN/m. Modelling this structure in SCIA (see Figure 9.12) results in a lateral displacement u of 1.4 mm. For the second equation, the length is increased to 9m, resulting in a lateral displacement u of 72 mm. These models result in the two following equations:

$u_1 = \frac{q*H_1^4}{8*EI} + \frac{q*H_1^2}{2*GA} = 72 = \frac{200*9000^4}{8*EI} + \frac{200*9000^2}{2*GA}$

$u_2 = \frac{q*H_2^4}{8*EI} + \frac{q*H_2^2}{2*GA} = 1,4 = \frac{200*3000^4}{8*EI} + \frac{200*3000^2}{2*GA}$

The first step when solving is to eliminate one of the unknowns, in this case GA is chosen. Subtracting the two equations after multiplying with the ratio H_1^2/H_2^2 leads to EI.

$9000^2/3000^2 = 9$

$72 = \frac{200*9000^4}{8*EI} + \frac{200*9000^2}{2*GA} -$

$12.6 = \frac{1800*3000^4}{8*EI} + \frac{200*9000^2}{2*GA}$

$59,4 = \frac{1.46*10^{17}}{EI} \Rightarrow EI = 2.476*10^{15} Nmm2$

Subsequently, GA can be calculated:

$GA = \frac{\frac{200*9000^2}{2}}{72 - \frac{200*9000^4}{8*2,476*10^{15}}} \Rightarrow GA = 1.63*10^9 N$

The stiffnesses can be simply calculated by hand to verify the method.

$EI = E*\frac{1}{12}*t*b^3 = 11000*\frac{1}{12}*100*3000^3 = 2.475*10^{15} Nmm2$

$GA = G*t*b = 5500*100*3000 = 1.65*10^9 N$

Since the results are close to identical, it can be concluded that the method works.

The method can now be applied to calculate the shear and bending stiffness of the modules. For module 0 this is done below. This configuration is chosen because for this design it is possible to check the results with hand calculations. The module is clamped at the bottom of the shear wall and side walls, a point load of 600 kN is applied at the top of the shear wall, therefore equation 9.1 should be used. The two equations are set up for the heights 2.6 m and 3.6 m so that the average height is 3.1 m as is the standard dimension. The corresponding displacements are 3.43 and 5.28 mm respectively. Note that the height of the shear wall is slightly smaller because the floor is raised by 170 mm and since the rigid support is placed underneath the shear wall the calculation is used with a reduced height of 2.43 and 3.43 m. The calculation can now be performed:

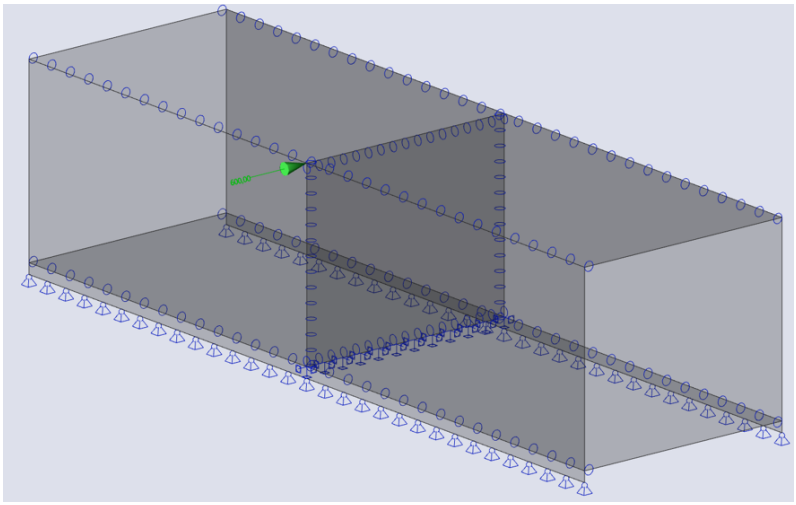

Figure 9.12: Model of module 0 used to determine the stiffness

$$u_1 = \frac{F*H_1^3}{3*EI} + \frac{F*H_1}{GA} = 5,28 = \frac{600*3430^3}{3*EI} + \frac{600*3430}{GA}$$

$$u_2 = \frac{F*H_2^3}{3*EI} + \frac{F*H_2}{GA} = 3,43 = \frac{600*2430^3}{3*EI} + \frac{600*2430}{GA}$$

The first step is to eliminate one of the unknowns, in this case GA is chosen. First, the equation of u_2 is multiplied with the ratio of the heights $H_2/H_1 = 1.41$. After that u_2 is subtracted with u_1 leaving the equation that can solve for EI. After that GA can be calculated by using the found EI.

$$5.28 = \frac{600*10^3*3430^3}{3*EI} + \frac{600*3430}{GA} -$$

$$4.84 = \frac{846*10^3*2430^3}{3*EI} + \frac{600*3430}{GA}$$

$$0.44 = \frac{4.02*10^{15}}{EI} \Rightarrow EI = 9.20*10^{15} Nmm2$$

Subsequently, GA can be calculated:

$$GA = \frac{600*10^3*3430^3}{5.28 - \frac{600*10^3*3430^3}{9.20*10^{15}}} \Rightarrow GA = 4.64*10^8 N$$

The obtained stiffnesses are verified in the next section.

VERIFICATION STIFFNESSES MODULE 0

In the previous section, the method shows good accuracy with the hand calculation for a simple shear wall. For the module design it is more difficult to calculate the stiffnesses by hand. The only module design for which this is possible is module 1. This module can be calculated as an I-beam where the shear wall is the web, the side walls are the flanges and the roof and floor do not contribute to the stiffness. The I-section is shown in Figure 9.13 whereafter the analytical calculation of EI and GA are performed.

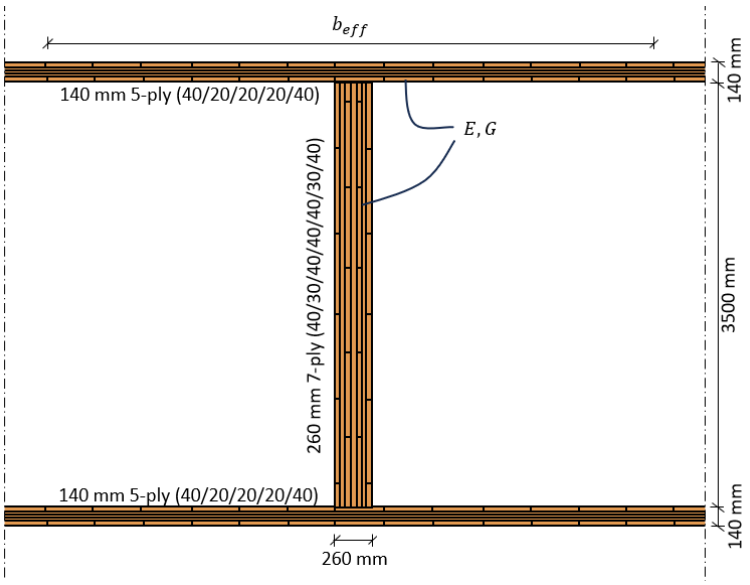

Figure 9.13: Module 1 shown as I-section

First, the effective width of the flanges should be determined. The research of J.J.A. Penners [47] investigated for CLT walls the influence of the transverse wall width on the effective width. The results are shown in Figure 9.14. The study found that a plateau is reached when the width keeps increasing. The side walls of the module are 12 m long, meaning the effective width would reach the plateau. Therefore, the effective width is taken as 800 mm. Another assumption is that γ is taken as 1 because the web and flanges are rigidly connected.

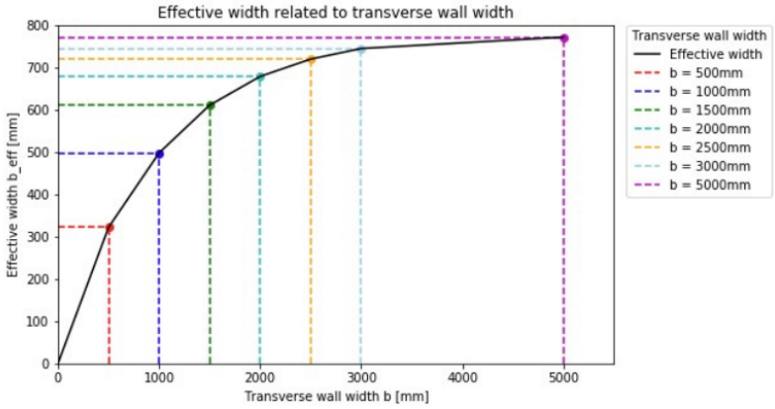

Figure 9.14: Effective width related to transverse wall width - Full cooperation [47]

Hand calculation EI and GA

$E = 11000 N/mm^2$
$G = 690 N/mm2$

Flange:

$b_{eff} = 800 mm$
$t_f = 140 mm$
$t_1 = 40 mm$, $a_1 = 1870 mm$
$t_3 = 20 mm$, $a_3 = 1820 mm$

$t_4 = 40mm$, $a_5 = 1770mm$

$I_f = \frac{1}{12} b_{eff} t_1^3 + t_1 b_{eff} a_1^2 + \frac{1}{12} b_{eff} t_3^3 + t_3 b_{eff} a_3^2 + \frac{1}{12} b_{eff} t_5^3 + t_5 b_{eff} a_5^2 = 2.65 * 10^{11} mm^4$
$A_f = t_f * b_{eff} = 112000mm^2$

Web:

$h = 3500mm$
$t_w = 260mm$
$t_0 = 160mm$

$I_w = \frac{1}{12} b_o h^3 = 5.72 * 10^{11}$
$A_w = t_w * h = 910000mm^2$

Stiffnesses:

$EI = E * (2I_f + I_w) = 1.26 * 10^{16} kNm^2$
$GA = G * (2A_f + A_w) = 7.82 * 10^8 kN$

Another way of calculating the shear and bending stiffness is by using reverse engineering. With equation 9.1 and SCIA results, the corresponding stiffness can be determined. With the following steps, EI and GA are calculated. First, the module is clamped at the bottom to make superposition possible. Then modelled with bending deformation only ($G = 10^{10}$) and shear deformation only ($E = 10^{10}$). The total force is then divided by the corresponding displacement. Subsequently, the corresponding values for EI and GA can be found with the equations $EI = \frac{\frac{F}{u_b} * H^3}{3}$ and $GA = \frac{F}{u_s} * H$. The calculation is performed below.

Bending stiffness EI:
$EI = \frac{\frac{F}{u_b} * H^3}{3} = \frac{\frac{600*10^3}{0.39} * 2930^3}{3} = 1.29 * 10^{16} Nmm^2$
$GA = \frac{F}{u_s} * H = \frac{600*10^3}{3.67} * 2930 = 4.79 * 10^8 N$

Finally, the calculated stiffnesses can be compared to those obtained from the 2 equations-2 unknowns method. As can be seen in table 9.9. For the bending stiffness, corresponding values were found. Even though there are some differences, they are within the agreeable limits. The shear stiffness results show bigger differences with the hand calculation. The hand calculation has a significant higher stiffness than the other methods. This is probably, because a too large effective width was considered which influences the shear stiffness. Because the other result does show good an identical result, the found value is still considered to be valid.

Table 9.9: Comparison of calculated stiffness values

2 eq.-2 unknown method		**Hand calculation**		**Forget-me-nots**	
EI $[Nmm^2]$	GA $[N]$	EI $[Nmm^2]$	GA $[N]$	EI $[Nmm^2]$	GA $[N]$
$0.92 * 10^{16}$	$4.79 * 10^8$	$1.26 * 10^{16}$	$7.82 * 10^8$	$1.29 * 10^{16}$	$4.79 * 10^8$

Appendix D: Results

MAIN EQUATIONS

For the main equations, the best fitting equations for the parameters width, height and force are presented. The equations were used to propose the main equations for the different module configurations

Module 0

Best fitting equations for b:

$$u_{M0} = \frac{4FH^2b}{(EI)_s(b^{1.2})} + \frac{1.5FH}{(GA)_s(\frac{b}{3} - 0.167)} \qquad \theta_{M0} = \frac{22FHb}{(EI)_s(b^3)}$$

Best fitting equations for H:

$$u_{M0} = \frac{4FH^2b}{(EI)_s(b^{1.2})} + \frac{1.2FH}{(GA)_s((\frac{b}{3} - 0.167)H^{0.3})} + 0.25 \qquad \theta_{M0} = \frac{22FHb}{(EI)_s(b^3)}$$

Best fitting equation for F:

$$u_{M0} = \frac{2FH^2b}{(EI)_s(b^{1.2})} + \frac{1.8FH}{(GA)_s(\frac{b}{3} - 0.167)} \qquad \theta_{M0} = \frac{22FHb}{(EI)_s(b^3)}$$

Module 1

Best fitting equation for b:

$$u_{M1} = \frac{10FH^2b}{(EI)_s(b^{1.9})} + \frac{2.22FH}{(GA)_s(\frac{b}{3} - 0.167)} \qquad \theta_{M1} = \frac{13FHb}{(EI)_s(b^3H^{0.7})}$$

Best fitting equation for H:

$$u_{M1} = \frac{10FH^2b}{(EI)_s(b^{1.9}H^{0.2})} + \frac{3.55FH}{(GA)_s((\frac{b}{3} - 0.167)H^{0.3})} \qquad \theta_{M1} = \frac{14FHb}{(EI)_s(b^3H^{0.7})}$$

Best fitting equation for F:

$$u_{M1} = \frac{10FH^2b}{(EI)_s(b^{1.9}H^{0.2})} + \frac{3.3FH}{(GA)_s((\frac{b}{3} - 0.167)H^{0.3})} \qquad \theta_{M1} = \frac{13FHb}{(EI)_s(b^{32}H^{0.7})}$$

Module 2

Best fitting equation for b:

$$u_{M2} = \frac{5FH^2b}{(EI)_s(b^{0.5})} + \frac{3FH}{(GA)_s(\frac{b}{3} - 0.167)} \qquad \theta_{M2} = \frac{8FHb}{(EI)_s(b^{2.8})}$$

Best fitting equation for H:

$$u_{M2} = \frac{8FH^2b}{(EI)_s(b^{0.5}H^{0.5})} + \frac{10FH}{(GA)_s((\frac{b}{3} - 0.167)H)} + 3.74 \qquad \theta_{M2} = \frac{10FHb}{(EI)_s(b^{2.8}H^{0.2})}$$

Best fitting equation for F:

$$u_{M2} = \frac{8FH^2b}{(EI)_s(b^{0.5}H^{0.5})} + \frac{10FH}{(GA)_s((\frac{b}{3}-0.167)H)} \qquad \theta_{M2} = \frac{10FHb}{(EI)_s(b^{2.8}H^{0.2})}$$

Module 3

Best fitting equation for b:

$$u_{M3} = \frac{150FH^2b}{(EI)_s(b^{1.15})} + \frac{10FH}{(GA)_s(\frac{b}{3}-0.167)} \qquad \theta_{M3} = \frac{4.2FHb}{(EI)_s(b^{3.1})}$$

Best fitting equation for H:

$$u_{M3} = \frac{160FH^2b}{(EI)_s(b^{1.15})} + \frac{10FH}{(GA)_s(\frac{b}{3}-0.167)} \qquad \theta_{M3} = \frac{4.2FHb}{(EI)_s(b^{3.1})}$$

Best fitting equation for F:

$$u_{M3} = \frac{150FH^2b}{(EI)_s(b^{1.15})} + \frac{10FH}{(GA)_s(\frac{b}{3}-0.167)} \qquad \theta_{M3} = \frac{4.2FHb}{(EI)_s(b^{3.1})}$$

EQUATION EXTENSION

The graphs that are used to determine the factors to account for the design options are presented here. First for the shear wall thickness factor $k_{sw,t}$ and after that for the connection stiffness factor k_c

SHEAR WALL THICKNESS

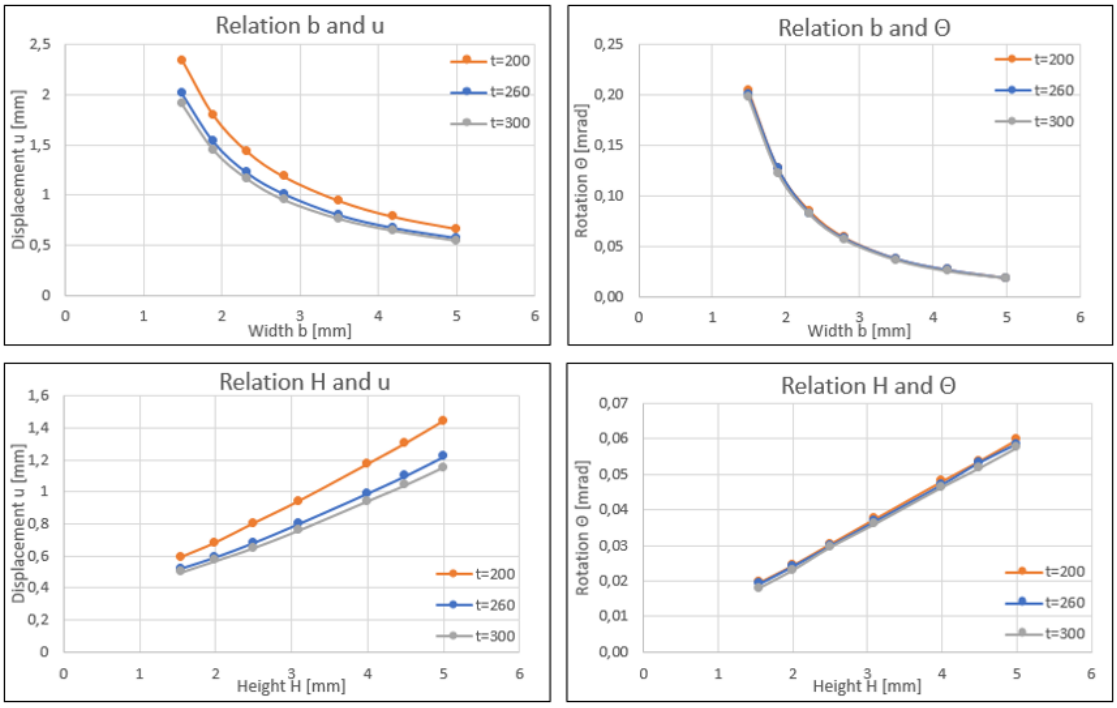

Figure 9.15: Relations for the varying shear wall thickness, module 0

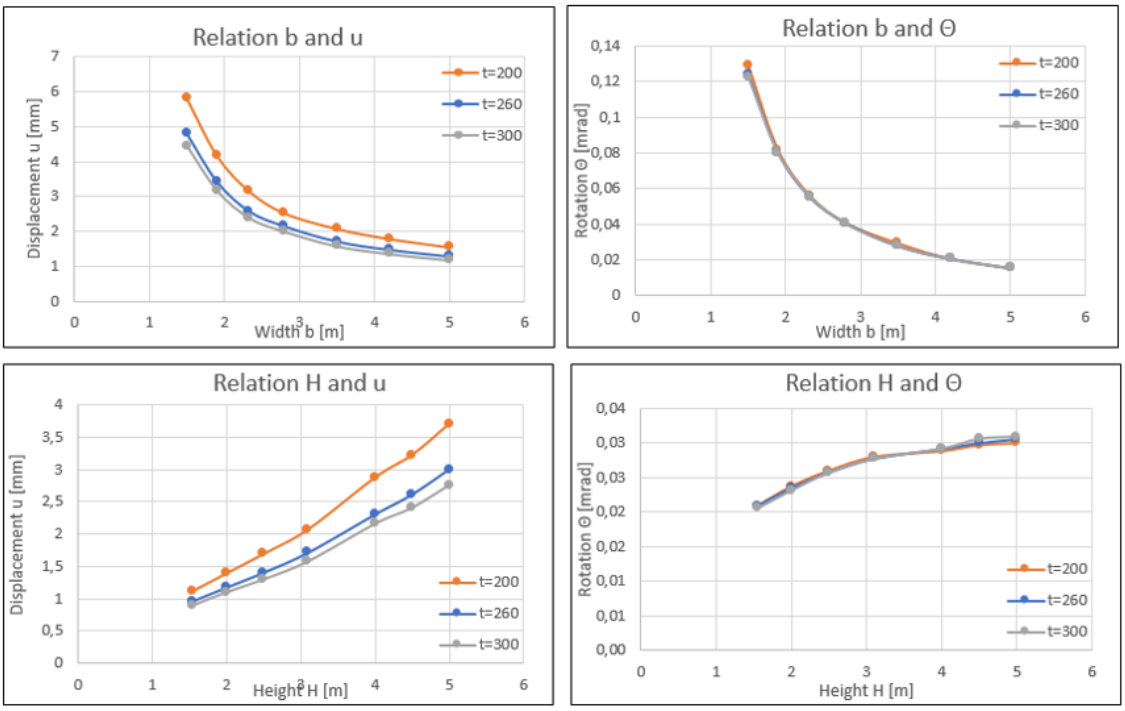

Figure 9.16: Relations for the varying shear wall thickness, module 1

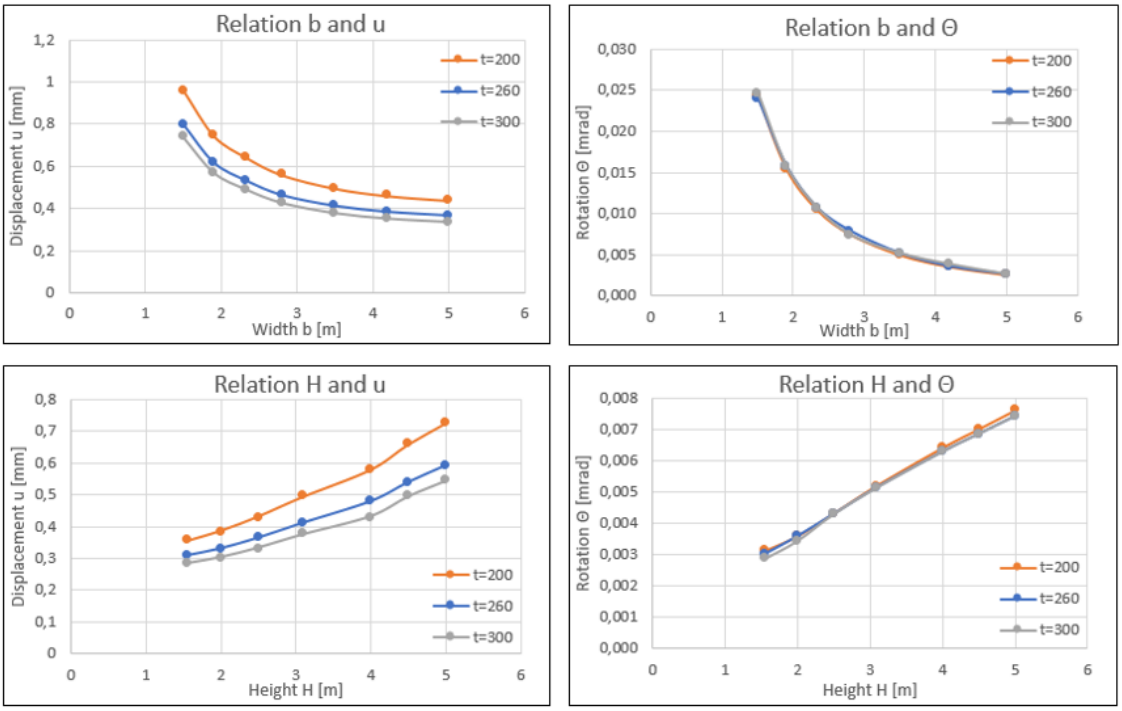

Figure 9.17: Relations for the varying shear wall thickness, module 2

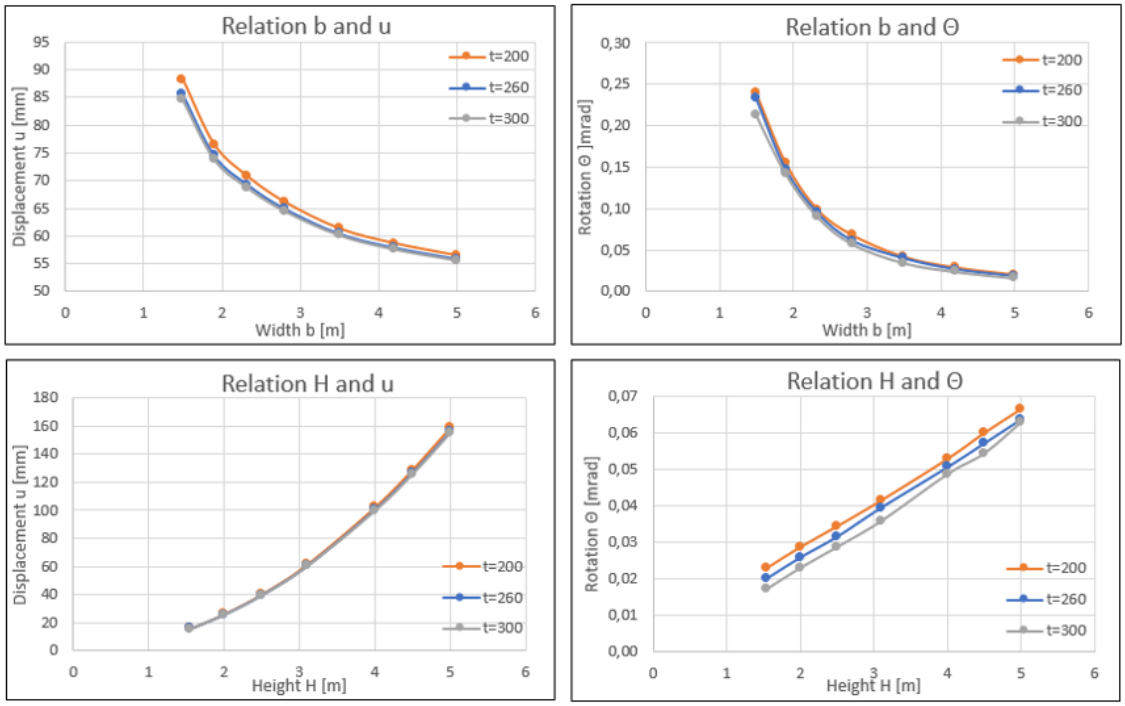

Figure 9.18: Relations for the varying shear wall thickness, module 3

CONNECTION STIFFNESS

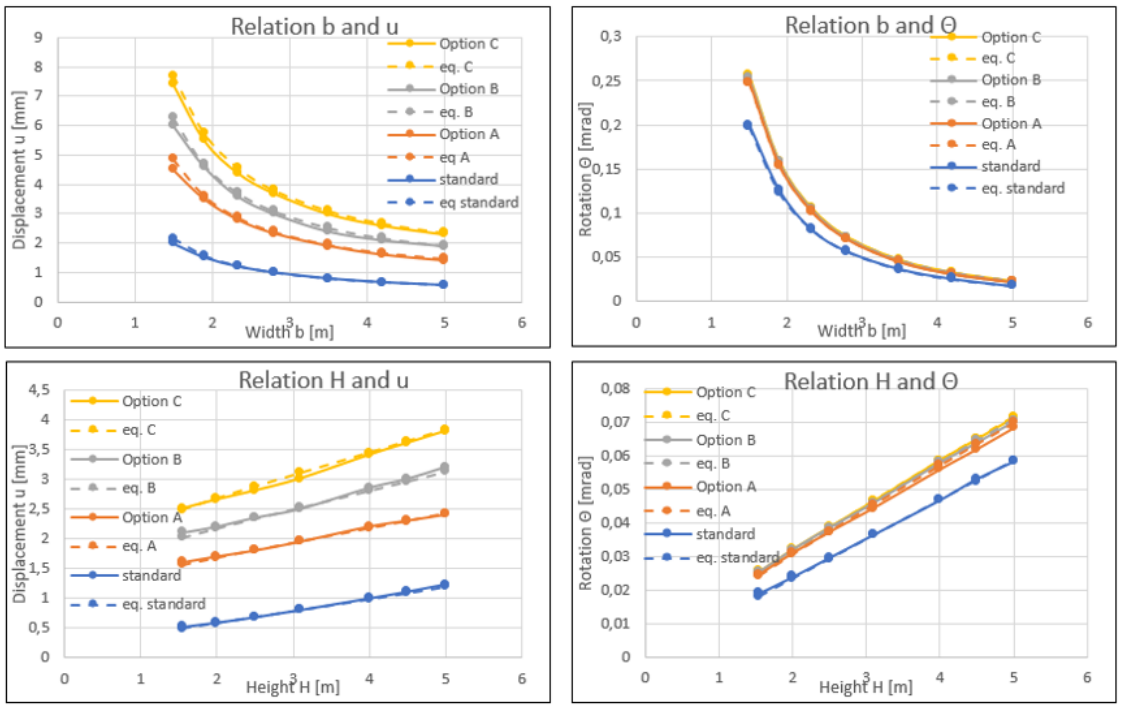

Figure 9.19: Relations for the varying connection stiffness, module 0

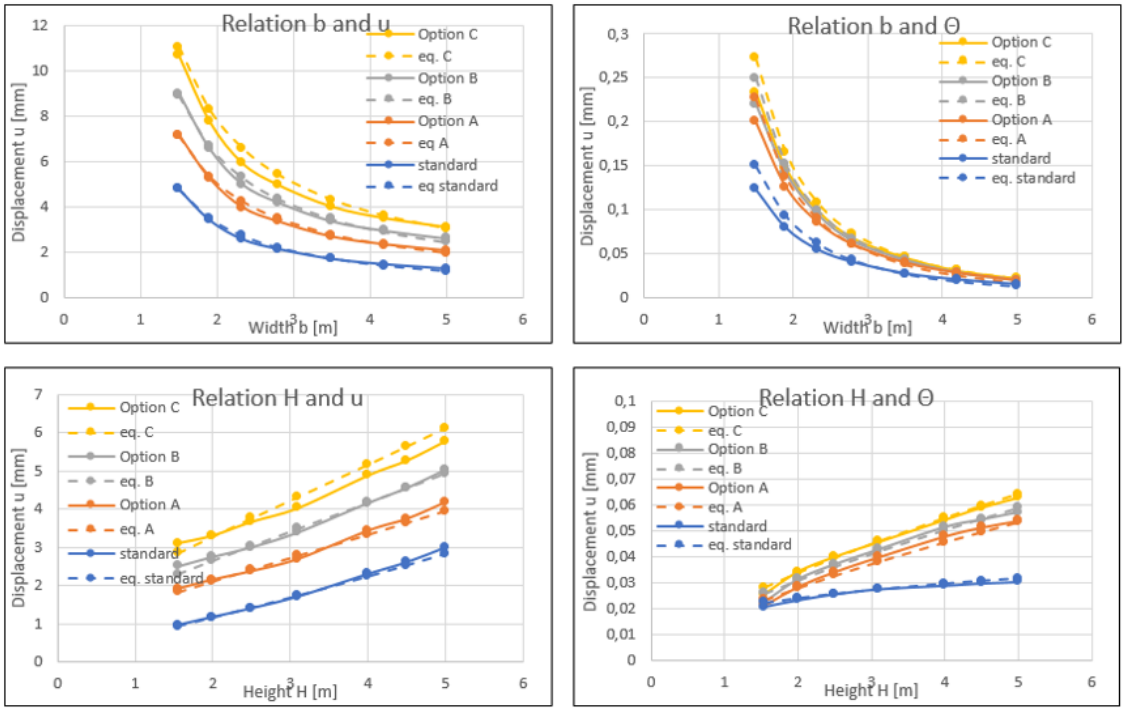

Figure 9.20: Relations for the varying connection stiffness, module 1

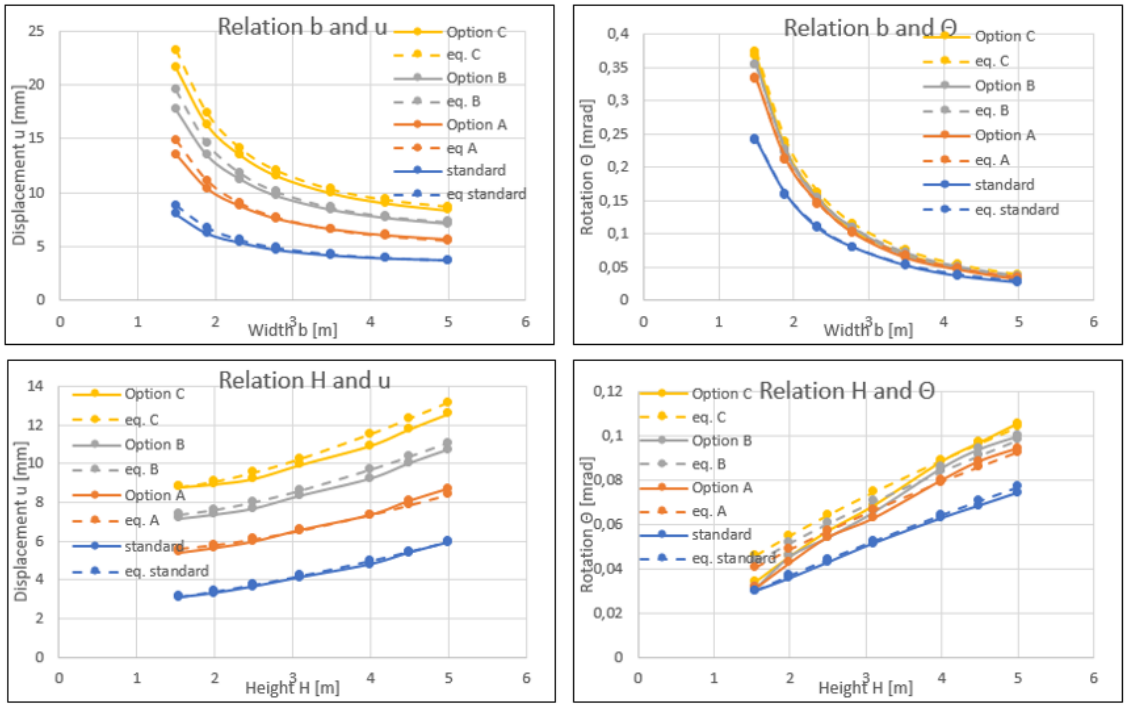

Figure 9.21: Relations for the varying connection stiffness, module 2

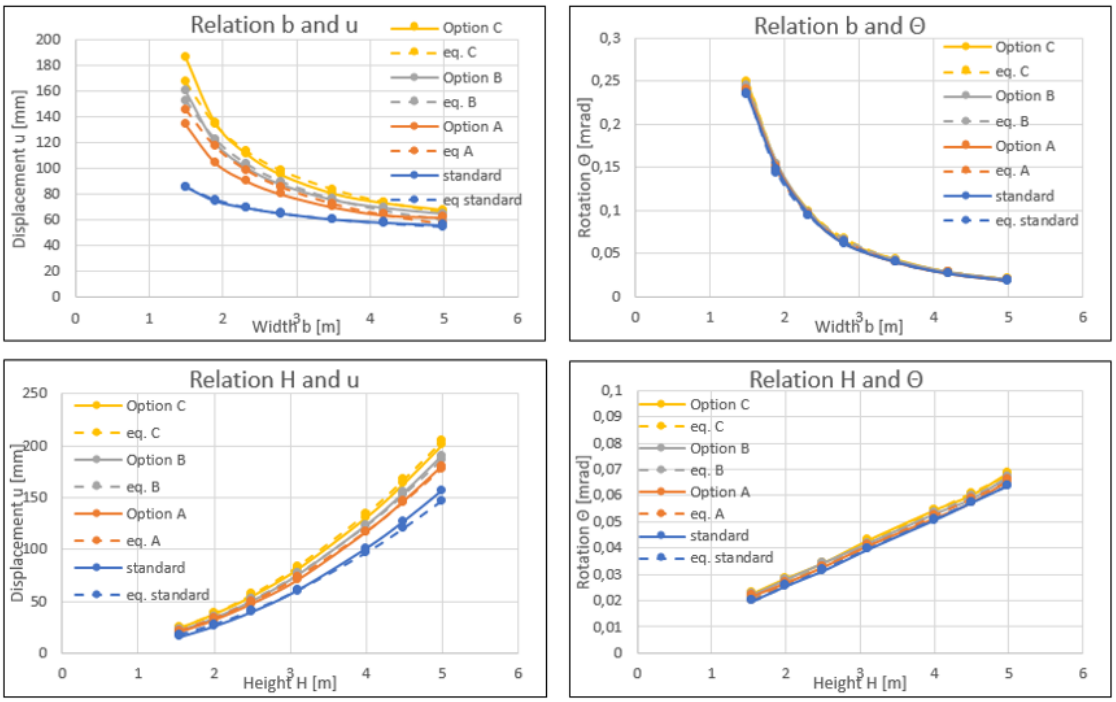

Figure 9.22: Relations for the varying connection stiffness, module 3